12-19-2023 2:00 PM

Towards Patient Specific Mitral Valve Modelling via Dynamic 3D Transesophageal Echocardiography

Patrick Carnahan, *The University of Western Ontario*

Supervisor: Peters, Terry M., *The University of Western Ontario*
Co-Supervisor: Chen, Elvis C.S., *The University of Western Ontario*
A thesis submitted in partial fulfillment of the requirements for the Doctor of Philosophy degree in Biomedical Engineering

Abstract

Mitral valve disease is a common pathologic problem occurring increasingly in an aging population, and many patients suffering from mitral valve disease require surgical intervention. Planning an interventional approach from diagnostic imaging alone remains a significant clinical challenge. Transesophageal echocardiography (TEE) is the primary imaging modality used diagnostically, it has limitations in image quality and field-of-view. Recently, developments have been made towards modelling patient-specific deformable mitral valves from TEE imaging, however, a major barrier to producing accurate valve models is the need to derive the leaflet geometry through segmentation of diagnostic TEE imaging. This work explores the development of volume compounding and automated image analysis to more accurately and quickly capture the relevant valve geometry needed to produce patient-specific mitral valve models.

Volume compounding enables multiple ultrasound acquisitions from different orientations and locations to be aligned and blended to form a single volume with improved resolution and field-of-view. A series of overlapping transgastric views are acquired that are then registered together with the standard en-face image and are combined using a blending function. The resulting compounded ultrasound volumes allow the visualization of a wider range of anatomical features within the left heart, enhancing the capabilities of a standard TEE probe.

In this thesis, I first describe a semi-automatic segmentation algorithm based on active contours designed to produce segmentations from end-diastole suitable for deriving 3D printable molds. Subsequently I describe the development of DeepMitral, a fully automatic segmentation pipeline which leverages deep learning to produce very accurate segmentations with a runtime of less than ten seconds. DeepMitral is the first reported method using convolutional neural networks (CNNs) on 3D TEE for mitral valve segmentations. The results demonstrate very

accurate leaflet segmentations, and a reduction in the time and complexity to produce a patient-specific mitral valve replica. Finally, a real-time annulus tracking system using CNNs to predict the annulus coordinates in the spatial frequency domain was developed. This method facilitates the use of mitral annulus tracking in real-time guidance systems, and further simplifies mitral valve modelling through the automatic detection of the annulus, which is a key structure for valve quantification, and reproducing accurate leaflet dynamics.

Keywords: Mitral valve, ultrasound, transesophageal echocardiography, segmentation, volume compounding, deep learning, patient-specific modelling

Summary for Lay Audience

Three-dimensional ultrasound is widely used for obtaining images of the heart for both preoperative-diagnostic and intraoperative-guidance purposes. For surgical procedures targeting the mitral valve, which controls the flow of blood from the left atrium to the left ventricle, 3D ultrasound images are acquired from a probe inserted into the esophagus which provides clear 3D images of the mitral valve and surrounding tissues. Our objective is to develop and validate systems that leverage advanced image processing approaches to improve information from diagnostic ultrasound and use this information for training and planning interventions. Ultrasound imaging of the heart can show some features in a high level of detail, like the mitral valve, but is very limited in use for important structures that lay in the left-ventricle. I propose a workflow for acquiring and compounding, or stitching, multiple separate 3D images together to reconstruct a single image showing the entire left side of the heart in a process similar to a panoramic picture, enabling clinicians to better plan for procedures. Additionally, automatic image segmentation, or labelling, will be used in a workflow for creating patient-specific silicone replicas of the mitral valve, which surgeons can use to practice procedures and compare various approaches to aid in the planning process. This will have applications in both surgical planning, as well as training, by providing a platform for clinical users to practice and evaluate the successfulness of a procedure.

Co-Authorship Statement

This thesis integrates several publications that are published or in preparation for submission. Details regarding the author's contributions to these manuscripts are provided below.

Chapter 2

Reference: P. Carnahan, J. Moore, D. Bainbridge, E. C. S. Chen, and T. M. Peters, "Multi-view 3D transesophageal echocardiography registration and volume compounding for mitral valve procedure planning," *Applied Sciences*, vol. 12, p. 4562, Apr. 2022

Contributions: My contributions include conceptualization, methodology development, development of software, data curation, validation, data analysis and visualization, and manuscript preparation. John Moore assisted with conceptualization, validation, manuscript review and editing. Daniel Bainbridge contributed to project conceptualization, methodology, data collection and validation. Elvis Chen contributed to project conceptualization, methodology, manuscript review, and served in a supervisory role in the project. Terry Peters provided resources, funding acquisition, project administration, manuscript review and editing, and served in a supervisory role on the project. All authors reviewed and agreed to the published version of the manuscript.

Chapter 3

Reference: P. Carnahan, O. Ginty, J. Moore, A. Lasso, M. A. Jolley, C. Herz, M. Eskandari, D. Bainbridge, and T. M. Peters, "Interactive-Automatic Segmentation and Modelling of the Mitral Valve," in *Functional Imaging and Modeling of the Heart*, pp. 397–404, Springer International Publishing, June 2019

Contributions: My contributions include project conceptualization, methodology and design, development of software, data curation, validation, data analysis and visualization, and manuscript preparation. Olivia Ginty contributed to data curation, validation, and manuscript preparation. John Moore assisted with conceptualization, validation, manuscript review and editing. Andras Lasso, Mathew Jolley and Christian Herz contributed to the development of software for this project. Mehdi Eskandari contributed to data curation, validation and data analysis. Daniel Bainbridge contributed to project conceptualization, methodology, data collection and validation. Elvis Chen contributed to methodology, manuscript review and served in a supervisory role in the project. Terry Peters provided resources, funding acquisition, project administration, and contributed to project conceptualization, manuscript review and editing, and served in a supervisory role on the project. All authors reviewed and agreed to the published version of the manuscript.

Chapter 4

Reference: P. Carnahan, J. Moore, D. Bainbridge, M. Eskandari, E. C. S. Chen, and T. M. Peters, "DeepMitral: Fully automatic 3D echocardiography segmentation for patient specific mitral valve modelling," in *Medical Image Computing and Computer Assisted Intervention – MICCAI 2021*, pp. 459–468, Springer International Publishing, 2021

Contributions: My contributions include conceptualization, methodology, development of software, data curation, validation, data analysis and visualization, and manuscript preparation. John Moore assisted with conceptualization, validation, manuscript review and editing. Daniel Bainbridge and Mehdi Eskandari contributed to data collection and validation. Elvis Chen contributed to manuscript review and served in a supervisory role in the project. Terry Peters provided re-

sources, funding acquisition, project administration, manuscript review and editing, and served in a supervisory role on the project. All authors reviewed and agreed to the published version of the manuscript. This chapter includes expanded results beyond the initial originally published work. I have included recent results obtained after we expanded our dataset and released it as a public resource. This chapter includes both the originally published results, as well as updated results with additional data, compared against the original.

Chapter 5

Reference: P. K. Carnahan, A. Bharucha, M. Eskandari, D. Bainbridge, E. C. S. Chen, and T. M. Peters, "Real-time mitral annulus segmentation from 4D transesophageal echocardiography using deep learning regression," in *Medical Imaging 2023: Image Processing* (I. Išgum and O. Colliot, eds.), SPIE, Apr. 2023

Contributions: My contributions include conceptualization, methodology, development of software, data curation, validation, data analysis and visualization, and manuscript preparation. Apurva Bharucha, Daniel Bainbridge and Mehdi Eskandari contributed to data collection and validation of results. Elvis Chen contributed to manuscript review and served in a supervisory role in the project. Terry Peters provided resources, funding acquisition, project administration, manuscript review and editing, and served in a supervisory role on the project. All authors reviewed and agreed to the published version of the manuscript.

Acknowlegements

I am profoundly grateful to my supervisors, Dr. Terry Peters and Dr. Elvis Chen, whose guidance and unwavering support have been instrumental throughout my Ph.D. journey. Their expertise, encouragement, and dedication have shaped my research and enriched my academic experience. Thank you Terry and Elvis for providing me the opportunity to explore the field of biomedical engineering research. My experience as a fourth-year computer science student working with you has led me down the path that led me to pursue research and postgraduate education. Terry, your profound knowledge and insightful feedback have challenged me to think critically and pushed the boundaries of my research. Your mentorship has been invaluable, and I am deeply appreciative of the time and effort you invested in my academic and personal growth.

I would also like to thank John Moore for his patience and guidance during my time with the VASST lab. Your insight and assistance in so many of my research projects was invaluable. John first introduced me to the heart valve modelling project within the lab which formed the basis for all of my graduate research. I would also like to thank my clinical collaborators Dr. Daniel Bainbridge, Dr. Apurva Bharucha, and Dr. Mehdi Eskandari for their assistance and expertise. Apu and Mehdi have been invaluable for their clinical insight and hard work collecting and annotating patient cases. Dan Bainbridge provided the foundation for my work on volume compounding, and has been readily available to help with anything from providing clinical perspective to helping with ultrasound data collection. To my other advisory committee members, Dr. Roy Eagleson, Dr. David Hocking, Dr. Peter Wang, thank you for your time and your guidance throughout my graduate studies.

To all of the members of the VASST lab who I had the pleasure of working with —thank you for the amazing times, and for making my time in the lab so

memorable. Olivia, thank you for your time and patience while I got up to speed in the lab. Leah, Dan, Hareem, Shuwei and Joeana, thank you for all the good times and memories, you have all made the lab a fun place to be and a hard place to leave.

To my amazing wife Kaitlyn —thank you for your unwavering love and support. It wasn't always easy but I always knew you were there for me know matter what. I don't have the words to describe how much your love and encouragement have meant to me, and just know I could not have done this without you. I know you wouldn't forgive me if I didn't also mention our cats, Louie and Gus, who never fail to come cheer me up when I'm stressed, and on occasion tried to offer their input on my work by walking across my keyboard. Last but not least, thank you to my family for all of your love, support and encouragement. I would never have made it to where I am without you to guide me. Trish, you have always been there for me, and I couldn't have asked for a better older sister. To my mom Kelly, thank you for everything you've done for me, and you're unwavering support in everything I do. In memory of my father Dale, I miss you so much and I know you would have been so proud of me. Thank you for always being there to talk to, and for encouraging me and fostering my interest in programming and computer science. You were always and will always remain to be an inspiration to me.

This work has been supported by many sources of funding, including the National Science and Engineering Council, Canadian Institute of Health Research, and Canadian Foundation for Innovation. Over the years, I have received scholarship funding from the Natural Science and Engineering Research Council and Ontario Graduate Scholarship Program.

Contents

List of Figures

List of Tables

List of Appendices

List of Abbreviations

1D One Dimensional 34, 35

2D Two Dimensional 10, 11, 20, 23, 31, 42, 60, 63

3D Three Dimensional 4, 10, 11, 13, 14, 19, 20, 22, 23, 28–32, 34–36, 38, 42, 43, 45, 47–51, 54–57, 59–61, 63, 68, 69, 71, 73–75, 77–79, 83–85, 87, 89–91

4D Four Dimensional 72, 78

AV Aortic Valve 1

BP Blood Pool 50, 51

CMR Cardiac Magnetic Resonance Imaging 9–12, 43, 87

CNN Convolutional Neural Network 22, 23, 60, 69, 74, 77, 85, 89–91

CPU Central Processing Unit 66, 67, 82

CT Computed Tomography 9–12, 25, 26, 38, 40, 42–45, 87, 88

ECG Electrocardiogram 11, 20, 32

FEM Finite Element Model 13

FFT Fast Fourier Transform 78, 79, 83, 84

GPU Graphics Processing Unit 43, 66, 67, 82, 83, 91

IGS Image Guided Surgery 24, 76

LA Left Atrium 2, 6, 10

LV Left Ventricle 2, 5, 6, 10, 15, 26, 42, 88

LVOT Left Ventricular Outflow Tract 7, 30, 88

MASD Mean Absolute Surface Distance 53, 54, 65, 66, 69

MV Mitral Valve 1–3, 6, 7, 9, 11–13, 15, 16, 18, 19, 31, 48, 52, 56, 75, 82

NCC Normalized Cross-correlation 33, 34

PM Papillary Muscle 3, 5

PV Pulmonary Valve 1

TEE Transesophageal Echocardiography 10, 14, 15, 17–19, 22–27, 29–33, 37–39, 41–45, 47, 49, 50, 54, 56, 59–61, 63, 68, 69, 71–75, 78, 87–91

TTE Transthoracic Echocardiography 10, 17

TV Tricuspid Valve 1

US Ultrasound 16–18, 37

Chapter 1

Introduction

1.1 Cardiology

The heart serves as the circulatory system's pump, facilitating the transportation of oxygen, nutrients, and metabolic waste throughout the entire body. Located in the thorax alongside the lung, this organ is approximately the size of a clenched fist. It is divided into two halves, the left and right side, each consisting of an atrium and a ventricle, as well as two valves apiece.

During the cardiac cycle, the myocardial muscle exerts the primary force required to propel blood out of the ventricles and into the great vessels, namely the aorta and pulmonary artery. In contrast, the atria play a relatively passive role, exerting minimal force and primarily receiving blood from the veins before it enters the ventricles.

Embedded within the fibrous cardiac skeleton, the valves ensure one-way blood flow during normal, non-diseased functioning. The heart is divided by four distinct valves. The mitral valve (MV) and tricuspid valve (TV) separate the atria from the ventricles, and are referred to as atrioventricular valves. Additionally, the aortic valve (AV) and pulmonary valve (PV) lie between the ventricles and the

great vessels. Due to their leaflet shape, they are also referred to as semilunar valves.

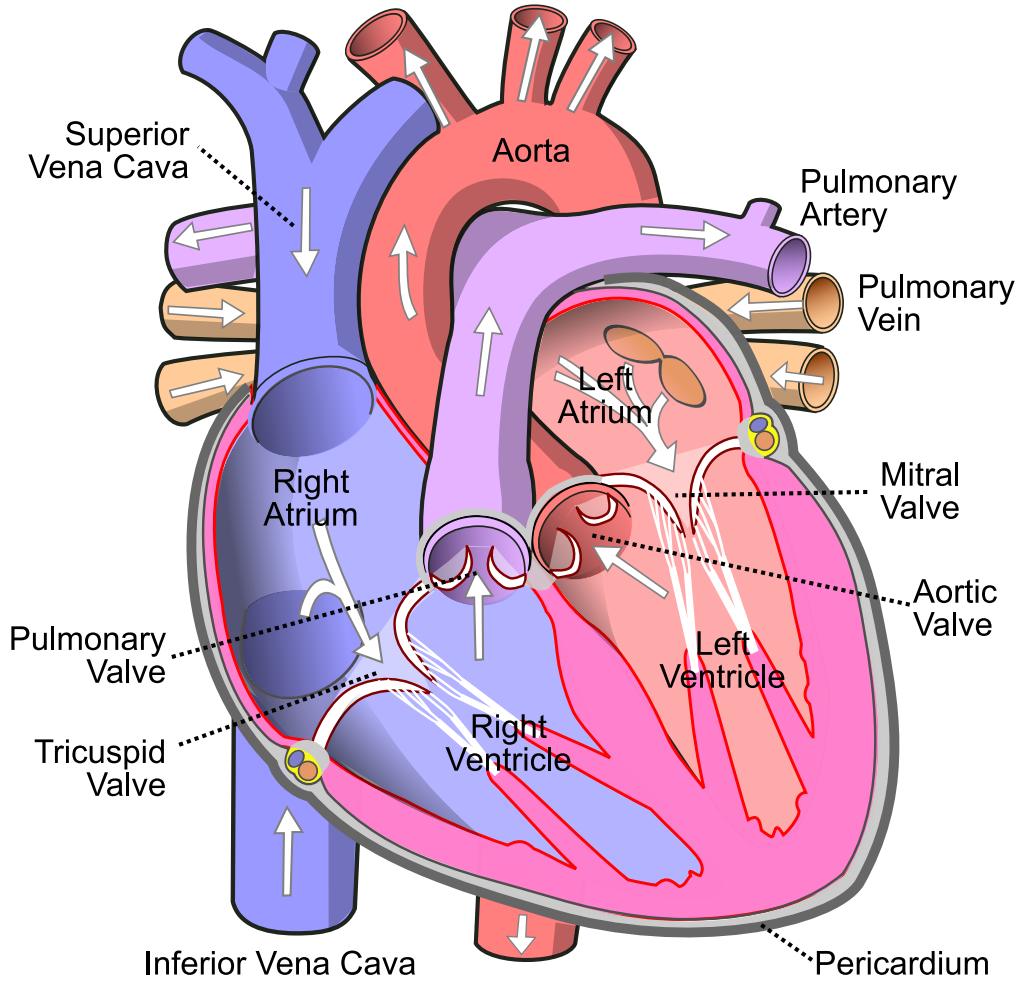

Figure 1.1: Illustration of the cross-sectional view of the heart with common anatomical features and blood flow directionality. Credit: Eric Pierce, 2006, Wikimedia Commons (CC BY SA 2.0).

1.1.1 Mitral Valve Anatomy

Leaflets

The MV separates the left atrium (LA) from the left ventricle (LV), and opens at diastole to allow the LV to fill, and closes at systole to prevent back-flow into the LA. The MV consists of two distinct leaflets that are attached to the atrioventricular

junction, supported by tendinous chords and connected to the papillary muscles (PMs). Clinicians commonly refer to these leaflets as the anterior and posterior leaflets due to their noticeable structural differences [5]. The two leaflets are composed of multiple thin layers of fibrous tissue, with a total thickness of approximately 1mm. They are anchored to the endocardial wall through the annulus, while the opposite end is known as the free edge [6].

The anterior leaflet exhibits a semi-circular shape and occupies about two-fifths of the annulus, while the posterior leaflet has a quadrangular shape and covers the remaining three-fifths of the annulus. The anterior leaflet is approximately twice as long, measured from the annulus to its free edge, compared to the posterior leaflet. At the junction where both leaflets meet, there are anterior and posterior commissures. These commissures are positioned a few millimeters away from the annulus and are located approximately above the corresponding papillary muscles. The posterior leaflet features two additional indentations along the free edge, which become visible during diastole when the MV opens. These indentations divide the leaflet into three scallops, known as P1, P2, and P3. Similarly, the corresponding segments on the anterior leaflet are labeled as A1, A2, and A3, as shown in Figure 1.2.

Above the free edge lies the coaptation zone, where both leaflets come into contact with each other during systole when the valve is closed. This area is typically rougher and irregularly thicker due to the insertion points of the chordae tendineae, in contrast to the rest of the leaflet.

The size of the coaptation area is generally associated with the effectiveness of mitral valve closure, and several studies have examined its correlation with surgical success rates [7, 8]. However, due to its relatively small size, polymorphic appearance, susceptibility to image artifacts, and potential confusion with chords, accurately quantifying the coaptation area from imaging data can be challenging.

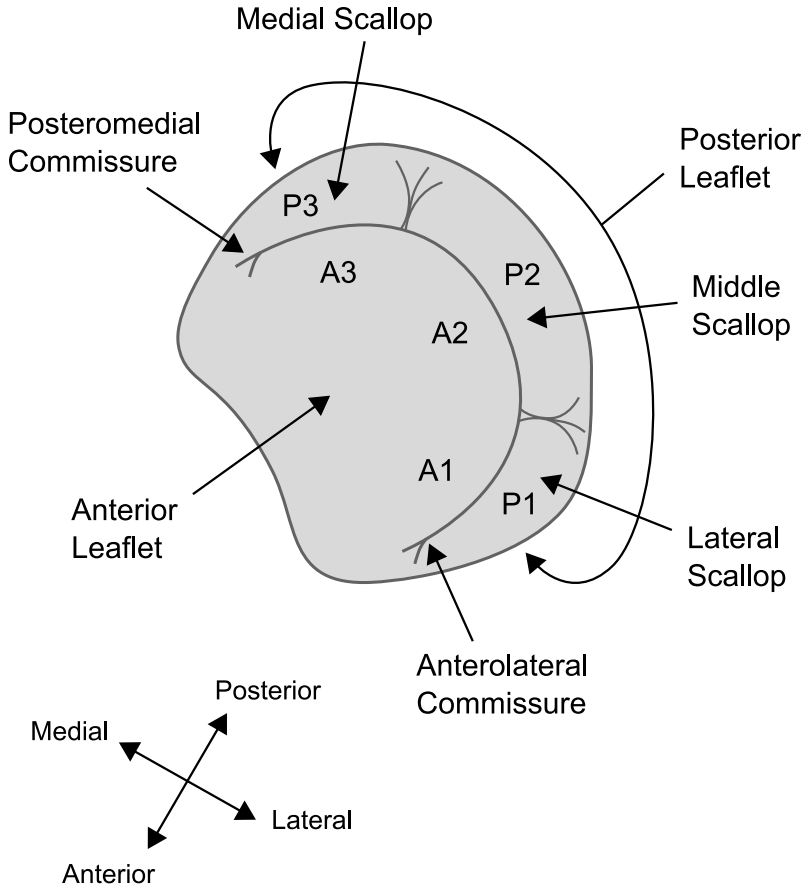

Figure 1.2: Illustration of the en-face view of the mitral valve with labelled leaflets. Credit: CardioNetworks, 2010, echopedia.org (CC BY SA 3.0).

Annulus

The mitral annulus is a D-shaped structure with a three dimensional (3D) contour that connects the leaflets to the endocardium. It is not planar and exhibits a prominent elevation between the trigones towards the atrioventricular region, resembling a saddle shape. The annulus incorporates several structures along its hinge point. The aortic valve is connected through fibrous continuity with the aortic mitral leaflet (anterior) and the right and left fibrous trigones [9]. This specific area of the annulus is primarily composed of fibrous tissue, making it less susceptible to dilatation. However, beyond this region, the remaining two-thirds of the annulus consist mainly of muscular tissue. In cases of significant mitral regurgi-

tation, it is common to observe dilation in this muscular portion of the annulus, as well as an increased likelihood of calcification [5].

Chordae Tendinae and Papillary Muscles

In a normal valve configuration, the leaflets are supported by fan-shaped chords that originate from the papillary muscles and insert into the leaflets. Depending on their attachment points, there are three types of chordae tendinae. The primary chords connect to the free edge of the rough zone present in both leaflets. Secondary chords attach to the ventricular surface within the rough zone, which corresponds to the body of the leaflet. Tertiary chords are exclusive to the mural (posterior) leaflet, which includes a basal zone, and directly attach to the ventricular wall [10].

The posteromedial PM contributes chords to the medial half of both leaflets, including the posteromedial commissure, P3, A3, and half of P2 and A2. Similarly, the anterolateral PM provides chords that attach to the lateral half of the mitral valve leaflets, specifically the anterolateral commissure, A1, P1, and half of P2 and A2. Within the secondary chords of the aortic (anterior) leaflet, two particular chords stand out as the largest and thickest. Referred to as strut cords, they originate from the tip of each papillary muscle and are considered to be the strongest.

The PM bundles are typically categorized as anterolateral and posteromedial, and they are situated along the mid to apical segments of the LV. The anterolateral PM is commonly observed to attach at the border between the anterolateral (lateral) and inferolateral (posterior) walls, while the posteromedial PM is located over the inferior wall of the LV. In most adults, the PM can consist of up to three heads, however, this distribution can vary significantly [11].

1.1.2 Mitral Valve Pathology

Heart valve disease generally presents as either stenosis, where the valve is restricted, or regurgitation, where the valve does not properly close and thus blood leaks back into the LA, or a combination of both [12]. Mitral stenosis arises primarily from post-inflammatory or rheumatic diseases, as well as congenital abnormalities. Valve area decreases from a typical measurement of around $4.0\,\mathrm{cm}^2$ to $1.0\,\mathrm{cm}^2$ or less, leading to elevated LA pressure and subsequent secondary pulmonary hypertension and right heart failure [13]. Conversely, a multitude of structural irregularities affecting the components of the mitral valve can lead to mitral regurgitation. Enlargement of the LA, annulus, or LV; alteration of leaflets and chordae due to myxoid transformation; as well as various modifications in the leaflets or papillary muscles can induce leakage in the mitral valve [14]. Mitral regurgitation can be classified as either primary regurgitation (an abnormality of the valve itself), or secondary regurgitation (an abnormality of the LV).

1.1.3 Valve Interventions

Surgical intervention is the most common therapeutic approach for patients with MV disease. Treatment options include tissue-preserving repair, or complete valve replacement, with the former being favored due to its association with more favorable long-term outcomes [15, 16]. Both repair and replacement are performed as open surgery requiring bypass, as well as minimally invasive approaches including port access and trans-catheter interventions [17]. Minimally invasive interventions are preferred where possible due to reduced recovery time, fewer blood transfusions and fewer septic complications [18]. However, minimally invasive procedures introduce a greater demand for training and imaging due to reduced access and surgeon vision [19].

Mitral valve replacement involves the surgical implantation of mechanical

prostheses, which necessitates the administration of anti-coagulation medication to counteract antibody attacks and the formation of blood clots [20]. Valve replacement requires careful consideration of subsequent restriction of the left ventricular outflow tract (LVOT), as well as potential migration or malposition of the implanted valve.

Mitral valve repair interventions aim to leave the existing valve in place and address the specific pathology causing regurgitation or stenosis. As such, valve repair includes a variety of techniques including annuloplasty rings, valve resection, leaflet clips and artificial chordae devices [21]. Annuloplasty rings are sutured into the MV annulus, with the aim of reducing the size of the valve opening to improve leaflet closure. The majority of patients undergoing valve repair will receive an annuloplasty ring in addition to other repair techniques [22].

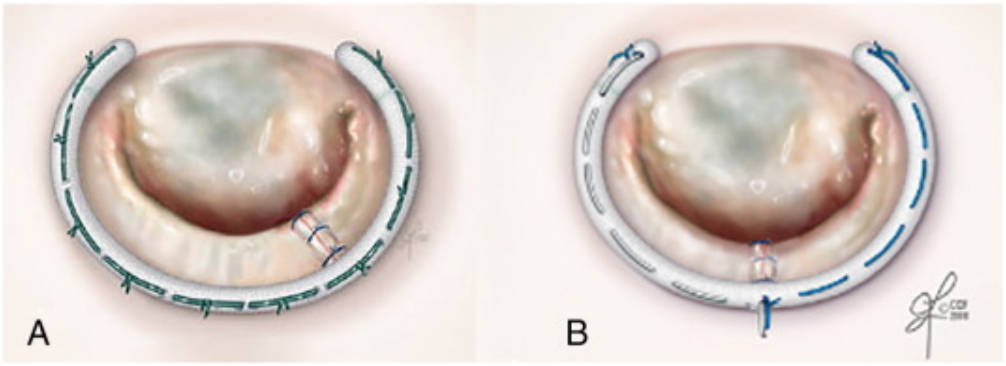

Figure 1.3: Examples of the annuloplasty ring on the mitral valve using a running suture technique (a), and an interrupted technique (b). Reproduced from Marin Cuartas *et al.* [23] (CC BY-NC-ND 4.0).

Triangular resection of the leaflet is commonly performed in cases of leaflet prolapse, and more recently has seen use in cases of degenerative disease [24]. In leaflet resection, a section of the leaflet is cut away, and the remaining leaflet is sutured together, addressing regurgitation caused by excess leaflet tissue. Leaflet resection is most commonly applied to the anterior leaflet, however can also be used on the posterior leaflet. Edge-to-edge, or Alfieri [25], repair is performed by

tethering the anterior and posterior leaflet edges to reduce the opening of the valve and limit regurgitation. Traditionally, using the Alfieri method, sutures were used to join the leaflets together, however, studies have indicated prevalence of mitral regurgitation after repair, suggesting additional techniques are needed [26]. More recently, devices such as the MitraClip (Abbott Laboratories, Abbott Park, IL, USA) have been introduced to simplify procedures. The MitraClip simulates edge-to-edge surgical technique by clipping the leaflets together instead of suturing [27].

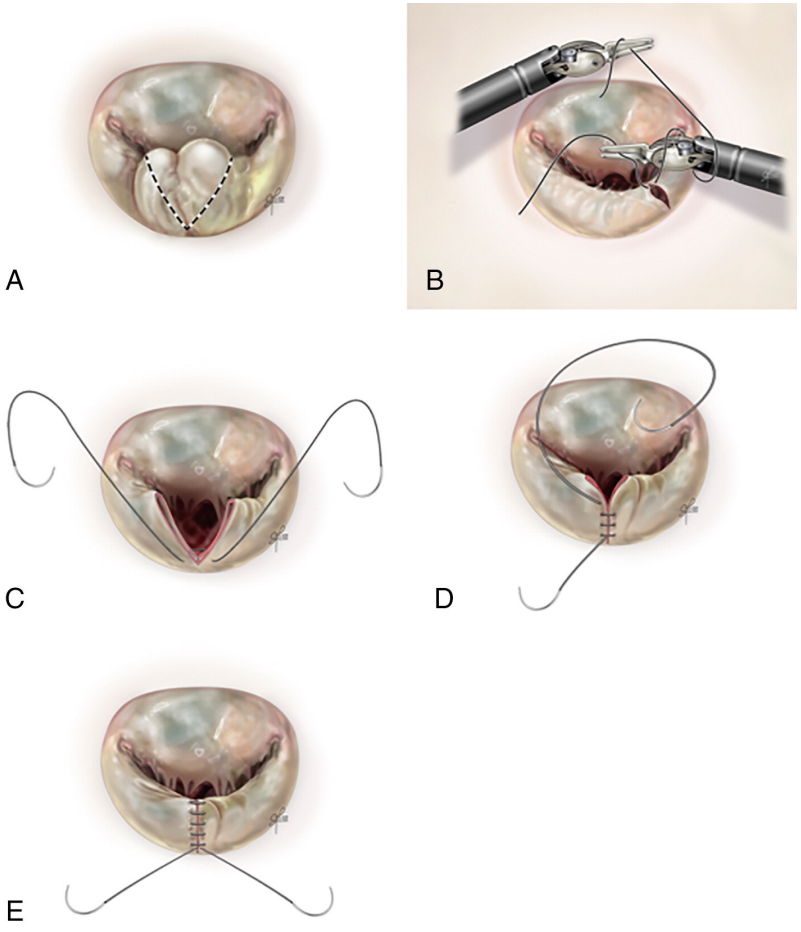

Figure 1.4: Example of posterior leaflet triangular resection. A: triangular resection of the posterior leaflet; B: posterior leaflet repair using running technique; C: repair of the posterior leaflet using ventricularization technique; D: running closure of the posterior defect; E: final stitch next to the annulus. Reproduced from Marin Cuartas *et al.* [23] (CC BY-NC-ND 4.0).

Artificial chordae can be implanted to address prolapse while preserving tissue,

in contrast to resection. This is often used when prolapse is caused by a ruptured chord. Expanded polytetrafluoroethylene sutures have been in use for artificial chordae since 1985, with the sutures being passed through the papillary muscle and leaflet to create varying chord structures [28]. More recently, minimally invasive chord implantation has been enabled by devices such as the NeoChord Artificial Chordae Delivery System (NeoChord, Inc., St. Louis Park, MN, USA), in which the device attaches to the leaflet in a beating heart, and allows the suture to be pulled down and anchored to the papillary muscle [29]. This allows for artificial chordae implantation without the need for pulmonary bypass, however places a much greater demand on interventional imaging for guidance.

Mitral stenosis can be treated by balloon valvuloplasty, and this is the preferred method of treatment due to preservation of the subvalvular apparatus and left ventricular geometry [30, 31]. Balloon valvuloplasty is performed by guiding a catheter to the valve, inflating a balloon to widen the valve opening, then deflating the balloon and removing the catheter. In cases where balloon valvuloplasty is not possible due to calcification, significant regurgitation, and severe chronic symptoms, patients will instead undergo valve replacement [30].

It is often unclear whether MV surgery, transcatheter repair, or ongoing medical therapy is the best option for specific patients from diagnostic imaging. Thus, choosing the treatment approach, or combination of approaches for an individual patient remains one of the largest clinical challenges in MV therapy [32].

1.2 Imaging the Mitral Valve

Accurate and clear imaging of the mitral valve is important for intervention planning, as well as intra-operative guidance. The mitral valve can be imaged using cardiac computed tomography (CT), cardiac magnetic resonance imaging (CMR),

and ultrasound, with ultrasound being the primary imaging modality used both preoperatively and intraoperatively [33].

1.2.1 Echocardiography

The mitral valve can be imaged using both transthoracic echocardiography (TTE), and transesophageal echocardiography (TEE). The primary form of ultrasound used is 3D TEE, which enables real-time imaging of the valve using B-mode imaging. Additionally, Doppler echocardiography is used for diagnostic purposes by measuring blood flow to identify stenotic or regurgitant valves. Ultrasound probes for 3D TEE imaging consist of a two dimensional (2D) phased-array transducer at the tip of a tube similar to that of an endoscope, with a handle to adjust the angle of the probe tip. The phased-array transducer enables real-time 3D ultrasound to be acquired. The TEE probe is extended down the esophagus with the patient under general anesthesia, with typical images being acquired from the mid-esophageal position, however, the probe can be extended further to acquire views from a trans-gastric position as well[34].

Mitral anatomy derived from 3D TEE correlates well with findings during open heart surgery [33]. Key views acquired using TTE imaging include the 2D short-axis and 2D long-axis views. Combined, these provide imaging of the LV and mitral leaflets, and enable measurement of LA and LV dimensions for deriving clinical measures such as stroke volume [36]. The typical view acquired with 3D TEE is the surgical, or *en-face* view, which captures the mitral valve from behind the LA with the probe in a mid-esophageal position.

1.2.2 Computed Tomography and Magnetic Resonance Imaging

Developments in cardiac CT and CMR have led to their increased use in valve imaging. CMR delivers high quality soft tissue contrast and flow measurements,

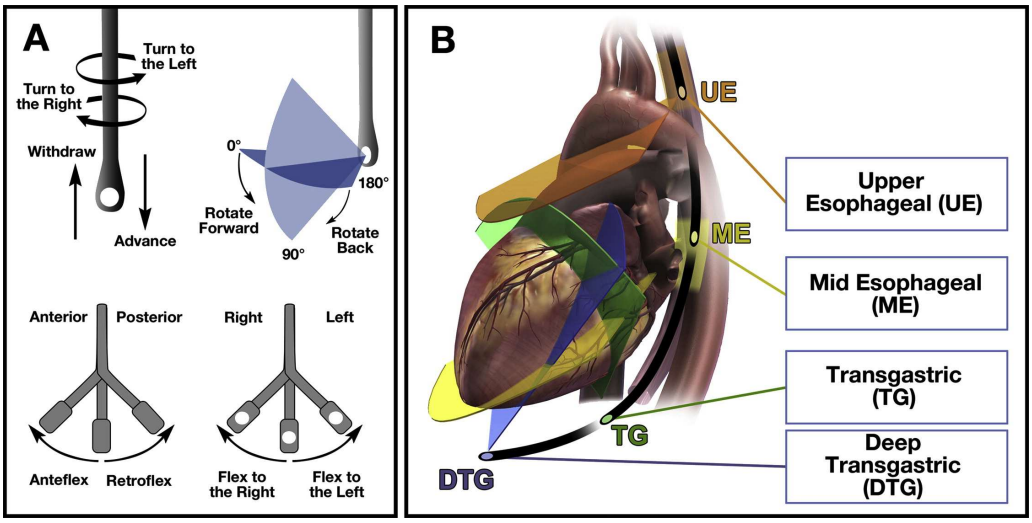

Figure 1.5: Terminology used to describe manipulation of the transesophageal echocardiographic probe during image acquisition. (A) Terminology used for the manipulation of the transesophageal echocardiographic probe. (B) Four standard transducer positions within the esophagus and stomach and the associated imaging planes. Reproduced with permission from Hahn *et al.* [35].

and has emerged as an adjunct to primary echocardiographic analysis [37]. However, CMR at this time is typically limited to 2D plus time slices, and is therefore not able to capture the complex 3D geometry of heart valves. The feasibility of CMR for use in planning MV interventions and predicting their success has not yet been demonstrated [38].

Advances in cardiac CT have enabled its wider use in pre-operative imaging of the mitral valve. Cardiac CT techniques use retrospective electrocardiogram (ECG) gating to acquire 3D plus time volumes with very high spatial resolution. Cardiac CT is used as a secondary imaging technique with patients being refered only when initial echocardiography assessment is deemed insufficient or inconclusive [33]. The use of CT is most common for valve replacement procedures where planning requires quantitative assessment to determine implant size, as well as to avoid impairment of the aortic valve. Recommendations for cardiac CT imaging suggest a heart rate of 60bpm or lower [39]. Additionally, the heart rate needs to

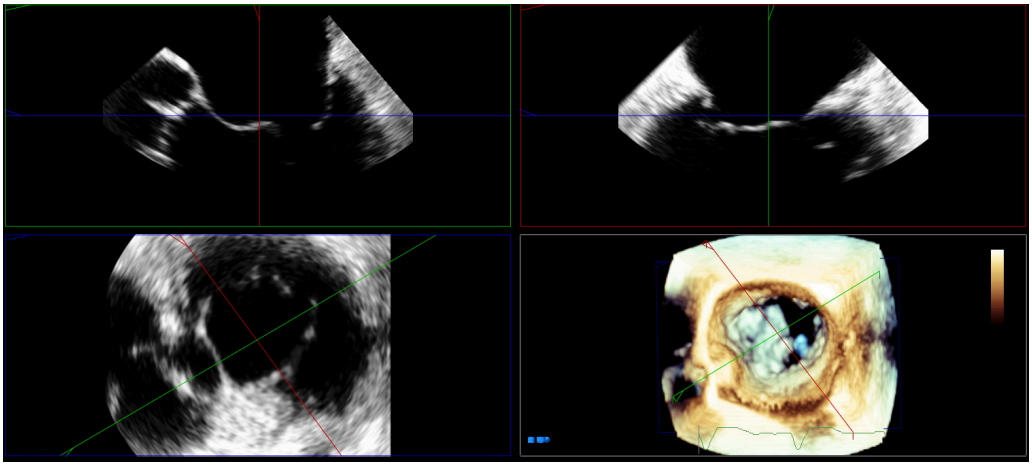

Figure 1.6: Example of en-face view of the mitral valve captured with a 3D TEE probe in the mid-esophageal position. Cross-sectional views include the anterior-posterior (top-left), commissure-commissure (top-right) and axial (bottom-left). Also shown is the 3D volume rendered view (bottom-right).

be regular to avoid misalignment artefacts [40]. The use of cardiac CT for valve repair planning is still under investigation and not formally recommended [36].

While future developments in CT and CMR may see their increased use for MV interventions, at this time echocardiography remains the standard-of-care diagnostic imaging approach used for patients [33].

1.3 Patient Specific Valve Modelling

Models of the mitral valve have long been of interest for investigating valve function, developing therapeutic devices, surgical training, and procedure planning. Porcine models have been used as an analogue for the human heart as they exhibit very similar anatomy and function [41]. Evaluation of artificial valves and research into the efficacy of repair techniques could be done using live animal models, however, running these studies can prove costly and time-consuming. Excised porcine valves have been used in conjunction with heart simulator devices to enable ex-vivo study [42]. As an alternative to porcine models, patient-specific modelling

has emerged to enable the study of valve function for an individual patient based on models derived from imaging. Various approaches have been demonstrated including computational models, static 3D printed models, and dynamic physical models with heart simulators [43, 44, 45].

1.3.1 Computational Models

Several research groups have explored the possibilities of in-silico modelling of MV mechanics, often utilizing finite element models (FEMs). Computational modelling studies have typically employed idealized geometries derived from mathematical models, or personalized geometries with limited clinical datasets [46, 43, 47]. The overarching goal has been to understand the significance of realistic material models and properties [48, 49, 50, 51], as well as the geometry of the annulus and subvalvular apparatus, concerning valve competence [52]. The overall goal of this area of research is to enable predicting the effects of therapy in advance and to obtain a better understanding of MV physiology with the goal of optimizing therapies. Several studies have been performed specifically modelling annuloplasty [53, 54], edge-to-edge repair [53, 55, 56] and MitraClip [57].

While computational modelling demonstrates promise in understanding valve behaviour and develop improved therapies, their use in surgical training is limited by the lack of physical interaction with the model. Surgical simulation using entirely virtual models has been demonstrated using haptic feedback devices, however the efficacy of these simulation systems is yet unclear [58].

1.3.2 Static Physical Models

Static 3D-printed replicas offer haptic and spatial appreciation of complex anatomy for both surgical training and procedure planning. Static valve replicas have been produced as direct-printed rigid models, as well as flexible models created using

3D-printed molds. Static models have been validated to demonstrate accurate replication of annular and leaflet geometry against native tissue evaluated intra-operatively [44, 59]. Rigid models of the mitral valve are primarily targeted at understanding the complex geometry of the valve structure. However, due to their rigid nature, they are of limited use for understanding the valve under dynamic conditions. Soft models made from silicone enable the simulation of surgical repair techniques. Nia *et al.* [60] were able to simulate the prospective surgical repair of a P2 prolapse within a static benchtop simulator using a deformable patient-specific mitral replica derived from 3D TEE. This work was subsequently followed by a successful real-life surgical repair matching the simulated procedure. Similarly, Yang *et al.* [61] showed correlation between morphological and mitral dimensions obtained on patient-specific silicone replicas and those obtained intra-operatively. The authors also found morphological parameters such as coaptation depth and leaflet/annulus ratio in repaired replicas to be associated with residual post operative mitral regurgitation therefore suggesting that these replicas can not only be used for procedural planning but also modelling post-repair outcomes.

Static mitral valve replicas derived from patient TEE imaging have been demonstrated to accurately reflect the geometry of the valve. Silicone valve replicas offer a platform for surgical simulation by enabling repair techniques to be practiced on a valve replica. However, there is no standardized approach for segmenting the valve geometry, 3D printing the valve replica or mold, and manufacturing valves, limiting the potential for translation of modelling work. Furthermore, static models are limited to interaction with a stationary valve, and valve function under dynamic conditions cannot be evaluated.

1.3.3 Dynamic Physical Models

Evidence indicates the volume of MV repair cases that a surgeon performs is a determinant not only of successful mitral repair rates, but also freedom from re-operation and patient survival [62, 63]. Current training for MV repair is limited to operating room observation, however, recent studies challenge this conventional approach and suggest introducing simulation as a way of ensuring resident's exposure to rare cases and high-risk procedures without compromising patient safety [64, 65].

Originally developed as an alternative to the use of live animal (porcine) models of the LV and mitral/aortic valves for testing new interventional procedures, heart simulator technology has been adopted widely by both industry for evaluation of technologies for imaging heart valves [66], and academia for the assessment of modelled heart valves [67]. Heart simulators enable the evaluation of dynamic valve replicas in hemodynamic environments. Dynamic patient-specific valve replicas created from patient TEE images have proven useful in surgical planning for specific cases [68]. Dynamic valve replicas extend the capability of static silicone replicas by enabling the performed repair to be tested in a heart-simulator and evaluated for residual regurgitation. As a tool for procedure planning, this would enable various repair approaches to be tested pre-operatively to select the surgical approach with the highest chance of success. Furthermore, for surgical training the impact of various simulated repairs can be directly seen in the heart-simulator.

Producing patient specific valve models requires extracting the valve geometry from image data. This is an application for automated valve segmentation from TEE volumes, as manual segmentation is a highly time consuming process. Existing segmentation algorithms have not been tailored for valve modelling, and have several drawbacks due to a different focus. As such, there is a need for im-

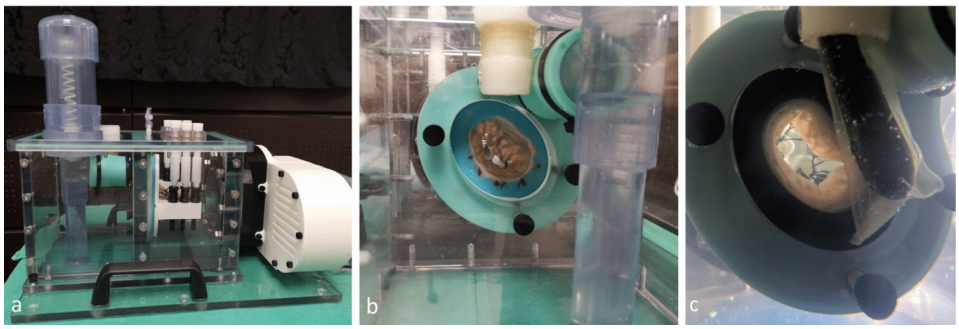

Figure 1.7: The Mitral Valve Simulator pulse duplicator. A: side view showing (from left) atrial reservoir/low pressure chamber with aortic outflow tower, left ventricle/high-pressure chamber with mounted valve assembly, and motor assembly; B: end view with TEE access port (top centre), and valve in place; C: closer end view with the TEE probe in place and chordae and papillary posts visible through the valve. Reproduced with permission from Ginty *et al.* [68].

proved segmentation specifically for patient-specific modelling, which is the focus of chapters three and four in this thesis.

1.4 Echocardiography Image Processing

Various image processing techniques can be applied to echocardiography volumes to enhance the clinical utility of standard imaging, as well as to automate measurement and quantification steps. Volume compounding approaches have been applied to ultrasound (US) imaging to improve image resolution and field-of-view, and show promise for use in cardiac imaging. Automatic segmentation of various anatomical regions of the MV apparatus can aid deriving quantitative measurements, and are a critical step in valve modelling applications.

1.4.1 Volume Compounding

Ultrasound compounding, or mosaicing, is the process of combining multiple seperate acquisitions into a single volume. This strategy has been proposed by several groups to address limitations of 3D ultrasound and improve imaging capa-

bility. By registering and blending together adjacent acquisitions from different poses, we can expand the field of view and address the issue of signal dropout, producing higher quality images with greater information for the clinician. Many US probes use stitching techniques to produce wider field-of-view volumes from a stationary position using an approach called elevational spatial compounding [69]. Additionally, several image compounding techniques have been proposed to register a set of ultrasound volumes acquired from different poses, all of which demonstrate improved image quality and provide an avenue for combining common cardiac ultrasound views into a single volume with reduced noise, reduced speckle, and fewer signal dropout artefacts[69]. Researchers have demonstrated 3D ultrasound compounding techniques with applications in cardiac, fetal and breast imaging [70, 71, 72].

Spatial compounding of cardiac US volumes has been demonstrated using TTE imaging, both with and without the use of external tracking. External tracking systems reduce the demand for image registration, as the pose of each acquisition is known. Image registration is only used for fine alignment in this case, however the requirement for incorporating a tracking system can be a limitation for clinical use. Tracker-less compounding relies entirely on registration to align the separate acquisitions, and can be less robust as a higher degree of overlap is required between images to successfully align them. The resulting volumes using spatial compounding demonstrate overall improved imaging. Although there is greater freedom of movement of the probe with TTE imaging, due to the presence of the ribcage and lungs the number of positions from which the heart can be imaged is limited, and structures at the back of the heart are challenging to view even with spatial compounding. In contrast, the use of spatial compounding of TEE volumes has been limited [73]. The range of motion of the probe is highly constrained in TEE, and is mainly limited to mid-esophageal and trans-gastric views of the heart. These

two probe positions are nearly orthogonal, and as such are a promising application of spatial compounding since a major limitation of TEE imaging is capturing structures parallel to the US beam.

1.4.2 Valve Segmentation

Valve segmentation is an important step for quantification of valve parameters, and patient-specific modelling applications. The rapid motion and considerable anatomical complexity of the MV are a challenge for precise image-based modeling. Quantification of the mitral valve is important for surgical planning, with key clinical measurements serving as indicators for repair complexity [74]. Common clinical measurements of interest for the mitral valve include annular diameter in the commisure-commisure and anterior-posterior axes, number of scallops on the leaflet, leaflet area, leaflet length and chordae length [75, 76, 77].

Beyond valve quantification for surgical measurements, accurate segmentation of the valve apparatus is a critical step for mitral valve modelling applications. Computational, static, and dynamic valve modelling all require accurate and consistent segmentation from patient image data. Traditionally, valve segmentation was done manually, however, this is a very laborious process and is subject to inter-user variability. Various semi-automatic and fully-automatic approaches have thus been developed with the goal for streamlining segmentation of the mitral valve.

Manual Segmentation

Manual segmentation of the mitral valve from TEE is a highly labor intensive task, often taking upwards of one hour to complete a single segmentation. Tools for performing manual segmentation often have several built-in functions to speed up the process, but general segmentation must be performed in a slice-by-slice

fashion. This is both time consuming, and can lead to in-continuities between adjacent slices and consequently a poor quality segmentation. Manual segmentation of the mitral valve has been shown to have high inter and intra-user variability due to the need for interpretation of unclear imaging, and difficulties capturing the 3D geometry. A study by Jassar *et al.* [78] reported inter-user variability using a surface distance metric ranging from 0.60 ± 0.17 mm to 2.38 ± 0.76 mm on different cases. Additionally, they report intra-operator variability on repeated acquisitions ranging from 0.46 ± 0.21 mm to 1.45 ± 0.62 mm. Due to the time requirements and variability in manual segmentation, there is a demonstrated need for automated approaches which can produce fast, robust and consistent results.

Semi-automatic Segmentation

Various semi-automatic approaches have been proposed in literature and industry to address the limitations of manual MV segmentation and assessment. Semi-automated approaches require some form of user input, often as a manual initialization that is further refined in an automated fashion. Semi-automated approaches can also be interactive, keeping the user in the loop as the segmentation is refined.

Burlina *et al.* [79] proposed an interactive approach which first delineates the entire left heart endocardial wall including the MV from 3D TEE images using active contours. Active contours are based on level-sets, and iteratively refine a segmentation contour based on an objective function often based on image gradients to detect edges. Following initial active-contour segmentation, thin tissue detection is used to identify the mitral leaflets. Thin tissue detection algorithms use an image filter that responds to opposing image gradients, leading to a stronger response in areas with thin structures such as the mitral leaflets. The motivation of the work of Burlina *et al.* was for personalized computational modelling, how-

ever, segmentation accuracy and runtime as well as size of the dataset have not been reported.

Schneider *et al*. [80] proposed in a series of publications a semi-automatic approach based on deformable modelling of the leaflets. This work aimed to produce segmentations over 3D plus time data, including the whole cardiac cycle. The approach consisted of several steps in a pipeline, beginning with annulus detection and tracking, segmentation of the annulus at diastole, and leaflet motion estimation with a deformable model [80, 81]. For automated annulus segmentation, the annulus plane was estimated using a least-squares fit through a thin tissue detector response. Then graph cuts are used to estimate the annulus and refined using active contour. The annulus is tracked throughout the cardiac cycle using optical flow tracking. Finally the leaflets are segmented in diastolic frames from several 2D planes rotated around the annulus normal and center, again using a combination of thin tissue detectors and graph cuts. Schneider *et al*. reported surface error of 0.8 mm on a dataset of fifteen patients. However, this method only represents the mitral leaflets as a single medial surface, rather than structures with thickness.

Commercial solutions implementing semi-automaic approaches are available, such as TomTec's 4D MV-Assesment tool (Tomtec Inc, Hamden, CT, USA), and Phlips' QLAB Mitral Valve Navigator tool with anatomic intelligence (Philips Healthcare, Andover, MA, USA). TomTec's solution automatically tracks manual delineations of the valve using optical flow through systolic frames only [75]. Philips Mitral Valve Navigator tool automatically selects the end-systolic frame based on the ECG waveform. Then the image is aligned by the user to a template guided by a schematic illustration. Finally, several key points are automatically placed by the software defining the annulus curve and leaflet coaptation. These points are then manually refined by the user. This tool was validated on fifty-two patient cases against manual segmentation and was demonstrated to have

good agreement with the manual ground-truth, as well as improving intra- and inter-user variability while reducing segmentation time [82].

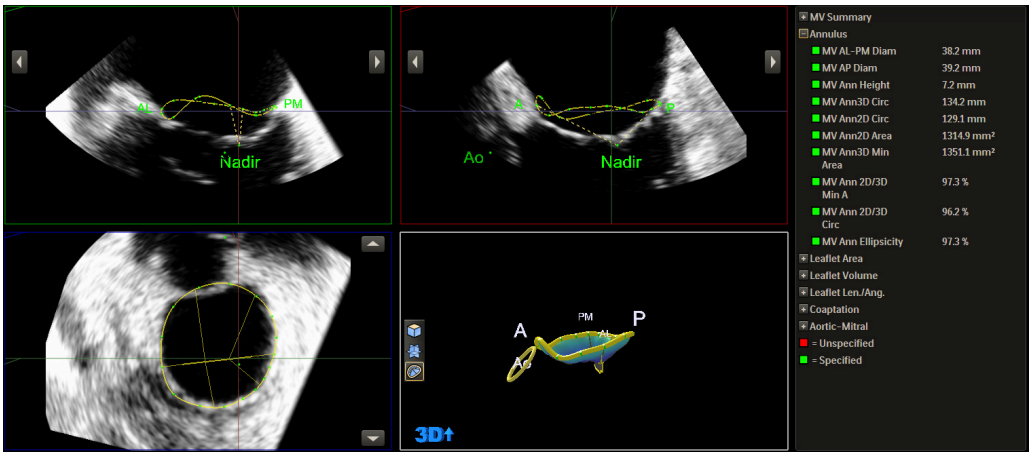

Figure 1.8: Philips Mitral Valve Navigator tool in the QLAB software package. Shown are the automatically placed key points, and the computed mitral annulus and leaflets. Derived measurements are shown in the panel on the right.

Semi-automated methods have shown promise in reducing time and improving reproducible in mitral valve segmentations. However, these methods can still introduce inter-user variability, and require varying levels of manual intervention to use. This limits the reduction in time possible with semi-automatic segmentations.

Fully Automatic Segmentation

Several fully automatic segmentation methods have been proposed with the goal of eliminating the need for manual initialization or adjustment, further improving segmentation times.

Ionasec et al. [83] describe a technique which uses a large database of manually labelled images and machine learning algorithms to locate and track valve landmarks. In this work, sophisticated biomedical models are employed to track and predict cardiac motion. This includes model-based tracking and delineation of

both the aortic and mitral valve apparatus. The biomechanical models can be tuned to patient-specific images via a set of parameters. This is done through a multi-step process beginning with global alignment and rigid motion estimation using feature detectors and a RANSAC estimator. Next, non-rigid local estimation is performed to further refine the model parameters using a machine learning estimator in the frequency domain, utilizing the discrete Fourier transform. Finally, non-rigid shape estimation is performed accross the full cardiac cycle using a combination of steerable features, a manifold-based shape model and probabilistic boosting trees [84]. While this method is fully automatic, the use of sparse landmarks potentially limits the patient-specific detail that can be extracted. This method takes roughly five seconds to compute, with reported accuracy of 1.54 ± 1.17 mm on a dataset of sixty five 3D plus time TEE sequences, with 1516 individual volumes.

Pouch et al. [85] also describe a fully automatic method which utilizes a set of atlases to generate a deformable template which is then guided to the leaflet geometry using joint label fusion. Multiple atlases are registered to the test image using deformable registration, and weighted voting schemes based on image similarity are used to fuse the associated labels from each atlas. A template mesh model is then registered to the resulting segmentation mask and regularized by additional terms to ensure smoothness. The surface error of this method is reported at 0.7 mm, however this is only achieved on healthy valves and performance is reduced when segmenting diseased valves. Additionally, this method is highly time consuming, taking several hours for deformable registration, with an additional thirty minutes for label fusion.

While existing methods have demonstrated the ability to accurately segment the mitral valve structure, they remain highly time-intensive. Furthermore, some of these published methods show decreased performance when applied to highly diseased valves, demonstrating limitations in patient-specificity. Convolutional

neural networks (CNNs) have been widely demonstrated to be effective for segmentation tasks. However, there has been limited work in using CNN segmentation approaches for mitral valve segmentation in 3D TEE imaging. However, 3D Unet based approaches have been used in other cardiac ultrasound applications such as automatic annulus detection [86]. Working in 2D, UNet has been used for mitral leaflet segmentation by taking a series of slices along the valve, and stitching together the resulting output into a 3D segmentation [87]. A major limitation of using only 2D slices is the lack of spatial consistency between slices, and an inability to account for dropout artefact. Thus far, a major limitation in the development of fully 3D CNN based approaches is data availability, as deep learning requires relatively large patient datasets. The lack of publicly available data also limits the ability to directly compare developed methods against each other, as there is no common benchmark to use. In this thesis, we report the first 3D CNN based segmentation method for the mitral valve, as well as the release of a publicly available dataset of 150 patient cases with 3D plus time sequences (Chapter 4).

1.4.3 Annulus Tracking

Segmentation of the mitral annulus is an important step in many cardiac applications. Current methods to delineate the mitral annulus often require extensive user interaction. Several methods have been proposed to automate mitral annulus segmentation, but often use methods which require sampling 2D planes from the 3D volume, discarding some of the contextual information contained in the original 3D volume. Identification of the mitral annulus shape during diagnosis for a number of applications including identifying pathologies, surgical planning and implant design[88, 89, 90]. The mitral annulus is currently typically identified using manual or semi-automated methods, such as the Mitral Valve Navigator tool in Philips QLab software, which introduces additional workload for clinicians. Ad-

ditionally, for trans-catheter mitral valve procedures, real-time annulus tracking significantly improves the procedure accuracy as part of an image guided surgery (IGS) system [91].

Prior methods have been developed that initially identify the mitral annulus using a manual approach, then apply image registration between subsequent ultrasound frames to warp the existing annulus, and in this way track and update the annulus shape and position in real-time [92]. These methods are effective for real-time tracking of the annulus, however they have the potential to accumulate error, as each position is updated based on the relative change compared to the previous frame. Additionally, correspondence to the previous frame can be lost, requiring re-initialization which may not be possible during surgery. Several methods which directly segment the annulus from ultrasound volumes have also been proposed. Early work based on optical flow can accurately identify the annulus, however it could only be applied to systolic images, and took 30-60 seconds to compute [81]. As a result, it is not possible to apply this technique for IGS applications, and for use in planning the annulus cannot be viewed at other cardiac phases. More recently, deep learning based approaches have been proposed, primarily by taking 2D cross-sectional images through the 3D volume, which are rotated around the mitral valve [93, 86].

1.5 Thesis Outline

The goal of this thesis is to address the challenge of producing patient-specific mitral valve models through the development of volume compounding and automated image analysis to more accurately and quickly capture the relevant valve geometry. Planning a surgical or transcatheter approach from diagnostic imaging for mitral valve procedures remains a significant clinical challenge. While TEE

is used as the primary imaging modality, it can suffer from poor image quality, signal dropout artefacts and limited field-of-view, contributing to the difficulty in planning an interventional approach. The development of simulation approaches utilizing patient-specific mitral valve models has shown promise for both training and planning for mitral valve interventions. However, a major barrier to producing accurate models of a patient's valve is the necessity of deriving the leaflet geometry from diagnostic TEE imaging.

In this thesis, I present a method to fuse multiple views acquired with a standard TEE probe to create an extended field-of-view volume (Chapter 2) to expand the range of anatomy that can be visualized for diagnostics and procedure planning. The remaining chapters are focused on the automated detection of relevant anatomy for patient-specific valve modelling from standard TEE images. I present first a semi-automatic segmentation algorithm for the mitral leaflets (Chapter 3), followed by a fully automatic approach (Chapter 4) made possible using a dataset created using the semi-automated method. Finally, I present a mitral annulus detection method (Chapter 5) that can track the annulus directly from the images in real-time. While the methods developed in this thesis utilize a Philips Epiq 7 cardiac ultrasound machine, the methods developed apply to any commercially available TEE system.

1.5.1 Chapter 2: Extended field-of-view cardiac ultrasound volume compounding

This chapter describes the methods used to register and blend multiple views acquired with a standard TEE probe without external tracking hardware. Standard TEE volumes can visualize the mitral valve, however, structures beyond the valve are difficult to see. Alternative imaging approaches such as cardiac CT are often needed to accurately image the sub-valvular structures, however, not all patients

are eligible for CT. The work explores the acquisition protocol used to acquire the separate views, as well as the registration algorithm used to align the volumes, and the blending strategy used to create the final image. The results indicate that I successfully demonstrated the creation of extended field-of-view volumes of the mitral valve and LV, which can clearly visualize otherwise difficult-to-see structures such as the chordae tendineae and papillary muscles using standard ultrasound hardware.

1.5.2 Chapter 3: Semi-automatic segmentation of the mitral valve

Identifying, or segmenting, the mitral leaflets from TEE volumes is an important step in diagnosis for quantification of the valve, as well as patient-specific valve modelling. Manual segmentation is a very time-intensive process and can have wide variability between users. This chapter describes a semi-automatic workflow that keeps the user in the loop with the goal of reducing the time required to produce segmentations of the mitral leaflets. This work explores the algorithms used to dynamically segment the leaflets with continuous user feedback. The results indicate that this workflow enables accurate segmentation with a reduction in the time required. This serves to simplify patient-specific valve modelling workflow and reduce the manual overhead required to derive measurements of the mitral valve from TEE volumes.

1.5.3 Chapter 4: Fully automatic segmentation of the mitral valve with DeepMitral

This chapter describes the methods used to produce fully automatic segmentations of the mitral leaflets, building upon the previous semi-automatic methods. Fully automatic segmentation is beneficial to minimize the manual effort required, as

well as produce greater consistency in the segmentations. Streamlining the process of segmenting the valve and generating a surface mold is important for the scalability and accuracy of patient-specific mitral valve modelling. I describe a deep learning architecture trained on a dataset created using the semi-automatic method to produce the labelled volumes. The results demonstrate state-of-the-art performance in segmentation accuracy, taking roughly five seconds to complete a single segmentation. This provides a platform for producing very fast and accurate segmentations that can be integrated into workflows for patient-specific valve modelling and valve quantification.

1.5.4 Chapter 5: Real-time mitral annulus detection

Delineation of the mitral annulus is an important step for valve quantification, patient-specific modelling, and real-time guidance applications. In this chapter, I describe a fully automatic, real-time mitral annulus segmentation approach based on a deep learning model. I present a novel approach using a regression model predicting a Fourier coefficient representation of the coordinates composing the annular ring directly from TEE volumes. This representation allows us to achieve real-time inference speed, enabling the use of this work in surgical guidance applications. Overall, the results of this work demonstrate state-of-the-art runtime speed, with good overall accuracy. The algorithm described can be integrated into a patient-specific modelling workflow to further reduce manual overhead, and can also enable more robust annulus tracking in surgical guidance applications.

Chapter 2

Extended field-of-view cardiac ultrasound volume compounding

In efforts to improve the field-of-view of standard TEE imaging, we present a volume compounding strategy to combine transgastric and mid-esophageal imaging of the mitral valve apparatus. This chapter presents the registration and blending methods and validation study of our volume compounding approach.

This chapter is adapted from the following manuscript:

[1] P. Carnahan, J. Moore, D. Bainbridge, E. C. S. Chen, and T. M. Peters, "Multi-view 3D transesophageal echocardiography registration and volume compounding for mitral valve procedure planning," *Applied Sciences*, vol. 12, p. 4562, Apr. 2022

2.1 Introduction

Three dimensional ultrasound imaging is used extensively as a diagnostic and guidance tool for cardiac procedures. Three dimensional echocardiography allows for the acquisition of volumetric data of the heart, which can be analyzed in any plane. The current standard of care for mitral valve procedures includes diagnos-

tic imaging with a 3D TEE probe[94, 95]. This method of imaging provides a clear view of the mitral valve, and including colour Doppler allows the cardiologist/-cardiac surgeon to identify the mitral valve pathology. While echocardiography is a powerful imaging technique, nevertheless it has some major limitations. The field of view is limited when using 3D transducers, which can limit the range of anatomy that can be easily viewed; structures further away from the image probe may suffer from poor spatial resolution, and thin structures parallel to the ultrasound beam, having no surfaces normal to the incoming wave, suffer from signal dropout artifacts.

Ultrasound compounding, or mosaicing, has been proposed by several groups to address limitations of 3D ultrasound and improve imaging capability. By registering and blending together adjacent acquisitions from different poses, we can expand the field-of-view and address the issue of signal dropout, producing higher quality images with greater information for the clinician. Several image compounding techniques have been proposed to register a set of ultrasound volumes, all of which demonstrate improved image quality [69], and provide an avenue for combining common cardiac ultrasound views into a single volume with reduced noise, reduced speckle, and fewer signal dropout artifacts. Researchers have demonstrated 3D ultrasound compounding techniques with applications in cardiac, fetal and breast imaging [70, 71, 72]. Common across all compounding methods are two critical steps: global registration of all volumes and blending the overlapping regions of the registered volumes to generate the resulting image [69]. Evaluation of registration frameworks has identified three main approaches consisting of sequential alignment, semi-simultaneous, and fully simultaneous registration [96]. Using a sequential alignment approach, each acquisition is registered to the next, however, this technique suffers from drift and error accumulation. The semi-simultaneous approach treats each volume in turn as the moving object

while the remaining volumes are fixed. This process is repeated for multiple cycles until convergence is met. Since only the parameters of a single transform need to be considered in optimization, this approach balances computational complexity with optimal global alignment as every volume is considered at every step. The final approach, fully simultaneous group-wise registration, optimizes the transformation parameters of all volumes simultaneously, applying a loss function as the sum of pairwise losses. This approach is optimal for registration quality, however is limited by computational complexity due to the number of parameters that need to be optimized.

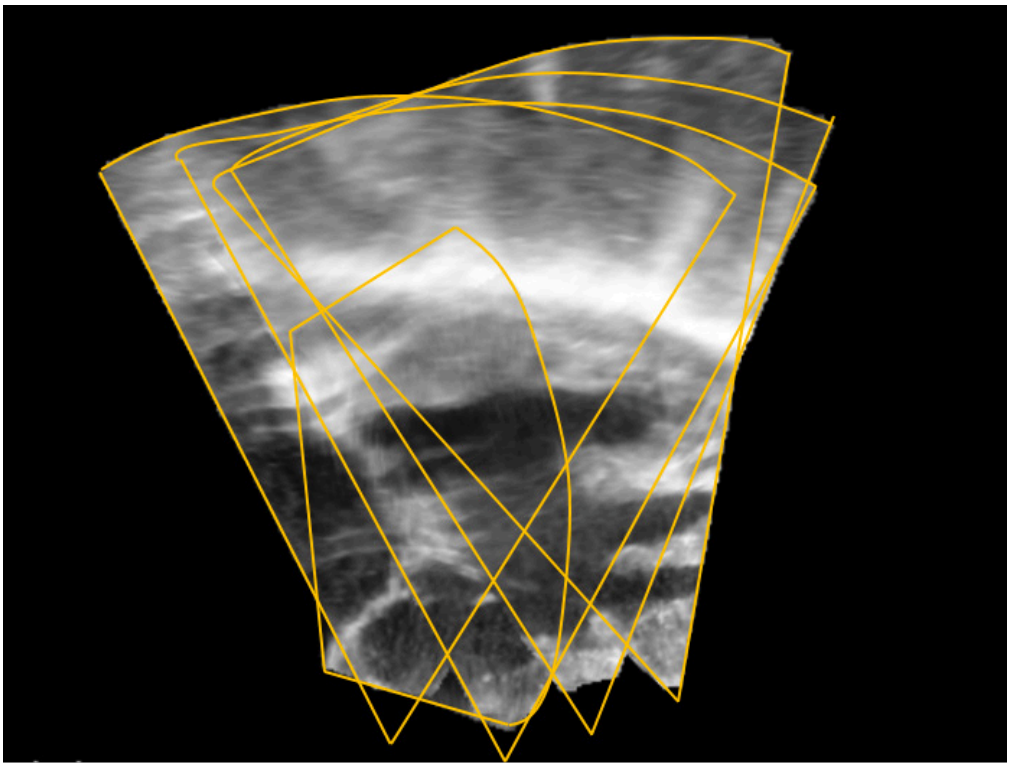

Figure 2.1: Compounded TEE volume of mitral valve with individual acquisitions outlined.

For mitral valve imaging using the standard mid-esophageal probe position, the limitations of 3D ultrasound result in the structures beyond the valve, including the chordae tendineae, papillary muscles and LVOT, being difficult to iden-

tify. While imaging from a different position (e.g. transgastric view) can capture these structures, the field-of-view limits the utility of these images as at these positions the entire mitral valve apparatus cannot be captured in a single volume. Currently, choosing the treatment plan that provides the greatest benefit to the patient is one of the biggest clinical challenges for cardiologists and cardiac surgeons [32]. Determining optimal neochord length is one of the main issues that cardiac surgeons must address in MV repair procedures [77], and it is particularly challenging to define this length due to a general lack of accurate anatomical information from standard diagnostic imaging, which includes only the mid-esophageal view of the mitral valve. Chordae tendineae length measurements are required for mitral valve procedures involving the implantation of artificial chordae [76]. It is nevertheless challenging to determine their optimal length because direct observation is limited to physical measurements made inside the flaccid heart during surgery, along with 2D transgastric long-axis images which require that the image plane be aligned with the entire chord to achieve accurate results [34]. While 3D transgastric TEE ultrasound is safe and easily acquired during routine TEE imaging (adding approximately 3-5 minutes to the procedure), it is rarely employed due to the limited visibility of the leaflets, and field-of-view limitations preventing the entire length of the chordae from being captured. Without the ability to see the entire subvalvular apparatus in the same image data as the standard mid-esophageal view of the leaflets, transgastric image information is of very limited clinical value.

In our prior work on volume compounding using TEE volumes, we explored a workflow using only the semi-simultaneous registration strategy, and a distance-based weighted average blending [97]. Our prior approach was able to successfully produce compounded volumes, however, the registration component of the workflow was not robust, could fail depending on the order in which the volumes were

processed, and the blending approach induced imaging artefacts. In this chapter, we propose an improved method to register and compound transgastric and mid-esophageal volumes utilizing a combination of semi and fully simultaneous registration with a novel weighting function for blending overlapping regions to reduce compounding artefacts. This provides an avenue for combining common cardiac ultrasound views into a single volume with reduced noise and fewer dropout artifacts. Many image compounding techniques involve the use of a tracked probe and were targeted at combining multiple transthoracic views [72]. Our method differs from these previous methods as it does not require any external tracking of the ultrasound probe, and it has been tailored for use with TEE probes to combine 3D mid-esophageal and transgastric volumes that can be acquired as part of a standard diagnostic imaging session. In the mid-esophageal volumes, the mitral valve is clearly visible, and in the transgastric views, the chordae are very clear, as these views are nearly perpendicular to each other. By combining both the mid-esophageal and transgastric views, we can maintain optimal imaging for both structures in a single compounded volume. Integrated leaflet and chordae geometry in a single volume will greatly improve the cardiac surgeons' ability to accurately measure the length of individual chordae (a crucial factor in neochordae repair techniques [77]) and to plan their repair strategy.

2.2 Materials and Methods

2.2.1 Image Registration

Following local REB approval, we adapted standard diagnostic TEE acquisition protocols to include multiple transgastric views in addition to the standard mid-esophageal view. Volumes were acquired using ECG gating to align each image with the appropraite phase of the cardiac cycle. Our imaging protocol requires

a minimum of one mid-esophageal acquisition and four transgastric acquisitions with at least 80 % spatial overlap or more between adjacent volumes for successful registration of the acquisitions (Figure 2.1). The acquisition frame-rates should remain constant to avoid temporal misalignment between subsequent image acquisitions. The transgastric acquisitions should begin at the mitral valve and proceed along the ventricle to the papillary muscles. Compounding is then accomplished by aligning over-sampled data through automated image registration, re-sampling the aligned volumes into a consistent output space, and generating the output image through the voxel-wise blending of the overlapping volumes. The compounding workflow is shown in Figure 2.2.

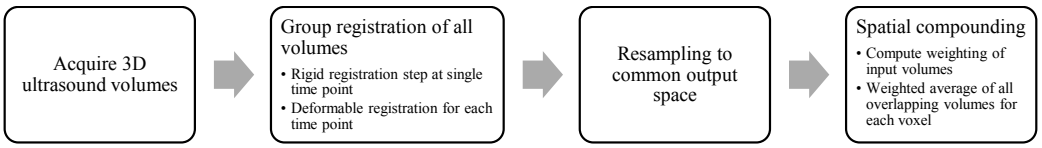

Figure 2.2: Workflow of TEE compounding for the mitral valve.

Performing image registration of multiple volumes can be achieved using pairwise, fully simultaneous, or semi-simultaneous approaches [98]. We implemented both the semi-simultaneous and fully simultaneous approaches described by Wachinger *et al.* [98]. This was performed as an extension of our initial work on this method, in which only the semi-simultaneous approach was used [97]. We first perform rigid registration at end-systole between all volumes using fully simultaneous group-wise registration, with the sum of pairwise normalized cross-correlations (NCCs) as the loss function. This gives us a rough global alignment of the volumes and is not dependent on input order. Then two cycles of semi-simultaneous registration are performed, which we found achieved better agreement between volumes than fully simultaneous alone. Finally, we utilize non-rigid registration in the semi-simultaneous framework at each frame in the acquisitions to account for slight deviations at different points of the car-

diac cycle due to imperfect synchronization. For both semi-simultaneous steps, the loss function used was the sum of NCC between the moving volume and each fixed volume. At each step, optimization was performed using adaptive stochastic gradient descent in a multi-resolution registration framework with four resolution levels, each of which smooths the image by a factor of 2 over the previous. We implemented this approach using the Elastix toolkit[1] on the 3D Slicer platform[2]. This open-source implementation of our work is available at `https://github.com/pcarnah/CardiacVolumeStitching`.

2.2.2 Image Blending

After the volumes are registered, re-sampling and compounding are performed at each cardiac phase to construct a 3D + time compounded volume with a wide field of view. Before compounding, the volumes are re-sampled to a common grid using cubic b-spline interpolation to ensure that there is complete voxel overlap between volumes, so that the blending step (a weighted average of all overlapping volumes at each voxel location), can be performed. The output grid is determined by the extent of all overlapping input images, using isotropic spacing equal to the minimum spacing in any dimension in any input image.

We evaluated multiple weighting strategies including the voxel-wise maximum, average, and weighted average using two different weighting schemes. The voxel weighting methods we compared were the scaled distance from the image probe, and a combination of distance from the probe and a feature detector based on the monogenic signal [99].

The monogenic signal is a generalization of the analytic signal to higher dimensions. In one dimensional (1D) signal processing the analytic signal is computed through the combinations of a signal with its Hilbert transformed counter-

[1] http://elastix.isi.uu.nl/
[2] https://www.slicer.org/

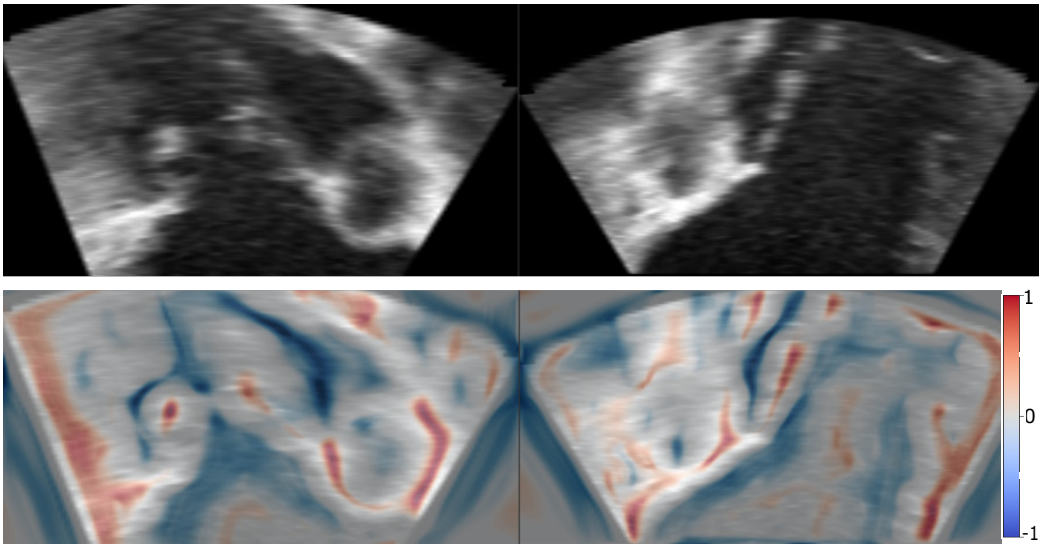

Figure 2.3: Original image (top), with oriented symmetry measure from monogenic signal (bottom).

part [100]. The monogenic signal is thus formed by combining a signal in a higher dimensional space, in this case 3D, with its counterpart transformed by a generalization of the Hilbert transform to higher dimensions. This method uses the Riesz transform, derived by Felsberg *et al.* [99], which is one such generalization of the Hilbert transform to Euclidean spaces of dimension greater than one. The 3D monogenic signal is composed of one even part, and three odd components, one for each spatial dimension. This is analogous to the real and imaginary components of the 1D analytic signal. The monogenic signal allows for the derivation of local energy and local phase, which correspond to overall local intensity and local structure, such as lines and edges, respectively. Previous work has shown the 3D monogenic signal to be useful in analyzing 3D volumetric ultrasound data[101]. The local phase measure derived from the monogenic signal had been previously demonstrated as part of an application-specific loss function for ultrasound compounding applications [102].

Through the use of multiple bandpass filters, the monogenic signal can be tuned to structures of different sizes, and derived measures can be averaged across

the different scales used. We use 4 filters tuned to spatial wavelengths of 6, 12, 24, and 32mm. As a feature detector, we use the oriented phase symmetry measure, which returns values from −1 to +1, with positive values being associated with features of interest and negative values being associated with background noise, as visualized in Figure 2.3. We implemented the 3D extension of the monogenic signal in Python. The distance function assigns higher weights to voxels closer to the image probe, with values ranging from 25 near the probe down to 0 with an inverse-square law dropoff, which we used to approximate the reduction in resolution further away from a phased-array ultrasound probe. For a single voxel position p in a source volume i, the expression for the distance from the image probe weighting d_i is

$$d_i(p) = 25\frac{\left(10 - \frac{10*\|p-o_i\|}{\max\limits_{q\in V_i}(\|q-o_i\|)}\right)^2}{10^2}, \tag{2.1}$$

where o_i is the position of the probe origin in volume i. The oriented symmetry weighting S_i is given as

$$S_i(p) = \begin{cases} 10 * s_i(p) & \text{if } s_i(p) < 0 \\ 25 * s_i(p) & \text{if } s_i(p) \geq 0 \end{cases}, \tag{2.2}$$

where s_i is the value of the oriented symmetry measure from the monogenic signal at position p in volume i. The combined weighting function W_i of distance and oriented symmetry is

$$W_i(p) = \max\left(0.5, S_i(p) + d_i(p)\right), \tag{2.3}$$

giving the sum of the two weights with a minimum value of 0.5. Both the dis-

tance weight d_i and symmetry weight S_i have a maximum value of 25, contributing equally to the overall voxel weighting. Finally, the expression for the final weighted average output intensity $F(p)$ is

$$F(p) = \frac{\sum_{V_i|V_i(p)>0} \big(V_i(p) * w_i(p)\big)}{\sum_{V_i|V_i(p)>0} \big(w_i(p)\big)}, \tag{2.4}$$

where $V_i(p)$ is the intensity value in volume i at position p, and w_i is either the distance weighting alone or the combined distance and oriented symmetry weighting.

A visual comparison of the results of applying the different blending approaches can be seen in Figure 2.4. The voxel-wise maximum approach produces a volume with very sharp features, but passes through any imaging artefacts and highlights registration errors. Simple averaging produces a smoother image, but lacks definition of smaller features, and boundary edges appear blurred. Distance weighted averaging further improves image quality, taking advantage of the increased US beam line density nearer to the probe and the corresponding increase in spatial resolution, but small features and edge boundaries are still blurred, and lack contrast to the background. The incorporation of the monogenic signal based feature detector into the weighting function helps to reduce this blurring, and makes the structures of interest more distinct without amplifying imaging and registration artefacts.

2.2.3 Data Acquisition

Three patients were imaged using our acquisition protocol under REB approval, using the Philips Epiq TEE system. These image sets were then registered and combined using each of the four blending approaches. Visual inspection of the

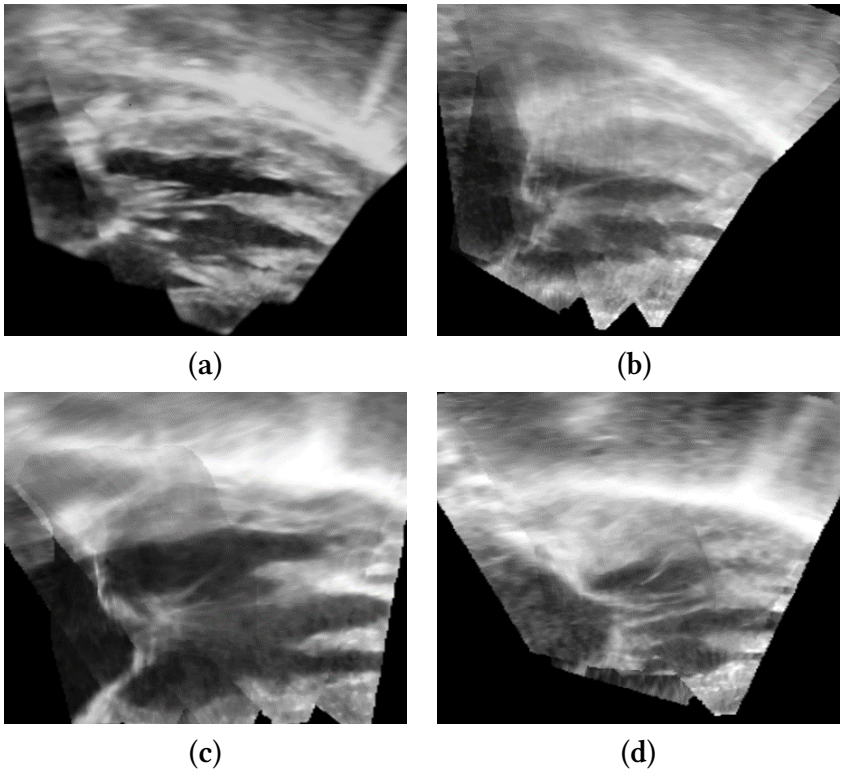

Figure 2.4: Results of blending functions max (**a**), average (**b**), distance weighted (**c**), and oriented symmetry plus distance weighted (**d**).

resulting volumes was performed by an echocardiography specialist, to verify apparent anatomical correctness, image quality, and clinical value. We validated the geometrical accuracy of this volume compounding approach on two excised porcine mitral valve units, shown in Figure 2.5. These valves were imaged using a Philips Epiq system with an X8-2T TEE probe, with volumes being captured sequentially from a mid-esophageal point, along a 3D printed path simulating the esophagus to a transgastric position. The valve was also stained with iodine and imaged with a cone-beam CT scanner (Medtronic O-Arm) to provide ground truth data. As shown in Figure 2.6, the ultrasound volumes were compounded using our described registration approach with the monogenic signal based blending method. Linear measurements were then made of the visible chordae structures in both volumes.

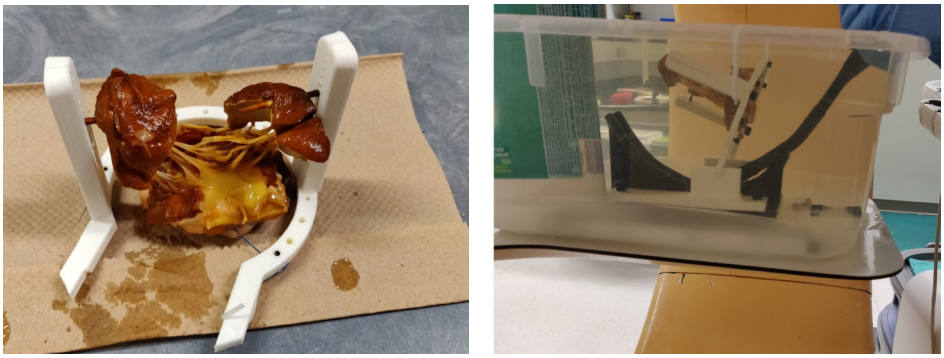

Figure 2.5: Excised porcine valve stained in iodine. Pictured on right is the valve being imaged using a TEE probe from a transgastric position.

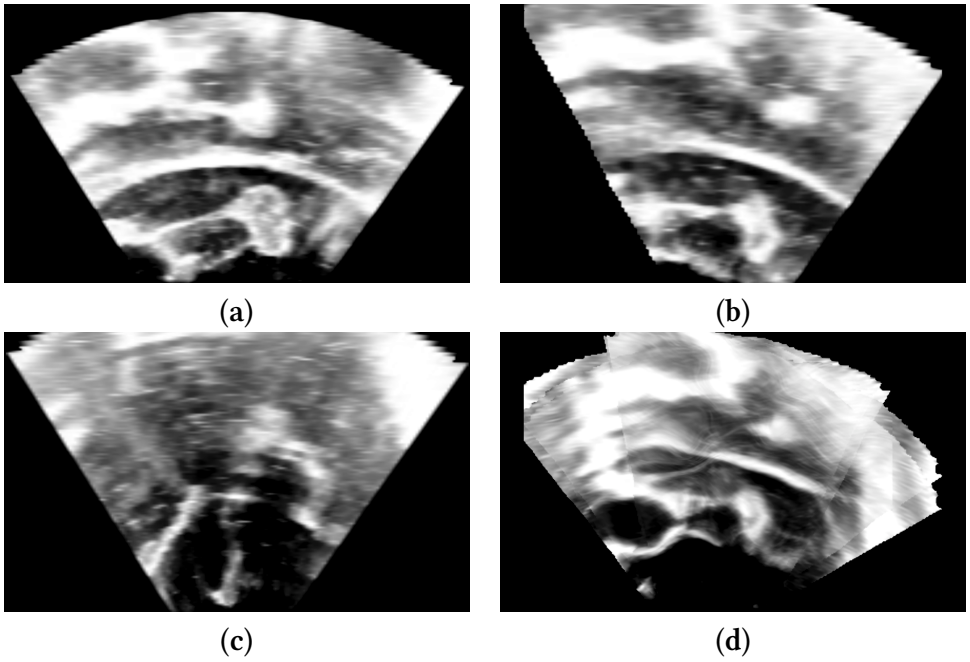

Figure 2.6: Original volumes simulating transgastric (**a**,**b**), and mid-esophageal (**c**) views of porcine valve unit. Resulting volume from compounding (**d**).

2.3 Results

2.3.1 Porcine Model

The compounded volumes visually replicated the anatomical structures visible in the ground truth CT scan. As shown in Figure 2.7, the mitral valve leaflets, papillary muscles, and individual chordae are clearly visible in the compounded volume. The compounded volume and CT are compared in Table 2.1 for each valve. For both volumes, four chordae that were easily visible in compounded echo and CT were measured from the papillary muscle tip to the leaflet insertion point, and the average absolute difference between US and CT length measurements was computed. The measured chordae lengths ranged from 22.1 mm to 36.4 mm.

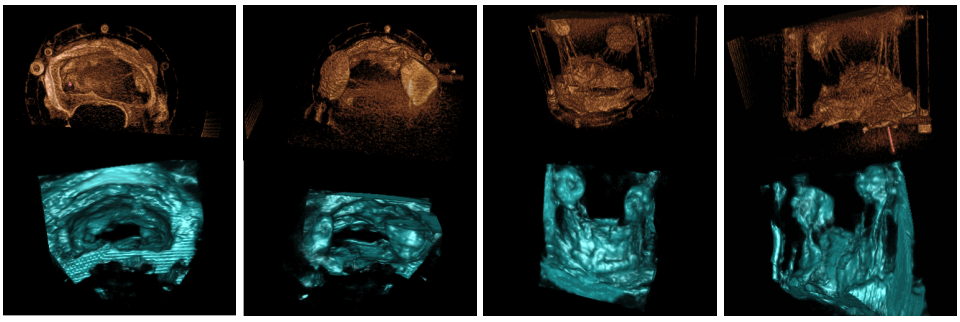

Figure 2.7: Side-by-side volume rendered comparisons from multiple view points of the CT data (top) and compounded echo (bottom).

Table 2.1: Volume comparison metrics between compounded echo and CT.

Excised Valve	Chordae Measurement Absolute Difference (mm)
Valve 1	0.7 ± 0.6
Valve 2	0.6 ± 0.6

2.3.2 Patient Images

We processed image volumes acquired from two patients to create compounded volumes that were visually inspected by a cardiac anaesthesiologist specializing

in echocardiography. The general consensus was that both volumes maintain acceptable clinical quality for the mitral valve leaflets, and that the chordae tendineae were very clearly visible in the volumes for both patients. The compounding process enabled the contrast between background noise and tissue to be more evident. Overall, compounded volumes exhibit an improvement in image quality, and include a wider field of view with little signal dropout, as shown in Figure 2.8. The overall conclusion was that these volumes represented an improvement over existing techniques, both in image quality, and range of structures visible.

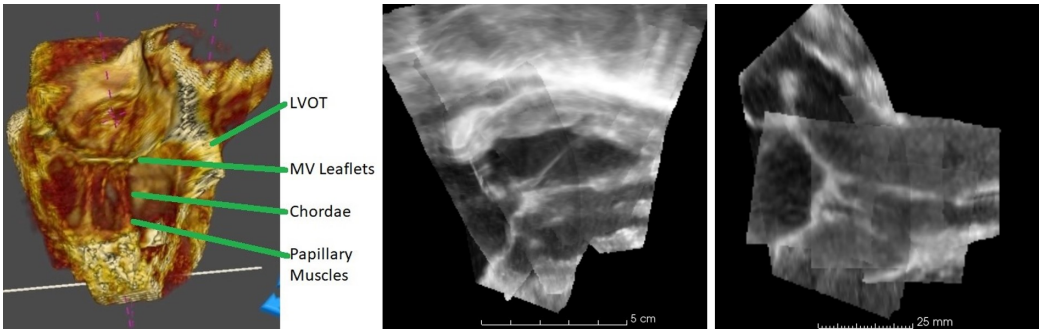

Figure 2.8: Visualizations of compounded TEE data from five different TEE volumes. Left, a volume rendered view. Middle, a commissure-commissure slice. Right, an AP slice.

2.4 Discussion

Spatial compounding has been demonstrated for many applications to improve field-of-view and image quality. Incorporating image information into the weighting function shows clear improvement over prior blending approaches. The combined distance and oriented symmetry weighting improves image quality and helps eliminate blending artefacts where the separate image acquisitions did not entirely agree. Compared to our previous results for this application, the registration strategy incorporating simultaneous group registration as the initial step

improved robustness, and eliminated the effect of initialization order, helping to prevent registration failure where the volumes do not reach alignment.

For the application of mitral valve procedure planning, we show that spatially compounded 3D echocardiography volumes are able to capture the complex structures in the LV. Utilizing spatial compounding reduces image noise and provides a single volume containing the mitral valve, chordae tendineae and papillary muscles, enabling clinicians to work from a single volume, instead of reconciling multiple separate volumes together. We demonstrate on porcine models that our spatial compounding method using a 3D TEE probe can reproduce the structures captured by a CT scan with high geometrical accuracy. Although the chordae appear thicker in the compounded volume, the separate individual chordae can still be identified from leaflet to papillary muscle. We found that the length of the chordae can be accurately measured from the compounded volume, as the thickening artefact does not affect the measurement of the length of the chordae.

The workflow described here can be integrated into the clinical standard-of-care, requiring only 4-5 acquisitions with approximately 80% overlap. Standard practice currently includes diagnostic 3D TEE for patients undergoing mitral valve procedures, and transgastric images are already acquired as part of this process in the form of 2D long-axis views in an attempt to capture the chordae in their entirety. This compounding technique enables the transgastric images to be acquired as a series of 3D volumes instead of the traditional 2D views, while still maintaining visibility of the entire chordae structures. Our workflow makes it possible for clinicians to map almost the entire chordal structure in 3D from leaflet to anchoring point in the LV, greatly improving the surgeon's ability to optimize lengths for introduced neochordae. Another instance where detailed, compounded 3D echocardiography has potential, is the early diagnosis of endocarditis, where individual 3D image volume analysis can often remain ambiguous [103]. The volumes

produced by applying 3D spatial compounding to TEE imaging capture the entire valve complex. Currently, many procedures require additional imaging in the form of cardiac CT/CMR to accurately perform diagnoses or plan for procedures [104]. Spatially compounded multi-view echocardiography has the potential to enhance the clinical imaging workflow by providing similar levels of information to cardiac CT at high frame rates, low cost and no radiation exposure to patients. Further validation of the clinical utility of this method will aim to demonstrate the effectiveness of compounded echo, in particular related to cases where currently cardiac CT is necessary.

Future work on this compounding method may include further improvements to registration speed and accuracy, as well as further exploration of blending approaches. Currently, the compounding process is performed offline due to computational requirements, with the process taking roughly one hour for a five volume data set of two beat acquisitions. However, further optimizations may enable a real-time compounding approach where the final volume is created as the volumes are acquired, which may also allow for guidance to be provided to the operator to ensure the volumes are collected with sufficient overlap. Incorporating image-based real-time tracking algorithms and graphics processing unit (GPU) acceleration may allow for active guidance of the volume acquisition relative to the initial position. Currently, this is a major drawback of the approach using offline processing, as in cases where the acquisitions have insufficient clarity or overlap, compounding will fail and the imaging session will have already concluded. Deep-learning based pose estimation and image registration also show potential for accelerating the volume compounding workflow. Real-time visualization of compounded ultrasound could be achieved by utilizing an initial alignment provided by these methods alongside simple averaging, with more computationally expensive processing steps performed offline to produce the final volume. This ap-

proach would enable a real-time preview of the results to the clinician to overcome the difficulties in adequate image acquisition, without sacrificing the accuracy of the alignment between volumes or quality of weighted image blending in the final compounded volume.

With improvements to the compounding process, extensions to the tricuspid valve could also be possible, extending the range of clinical applications for this work. Additional validation of the compounding approach for mitral chordae on a larger cohort of patients would be necessary to evaluate how accurately artificial chordae lengths can be predicted from these extended volumes. Further work needs to be performed to evaluate the effects of multi-view compounding on image quality using additional patient image data. Quantitative evaluation of image quality on a larger image set could be carried out by looking at potential improvements in the contrast-to-noise ratio and image sharpness, as described in prior volume compounding work [71, 72].

2.5 Conclusions

We have described a workflow for capturing a series of volumes using a TEE probe during standard diagnostic imaging that can then be registered and compounded together. We demonstrate improvements to the compounding process in registration robustness and final image quality. These compounded volumes capture the sub-valvular structures of interest for cardiac procedure planning. Capturing the necessary additional volumes can be performed while only adding an additional ten minutes to the time for the current standard of care diagnostic imaging protocol. We validate the geometrical accuracy of the compounding approach on two excised porcine valves, finding measurement error between compounded ultrasound and ground-truth CT to be 0.7 ± 0.6 mm and 0.6 ± 0.6 mm respectively.

This method is able to provide clinicians with a single volume that captures the mitral valve and the sub-valvular structures using existing standard-of-care ultrasound imaging. For patients who are not eligible for cardiac CT imaging, this provides an alternative approach that captures the same anatomical detail which may not otherwise be visible. Furthermore, we can incorporate the additional detail available in compounded volumes to create more accurate patient-specific models, particularly in regard to the papillary muscles and chordae tendineae. Overall, this represents potential improvements in both diagnostics and procedure planning from 3D TEE imaging.

Chapter 3

Semi-automatic segmentation of the mitral valve

Patient-specific mitral valve modelling requires the accurate identification of the leaflet geometry from diagnostic imaging data. This chapter presents a semi-automatic workflow for segmenting the mitral valve and validation results on expert ground-truth segmentations.

This chapter is adapted from the following manuscript:

[2] P. Carnahan, O. Ginty, J. Moore, A. Lasso, M. A. Jolley, C. Herz, M. Eskandari, D. Bainbridge, and T. M. Peters, "Interactive-Automatic Segmentation and Modelling of the Mitral Valve," in *Functional Imaging and Modeling of the Heart*, pp. 397–404, Springer International Publishing, June 2019

3.1 Introduction

The mitral valve is an anatomically complex, dynamic structure integral for efficient blood flow and therefore healthy cardiac output. When it becomes dysfunctional, it causes mitral regurgitation, and patients can face declining cardiovascular health leading to cardiac failure and death. Furthermore, mitral regurgitation is

the most common valvular disease affecting approximately 10% of those over 75 years old [105]. The preferred intervention for mitral regurgitation is repair, due to superior patient outcomes compared to replacement [15, 16]. However, the repair must be tailored to the patient-specific anatomy and pathology, which requires expert training and experience. Consequently, there is a need for patient-specific models that can permit the training and procedure-planning of patient-specific repairs to minimize its learning curve and preventable errors [106, 19]. Previous work has demonstrated the potential for patient-specific valve modelling for both surgical training as well as preoperatively predicting surgical outcomes [45]. The cause of mitral regurgitation varies across patients, as any failure of these structures can compromise the efficacy of the valve.

In order to prepare patient-specific models, the mitral valve must first be extracted from patient image data. Segmentation of the mitral valve is challenging in that it requires the capture of dynamic complex anatomy. There is no intensity-based boundary between leaflets and adjacent heart tissue, and distinguishing between the anterior and posterior leaflets in the coaptation zone during systole is difficult due to the lack of an intensity-based boundary. Additionally, in diastole there can be signal dropout which appears as gaps in the leaflets. To facilitate clinical use and repeat-ability, several mitral leaflet segmentation methods have been proposed. These methods focus on varying goals between deriving quantitative valve measurements and extracting annular and leaflet geometry from 3D TEE images. Burlina et al. [79] proposed a semi-automatic segmentation method based on active contours and thin tissue detection for the purpose of computational modelling. Scheinder et al. [80] proposed a semi-automatic method for segmenting the mitral leaflets in 3D TEE over all phases of the cardiac cycle. This method utilizes geometric priors and assumptions about the mechanical properties of the valve to model the leaflets through coaptation with a reported surface error of 0.8 mm.

However, this method only represents the mitral leaflets as a single medial surface, rather than structures with thickness. Additionally, several fully automatic methods have been proposed that are based on population average atlases. Ionasec et al. [83] describe a technique which uses a large database of manually labelled images and machine learning algorithms to locate and track valve landmarks. While this method is fully automatic, the use of sparse landmarks potentially limits the patient-specific detail that can be extracted. Pouch et al. [85] also describe a fully automatic method which utilizes a set of atlases to generate a deformable template which is then guided to the leaflet geometry using joint label fusion. The surface error of this method is reported at 0.7mm, however, this is only achieved on healthy valves and performance is reduced when segmenting diseased valves.

Automatic 3D segmentation methods offer significant implications for the feasibility of patient-specific modelling in clinical use. While existing methods have demonstrated the ability to accurately segment the mitral valve structure, they remain highly time-intensive. Furthermore, some of these published methods show decreased performance when applied to highly diseased valves, demonstrating limitations in patient-specificity.

We aim to develop a segmentation method that can be applied to both normal and highly diseased valves, to extract patient-specific leaflet geometry. Our focus is on delineating the leaflet surfaces for the purpose of creating molds for our related patient-specific MV modelling project, where silicone is applied to the molds to create valves for use in surgical training and planning [45]. To accomplish this, we propose a semi-automatic segmentation method based on active contours that iterates using a user-in-the-loop strategy.

3.2 Methods

3.2.1 Image Acquisition and Data Sets

Fifteen patients with mitral valve regurgitation undergoing cardiac surgery were imaged preoperatively using Philips Epiq and iE33 systems as per clinical protocol. Of the fifteen patient datasets, six were acquired at King's College Hospital, London, UK, from patients with severe mitral regurgitation, and nine were acquired at University Hospital, London, Canada. The 3D TEE images were exported into Cartesian DICOM format, which were imported into 3D Slicer using the SlicerHeart module [107]. Images at end-diastole were selected for image analysis. The exported Cartesian format images have voxel spacing in the axial direction of 0.3 mm to 0.6 mm.

3.2.2 Semi-Automated Image Analysis

Our software has been developed in the 3D Slicer[1] platform and employs The Insight Segmentation and Registration Toolkit (ITK)[2] software package. All code is publicly available on GitHub[3]. To account for the high variability in TEE data the iterative steps in our method do not use a fixed stopping point. Instead, the user runs the segmentation steps in increments until they are satisfied with the results, leading to an ideal compromise between human judgement in ambiguous cases and guided automatic segmentation for ease of use and time efficiency. In addition, a user can view the result of the next step of the segmentation, compare it to the previous step, and make manual adjustments between active contour steps. We base our segmentation on the end diastole image where the leaflets are least likely to experience signal dropout, but where the anterior and posterior boundary

[1] www.slicer.org
[2] www.itk.org
[3] https://github.com/pcarnah/SlicerMitralValve

is still clearly identifiable.

Before beginning the segmentation process, the user must define the valve annulus by placing a series of twelve points radially along the leaflets where they meet the atrial wall. The hinge point of the leaflets is identified by observing adjacent frames in the acquisition sequence to see the leaflet in motion. This is accomplished through the SlicerHeart software, which facilitates the placing of the points and fits them with a smooth annulus curve [108]. This annulus definition is used throughout the automated process to provide context for the valve centre, orientation and boundaries.

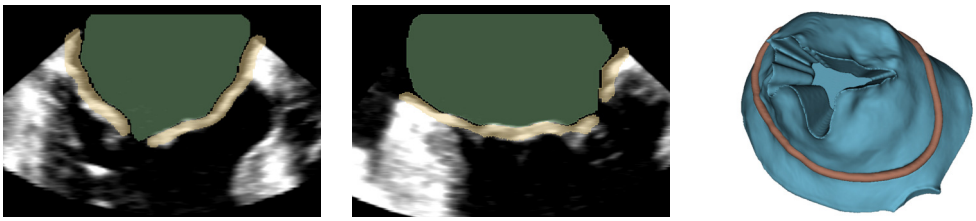

(a) (b) (c)

Figure 3.1: Cross sectional views of a 3D TEE image and segmentation (a,b), with the blood pool segmentation shown in green and the leaflet segmentation shown in yellow. Rendering of extracted proximal surface mold (c).

Blood Pool Segmentation

We first segment the atrial blood pool (BP), which provides context for the leaflet segmentation as well as the leaflet surface extraction. The image is first processed using a Gaussian filter with a variance of 1.0 mm, followed by a gradient magnitude filter. This creates a feature image highlighting the contrast edges, which determines the speed of the active contour growth. The centre of the defined annulus is used to initialize a geodesic active-contour filter from ITK that grows to complete the BP segmentation, as pictured in Figure 3.1. The active contour process is run with curvature, advection, and propagation scaling parameters of 1.2, 1.0, and 0.9 respectively. The curvature parameter controls boundary smoothing,

while the advection parameter influences attraction to edges. The propagation scaling parameter applies an inwards or outwards force on the contour boundary creating a bias to either grow or shrink.

Shrinking Leaflet Segmentation

The boundary region of the BP segmentation within a distance of 11 voxels, or ~5.0 mm is taken as the initial estimate for the leaflet segmentation. This estimate is refined using another active contour approach which shrinks the segmentation down to the desired result. The active contour approach used here differs from the one used in the BP segmentation mainly in that it is biased to shrink. The parameters used for this phase are 0.9, 0.1, and -0.4 for curvature, advection and propagation scaling respectively. As the active contour process iterates, the segmentation pulls back to the leaflet boundaries as pictured in Figure 3.1. Since our approach is interactive, the user is able to view adjacent image frames during the segmentation process to better inform their decision on the ideal stopping point. In addition, a volume rendered view can also be displayed alongside a 3D mesh of the segmentation, again providing more information to the user for completing the guided segmentation.

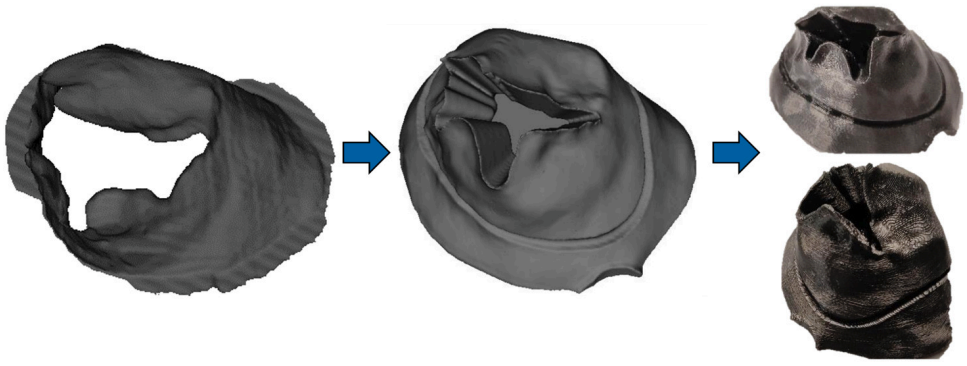

Figure 3.2: Extracted atrial surface (left) to generated 3D mesh (middle) to 3D printed positive molds (right).

Proximal Surface Extraction

For manufacturing our physical MV models as described in previous work [45], we require a geometric model of the valve surface proximal to the TEE transducer. The proximal surface is extracted from the leaflet segmentation using the defined annulus for context. Before proceeding, we utilize the "Segmentations" modules of 3D Slicer to produce a closed-surface mesh representation of the leaflet segmentation. Subsequent processing is achieved using VTK[4] on PolyData meshes. The atrial surface algorithm is described in algorithm 1, and an example of the resulting extracted surface can be seen in Figure 3.2.

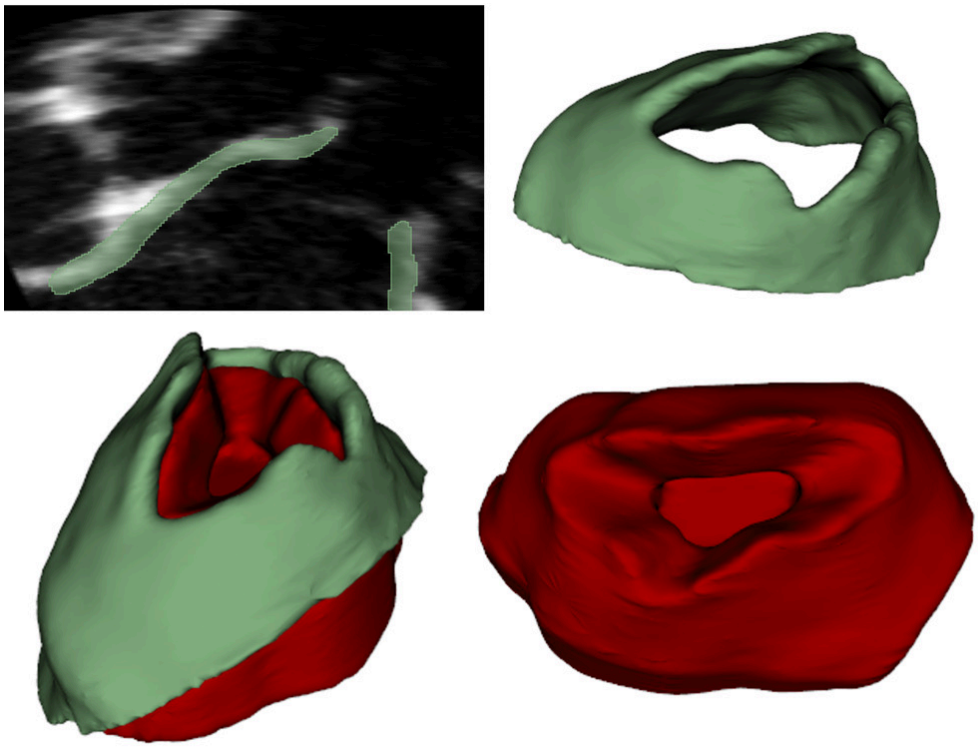

Figure 3.3: Cross section of 3D TEE volume (top-left). 3D representation of leaflet segmentation shown in green (top-right, bottom-left), positive mold generated from atrial surface shown in red (bottom-left, bottom-right).

The extracted atrial surface is then thickened inwards towards the midplane centre by 2.0 mm using linear extrusion, and the portion below the midplane centre

[4]https://vtk.org/

Algorithm 1: Algorithm to extract only atrial surface portion of segmentation mesh

```
Data: m segmentation mesh
Result: extracted atrial surface mesh
Construct OBBTree from m;
Construct cylinder c with midplane normal as axis, at midplane centre,
  with height 40mm and radius 10mm;
for each point p in m do
    if p is above midplane then
        Use OBBTree to compute interesection between m and line from p
          to midplane centre;
        Discard point if self-intersection;
    else
        Find line l from p to closest point on cylinder;
        Compute angle a between mesh normal at p and line l;
        Discard point if angle a > 1.5 rad
    end
end
```

is filled in. To construct a flat base, the mold's bottom half is extruded downwards and clipped to account for any regions with a short segmentation. The results of this process can be seen in Figure 3.3.

3.3 Evaluation and Results

To evaluate the accuracy of the proposed segmentation method, we compared automated segmentations to expert manual segmentations for images from 15 subjects. The ground truth expert segmentations were created using manual segmentations performed by two clinical users. Our semi-automatic system was then used on the same images and reference frames. Our system was employed with no manual user intervention between iterations in order to perform a baseline assessment of the algorithm independent of manual influence. Comparisons were made using the mean absolute surface distance (MASD) between the boundaries of the complete segmentations, as well as the MASD between the extracted proximal

surfaces.

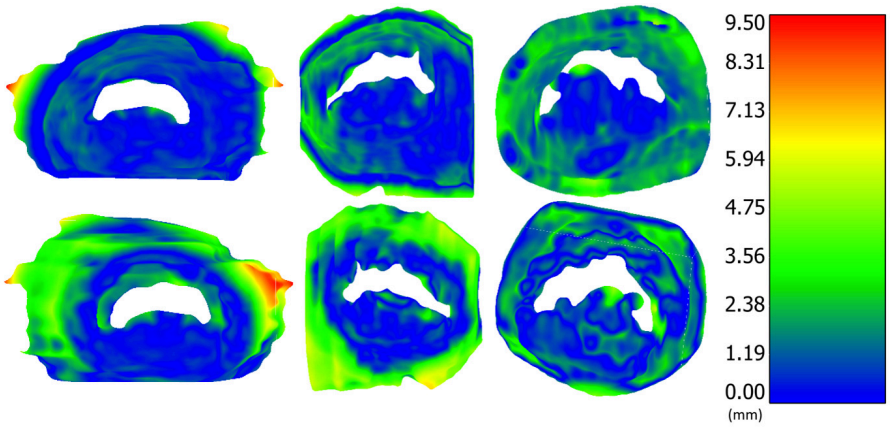

Figure 3.4: Distance maps of the proximal segmentation surface (top) and the distal segmentation surface (bottom) for 3 cases. The largest regions of error are located where the leaflets meet the atrial wall, as well as near the valve commisures.

The results indicate a MASD for the proximal surface of 1.01 ± 0.13 mm, which is on the order of one to two image voxels along the depth of the image. The MASD for the complete valve boundary is higher at 1.40 ± 0.26 mm, or two to three image voxels. The maximum local error observed was 9.4 mm occurring at the boundary between the leaflet and the surrounding atrial tissue. The average completion time using the proposed semi-automated segmentation method was 8.93 ± 2.31 min, compared to the manual segmentation times which averaged 55.84 ± 12.87 min. There was an overall average speedup of 46.47 ± 10.64 min using the semi-automated method over performing manual tracings.

3.4 Discussion

The proposed semi-automatic guided segmentation method enables the extraction of mitral leaflet geometry from 3D TEE in a 3D printable form. This method allows a user to rapidly segment the mitral valve at end-diastole to extract its atrial surface for generating a patient-specific mold with minimal effort. The interactive, iterative nature of this segmentation system allows it to be used on a wide variety

of pathological valves, as well as consistently work with a large range of image qualities from different systems.

Our results indicate similar overall performance to other semi-automatic methods and is on the same magnitude as previously reported inter observer variability of 0.60 ± 0.17 mm [78]. They are also consistent with previous studies which have observed that the greatest variability in manual and automatic segmentations occurs at the boundaries of the model, rather than at the leaflet surfaces. As Figure 3.4 shows, we see a boundary displacement of 1mm or less for most of the leaflet surface, and see larger displacement only at the boundary of the leaflet as well as the chordae attachment points. This is a result of the somewhat arbitrary, non-contrast boundary between the leaflets, the atrial wall, and the surrounding tissue. In addition, our method shows improved results when only considering the atrial valve surface, the surface of the valve more proximal to the TEE probe. This region shows the best image contrast and is consequently the most consistently identified between manual and automatic segmentations. Furthermore, since we do not rely on any prior data or image atlases, our system does not demonstrate any biases or drop in performance for previously unseen valve geometries. This is a critical consideration when modelling highly diseased valves for preoperative planning, as a wide variety of valve geometries can be observed. For the purposes of patient-specific valve modelling, prior work has demonstrated the creation of physical valve models using silicone and 3D printed molds based on the proximal valve surface [45]. Our method is well suited to the task of extracting mitral valve geometry for the creation of patient-specific models such as these.

3.4.1 Limitations and Future Work

In cases of very poor image quality, the automated segmentation may miss regions of dropout, or fail to capture the exact valve geometry. Expert users performing

these same segmentations often use other points in the cardiac cycle to inform their segmentation. Adapting this software to utilize additional time points may help to improve the robustness of the method in very difficult cases. In addition, color Doppler images are often captured in order to diagnose mitral valve regurgitation. This additional information could be used to increase the accuracy of segmentations as it contains information about the flow of blood between the leaflets. Further work validating the effectiveness of this system may be necessary to ensure it accurately captures patient-specific detail across healthy, mildly diseased and severely diseased valves. Our semi-automatic segmentation technique was used as part of a prospective study which aimed to validate the effectiveness of our dynamic silicone-based valves for predicting surgical outcomes [68].

3.5 Conclusion

Identifying, or segmenting, the mitral leaflets from TEE volumes is an important step in diagnosis for quantification of the valve, as well as patient-specific valve modelling. Manual segmentation is a very time-intensive process and can have wide variability between users. In this chapter, we present a technique that enables the extraction of mitral leaflet geometry from 3D TEE for creating 3D printed models used in creating accurate patient specific physical models. Segmentations from our software successfully replicate gold-standard MV segmentations within reasonable tolerance with respect to image resolution. The overall mean surface distance analysis demonstrates that our software can extract the proximal surface of the MV to within approximately one millimeter. This level of accuracy is suitable for patient-specific mitral valve modelling applications. Through the integration of a semi-automated segmentation approach, and subsequent mesh modelling steps into a user friendly 3D Slicer module, we have simplified the process to gen-

erate a 3D printable mold from patient image data. This segmentation software represents a critical step towards improving the translatability of the mitral valve modelling process by reducing the time required for completing an accurate mitral valve segmentation and automating part of the overall workflow.

Chapter 4

Fully automatic segmentation of the mitral valve with DeepMitral

This chapter presents improvements upon the results from Chapter 3 through the adoption of deep learning to create a fully automatic segmentation system with improved accuracy and runtime.

This chapter is adapted from the following manuscript:

[3] P. Carnahan, J. Moore, D. Bainbridge, M. Eskandari, E. C. S. Chen, and T. M. Peters, "DeepMitral: Fully automatic 3D echocardiography segmentation for patient specific mitral valve modelling," in *Medical Image Computing and Computer Assisted Intervention – MICCAI 2021*, pp. 459–468, Springer International Publishing, 2021

4.1 Introduction

As discussed previously in Chapter 3, a key step in patient-specific modelling workflows is delineating the mitral valve leaflets in patient ultrasound image data. Extracting the patient-specific leaflet geometry which is used to form the basis of the silicone valve replica remains a challenge. Performing manual segmenta-

tions is very time consuming, taking upwards of two hours, which is a serious bottleneck in modelling workflows. Several mitral leaflet segmentation methods have been proposed, targeting a number of different applications. These methods focus on varying goals between deriving quantitative valve measurements and extracting annular and leaflet geometry from 3D TEE images. These methods can be divided into two categories: semi-automatic and fully automatic approaches. The semi-automatic approaches all require some level of user intervention during the segmentation process, while fully automatic methods do not.

In our prior work presented in Chapter 3, we developed a semi-automatic approach designed for patient-specific valve modelling and reported a surface error of 1.4 mm overall, and an surface error of 1.0 mm for the atrial surface critical in mitral valve model creation [2]. Previous semi-automatic methods have also been presented in the literature. Scheinder *et al.* [80] proposed a semi-automatic method for segmenting the mitral leaflets in 3D TEE over all phases of the cardiac cycle, reporting a surface error of 0.8 mm. Burlina *et al.* [79] proposed a semi-automatic segmentation method based on active contours and thin tissue detection for the purpose of computational modelling, reporting errors in the range of 4.0 mm to 5.0 mm.

Several fully automatic methods have been proposed that are based on population average atlases. Ionasec *et al.* [83] describe a technique which uses a large database of manually labelled images and machine learning algorithms to locate and track valve landmarks, reporting a surface error of 1.5 mm. While this method is fully automatic, the use of sparse landmarks potentially limits the amount of patient-specific detail that can be extracted. Pouch *et al.* [85] also describe a fully automatic method that employs a set of atlases to generate a deformable template, which is then guided to the leaflet geometry using joint label fusion. The surface error of this method is reported as 0.7 mm.

Automatic 3D segmentation methods offer significant implications for the feasibility of patient-specific modelling in clinical use. While existing methods have demonstrated the ability to accurately segment the mitral valve structure, they remain highly time-intensive. Furthermore, some of these published methods show decreased performance when applied to highly diseased valves, demonstrating limitations in patient-specificity. CNNs have been widely demonstrated to be effective for segmentation tasks. However, to our knowledge no CNN segmentation approaches have been reported for mitral valve segmentation in 3D TEE imaging, although 3D Unets have been used in other cardiac ultrasound applications such as automatic annulus detection [86]. Working in 2D, UNet has been used for mitral leaflet segmentation [87].

In this chapter, we present DeepMitral, a 3D segmentation pipeline for mitral valve segmentation based on the 3D Residual UNet architecture [109]. We demonstrate the feasibility of CNN based segmentation for 3D TEE images, and establish a baseline of performance for future methods. DeepMitral will have applications in patient specific valve modelling, enabling improvements in the workflow. DeepMitral has been made open source including our trained model and is freely available on GitHub[1].

There are several key roadblocks to the development of image analysis techniques in the medical imaging domain. In the computer vision domain, ImageNet [110] was transformational to research and development because it highlighted the importance of data curation and availability to feature and algorithm generation. In the medical imaging field, the curation of large datasets is particularly challenging due to the need for clinical expertise to annotate images, and privacy concerns limiting the sharing of data [111]. For algorithm design, sufficient quantities of data are necessary to ensure that the methods generalize to the

[1] `https://github.com/pcarnah/DeepMitral`

broader population, a problem made evident with the onset of deep learning-based approaches. Furthermore, transparency in the validation approach used is necessary for reproducibility, and when the data used is not made public, we cannot effectively evaluate a reported method. This makes it difficult to compare new algorithms directly against the existing state-of-the-art, and we must instead rely on reported results by the authors. Image analysis competitions address these concerns by centralizing the curation of high-quality datasets which are released to the research community, and the consistent evaluation of submitted methods fixed test set. This serves to increase data availability to the wider community, as well as expedites the development cycle for new approaches. Currently, there are no public challenges or datasets of 3D TEE imaging of the mitral valve, which has been a major limiting factor in the evaluation and comparison of different methods. In this chapter, we report the curation and release of a dataset consisting of 150 cases of mitral valve TEE images with expert annotation, released as an image segmentation competition.

4.2 Methods

4.2.1 Data Acquisition

Patients with mitral valve regurgitation undergoing clinical interventions were imaged preoperatively as per clinical protocol with appropriate ethics approval using a Philips Epiq system with an X8-2T transducer. The 3D TEE images were exported in a Cartesian DICOM format, and the SlicerHeart module was used to import the Cartesian DICOM files into 3D Slicer[2] [107]. Images at end-diastole were selected for image analysis due to the need for manufacturing patient-specific valve replicas from this cardiac phase. The exported Cartesian format images have

[2] https://slicer.org

voxel spacing in the axial direction ranging from 0.3 mm to 0.6 mm, and spacing in the lateral directions of 0.4 mm to 0.7 mm.

We initially collected a total of 48 volumes, which were divided into training, validation and testing partitions with 36, 4, and 8 volumes respectively. Annotations for the training and validation sets were performed in 3D Slicer by multiple trained users. These segmentations were performed via manual refinement of the output of our previous semi-automatic segmentation tool as described in chapter 3 [2] and were then reviewed and modified as necessary by a single experienced user to ensure consistency. The test set was annotated entirely manually by two cardiac imaging clinicians using 3D Slicer. All model selection was performed on this initial dataset.

Subsequently, we collected an additional 150 cases, which were initially segmented with DeepMitral and manually edited where necessary by an expert clinical user. We report results for both our initial dataset, and our combined final dataset after retraining our model, keeping the network architecture consistent for direct comparison. We released the additional 150 cases as a standalone public dataset as part of the MVSEG2023 MICCAI challenge[3].

4.2.2 Model Selection

Our initial training and validation sets of 36 and 4 cases were used to perform model selection and hyper-parameter tuning on a variety of network architectures including Residual UNet, VNet, AHNet and SegResNetVAE [109, 112, 113, 114]. We trained each network with a selection of hyper-parameters and computed mean Dice coefficient scores, mean surface error scores, and mean 95 % Hausdorff distance on the validation set. The best performing version of each network architecture is shown in Table 4.1. Of the models, the Residual UNet architecture achieved

[3] `https://www.synapse.org/MVSEG2023`

Table 4.1: Validation metrics for the tested network architectures.

Network	MASD (mm)	95 % Hausdorff (mm)	Dice Coefficient
Residual UNet	0.5	3.4	0.8
VNet	0.5	4.1	0.8
AHNet	0.7	5.2	0.8
SegResNetVAE	0.7	4.2	0.8

the best performance with respect to all validation scores, so it was chosen as our final network for use in the DeepMitral pipeline.

4.2.3 DeepMitral Pipeline

Our 3D TEE volume segmentation platform was built using the MONAI[4] framework, that provides domain-optimized foundational capabilities for developing healthcare imaging training workflows. This platform includes the implementation of many common network architectures for both 2D and 3D data, as well as a number of medical imaging focused pre-processing methods.

Our workflow begins with a sequence of pre-processing operations from the MONAI framework. First, we load the images, and transform them into channel-first representation according to PyTorch image conventions. Next, we isotropically re-sample the volumes to 0.3 mm spacing, using bilinear re-sampling for the image data and nearest neighbour re-sampling for the label. Following re-sampling, we re-scale the image intensities to the range of 0.0 to 1.0, then crop the images to the foreground using the smallest possible bounding box that includes all non-zero voxels. Finally, random sampling is performed on the volumes, taking 4 samples of size 96x96x96, centered on voxels labelled as leaflet. The final random sampling step is recomputed at every epoch during network training. No data-augmentation was performed, as adding rigid or deformable spatial trans-

[4] `https://monai.io/`

formations resulted in no improvements in validation metrics, and a reduction of training speed.

Our network uses a Residual UNet architecture [109], implemented by the MONAI framework, with 5 layers of 16, 32, 64, 128 and 256 channels respectively. Each of these layers is created using a residual unit with 2 convolutions and a residual connection. Convolutions are performed with stride 2 at every residual unit for up-sampling and down-sampling. The complete network architecture is shown is Figure 4.1.

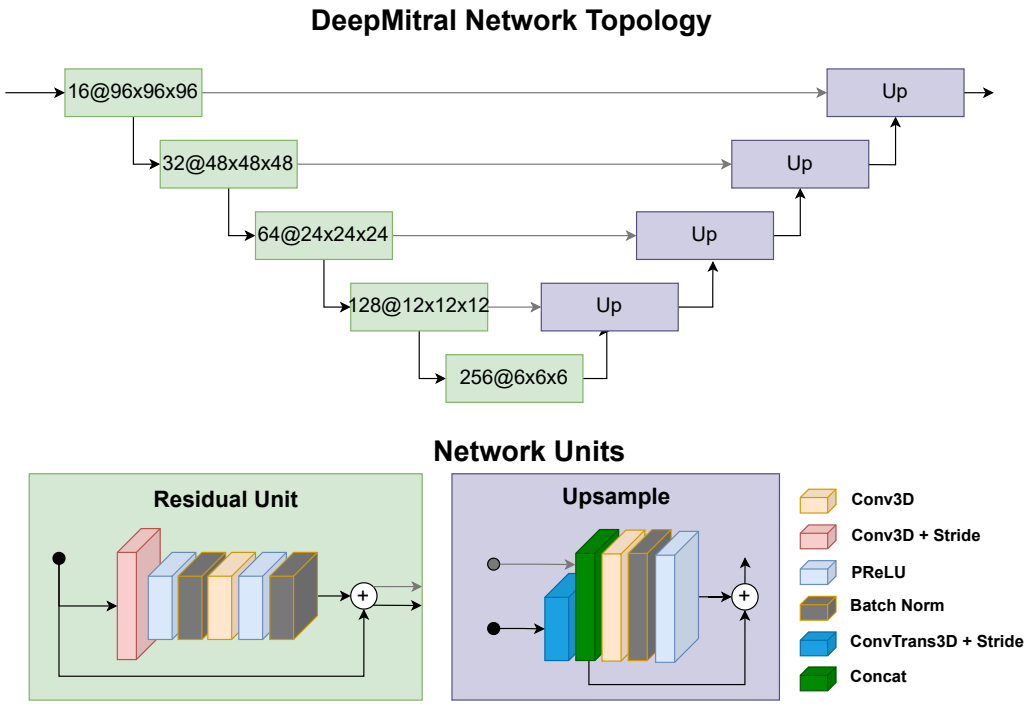

Figure 4.1: Network diagram showing Residual U-Net architecture used by DeepMitral. The downsample path consists of Residual Units with strided convolutions. The upsample path uses Residual Upsample Units with transposed convolution. Skip connections are included at each layer of the network.

We trained our model using batch sizes of 32, composed of 8 different volumes, with 4 random samples being taken from each volume. Training was performed for 1500 epochs using an Nvidia RTX6000 graphics card with 24GB of ram. The training process took roughly 3 hours on our initial dataset for DeepMitral v1,

and 22 hours on our expanded dataset for DeepMitral v2. We employed the Adam optimizer, with an initial learning rate of 1×10^{-3}, which is reduced to 1×10^{-4} after 1000 epochs [115]. Batch normalization is used to help prevent over-fitting of the model.

4.2.4 Evaluation

Final evaluation of our pipeline is performed using a separate test set consisting of eight volumes with ground truth annotations that were performed manually by two cardiac imaging clinicians. Prior to evaluating our model, we retrained the network using combined training and validation sets. The primary comparison metrics are the MASD between the boundaries of the complete segmentations, as well as the 95 % Hausdorff distances, and Dice coefficient scores. We report the validation metrics for the same eight test cases using both our initial model, DeepMitral V1, and a retrained version of the same architecture using an expanded dataset, DeepMitral V2.

4.3 Results

DeepMitral v1 trained on our initial dataset achieved a MASD of 0.59 ± 0.23 mm, average 95 % Hausdorff distance of 1.99 ± 1.14 mm, and a Dice score of 0.8. In all 8 volumes used for testing the mitral leaflets were successfully segmented, with no cases of complete failure to identify the leaflets. Overall, the scores are consistent among 6 of the 8 examples, with 2 examples exhibiting lower performance. In one instance, case P3, the leaflets are under-segmented near the leaflet tips, and in another instance, P8, the chordae tendineae are mis-labelled as leaflet, as seen in Figure 4.2. We see the corresponding metrics for these cases in Table 4.2, which show higher surface distance errors and worse dice scores than the other cases.

Table 4.2: MASD, 95 % Hausdorff Distance and Dice Coefficient scores for each of the eight volumes in the test set for DeepMitral v1.

Test ID	MASD (mm)	95 % Hausdorff (mm)	Dice Coefficient
P1	0.43	1.18	0.84
P2	0.37	1.10	0.87
P3	1.04	3.53	0.65
P4	0.53	1.49	0.83
P5	0.49	1.25	0.83
P6	0.42	1.37	0.85
P7	0.71	1.97	0.76
P8	0.76	4.02	0.82
Average	0.59 ± 0.23	1.99 ± 1.14	0.81 ± 0.07

After expanding our initial dataset from 48 cases to 198 cases, we retrained our model and recomputed our evaluation metrics. Version two achieves a MASD of 0.52 ± 0.16 mm, average 95% Hausdorff distance of 1.60 ± 0.58 mm, and a Dice score of 0.8. For the six cases in which DeepMitral v1 achieved good results, limited improvement is shown. However, for cases three and eight in which v1 had poor performance, v2 has demonstrated improved results in line with the remaining six cases. Overall, we note a small improvement in each metric, with better consistency across all cases using DeepMitral v2, trained on a much larger dataset.

4.3.1 Inference Runtime Performance

Deep learning segmentation methods enable predictions to be performed for low computational cost. We evaluated DeepMitral's inference speed on our test set using both central processing unit (CPU) only (Intel i7-6700K) and GPU acceleration (Nvidia GeForce GTX 1080). The size of the volumes range from approximately 160x160x160 to 300x200x200 voxels. Using only the CPU for inference, DeepMitral takes on average 9.50 ± 2.26 s to perform the inference itself, and 11.40 ± 2.28 s for overall runtime including startup overhead. When using GPU acceleration,

Table 4.3: MASD, 95 % Hausdorff Distance and Dice Coefficient scores for each of the eight volumes in the test set for DeepMitral v2.

Test ID	MASD (mm)	95 % Hausdorff (mm)	Dice Coefficient
P1	0.40	1.29	0.84
P2	0.37	1.12	0.87
P3	0.76	2.84	0.75
P4	0.51	1.34	0.84
P5	0.45	1.18	0.85
P6	0.37	1.26	0.87
P7	0.78	1.91	0.73
P8	0.51	1.88	0.82
Average	0.52 ± 0.16	1.60 ± 0.58	0.82 ± 0.05

these times are reduced on average to 3.50 ± 0.53 s for inference and 5.69 ± 0.66 s for overall runtime. DeepMitral achieves fast inference times on both CPU and GPU, with GPU acceleration reducing runtime by a factor of two on average. Additionally, startup overhead is consistently around 2.0 s for both CPU and GPU. This overhead would only occur once in the case of performing inference on multiple volumes in a single run.

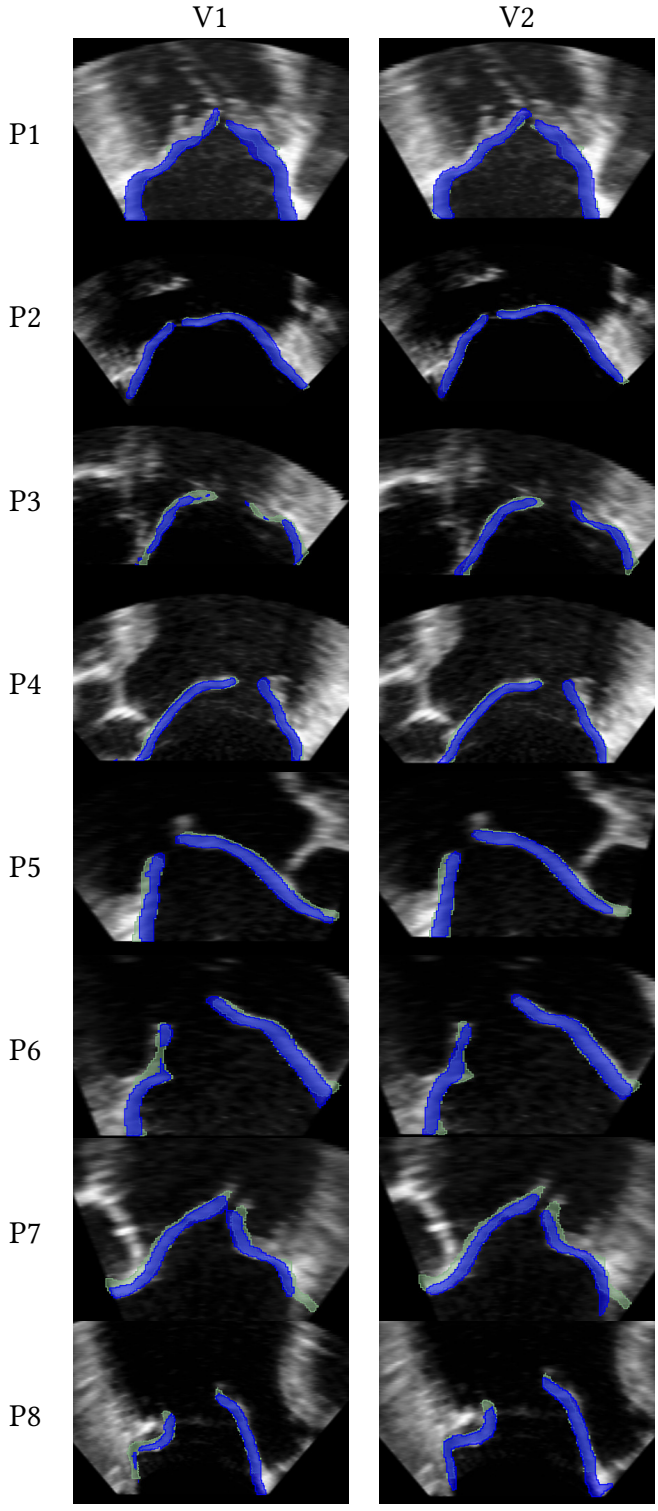

Figure 4.2: Cross sectional views of 3D TEE images and segmentations for each volume in our test set for DeepMitral versions one and two. Ground-truth label is shown in green, and predicted label is shown in blue.

4.4 Discussion

These results demonstrate the feasibility of CNN based techniques for mitral valves segmentations in 3D TEE volumes. Trained with a relatively small dataset, DeepMitral achieves an improvement in accuracy over the existing state of the art approaches. Average surface error is reduced to 0.6 mm on average, where the best performing existing methods report an error of 0.7 mm. Additionally, our reported error is almost equal to typical inter-user variability, which was previously reported as 0.60 ± 0.17 mm [78]. Our reported MASD is approaching the axial resolution of the ultrasound volumes, which is approximately 0.5mm on average. These results indicate that while DeepMitral v1 is accurately labelling the valve leaflets overall, we note the 95 % Hausdorff distances are typically larger, in the range of 1.0 mm to 4.0 mm. We can see in Figure 4.3 that there are small regions of the leaflets where accuracy is worse, contributing to these larger 95 % Hausdorff errors, while the majority of the leaflet surface maintains sub-millimetre error. For P8, we see that the leaflets themselves are well identified, however the large protrusion where the chordae were mis-identified contributes to the poor error metrics in the case. In Figure 4.4 we see the same two cases segmented using DeepMitral v2, and the improvement in the boundary regions is evident. This demonstrates the benefit and necessity of increasing the size of the training dataset when using deep learning to improve generalizability.

Our results suggest deep learning-based approaches are able to capture unique valve features. Although we tested DeepMitral on exclusively diseased valves, as demonstrated by our test data, there is a range of distinct valve geometries, all of which are accurately identified by our model. The areas of poor performance are not due to systematic geometrical bias, but are instead caused by poor image data and mis-identified structures.

CNN based approaches are particularly beneficial for use in valve modelling

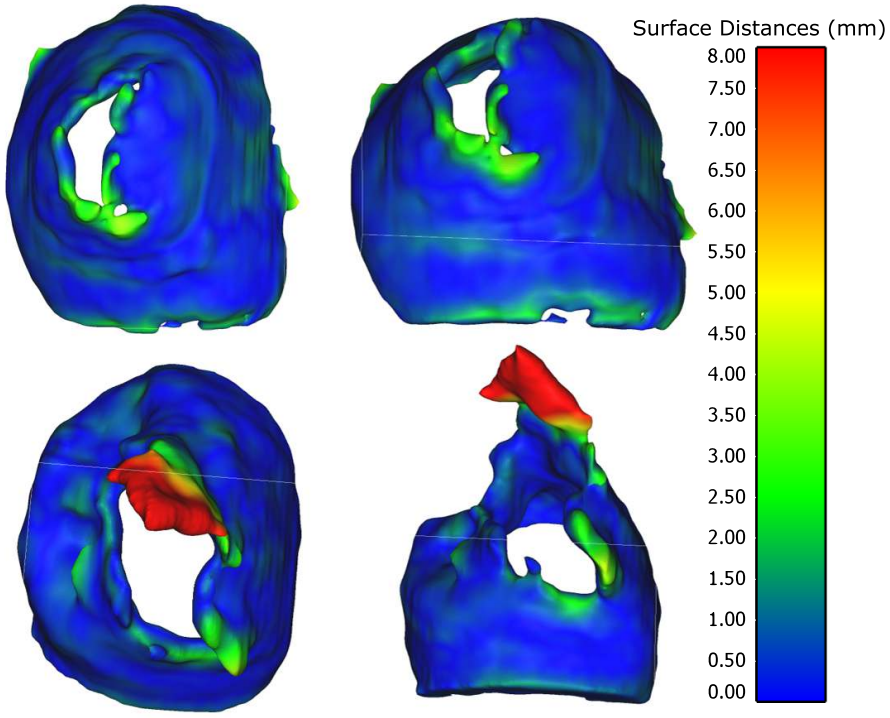

Figure 4.3: Distance comparison heatmaps for P4 (top) and P8 (bottom), showing the distribution of error across the leaflet segmentation for predictions using DeepMitral v1.

applications since they eliminate the computational time that prior methods have reported, ranging from 15 minutes to 3 hours for a single segmentation. Deep learning methods instead can perform a segmentation in seconds, which removes a large bottleneck in valve modelling workflows. Additionally, since these methods are fully automatic, the resulting segmentations will be more consistent than semi-automatic or manual approaches, where individual users can vary greatly on how much of the atrial wall they label as leaflet. DeepMitral produces accurate segmentations in most cases, however in instances where the segmentation is sub-optimal manual editing of the result is still possible. DeepMitral has been integrated into our 3D Slicer module described in Chapter 3, allowing for an initial segmentation to be created very quickly, and then be verified and edited if necessary before being used in any downstream applications. We successfully employed

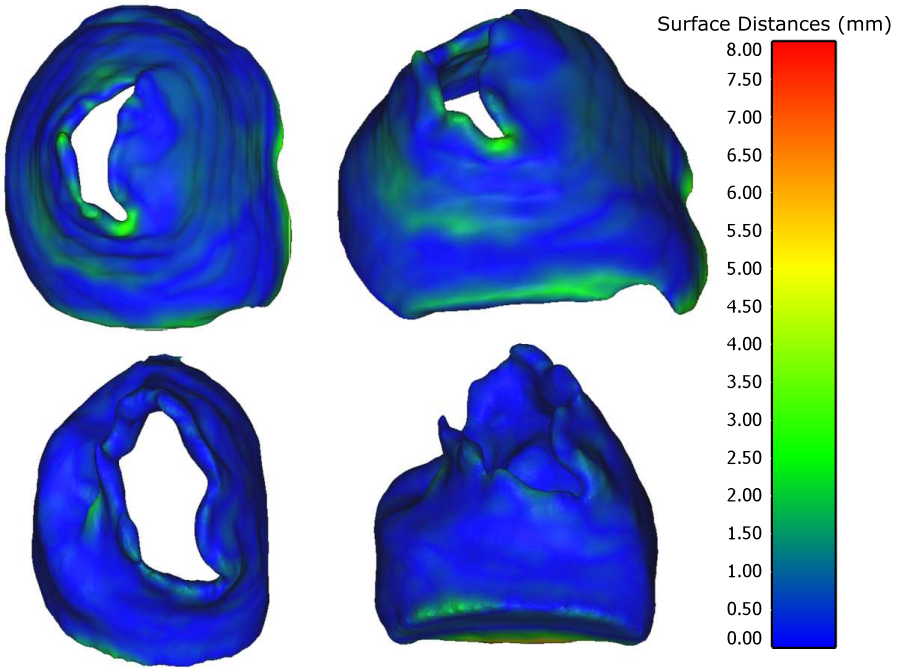

Figure 4.4: Distance comparison heatmaps for P4 (top) and P8 (bottom), showing the distribution of error across the leaflet segmentation for predictions using DeepMitral v2.

this approach using DeepMitral v1 to produce an additional 150 cases with manually refined s for further training. This module including DeepMitral has also been used for producing segmentations for a further study validating dynamic patient-specific mitral valves.

4.4.1 Public Dataset

To directly compare various segmentation methods against each other, a consistent benchmark dataset is desireable. To date, there has been no publicly available dataset of mitral valve imaging using 3D TEE. As part of the MICCAI 2023 conference, we organized a challenge titled *"Segmentation of the Mitral Valve from 3D Transesophageal Echocardiography"*, in which we curated and released a dataset of 150 cases with TEE imaging and expert ground-truth segmentations. These cases represent a subset of the data used to train DeepMitral v2. This dataset includes

only a single time-point selected at end-diastole, and not the full cardiac cycle.

Through the curation and release of a high-quality dataset, we aim to provide a benchmark for future work on mitral valve segmentation. This will enable further development and improvement of segmentation algorithms with the ability to report results using a consistent dataset. We plan on further iterating on this challenge to include additional tasks such as full-cycle four dimensional (4D) segmentation, annulus tracking, and papillary muscle segmentation.

4.4.2 Limitations and Future Work

DeepMitral v1 fails to differentiate between chordae and leaflet in some images where the chordae are very clear, as seen in case P8 and to a lesser extent case P6 in Figure 4.2. The initial dataset has a lack of training data where chordae are strongly delineated in the image, as this rarely occurs in TEE imaging. As a result, our model tends to classify the chordae as leaflet, as it presents as a similar image feature when visible. This has been partially addressed through the expansion of our dataset, and improved results at differentiating chordae are evident in DeepMitral v2. This could be developed upon in future work by including an additional label for the chordae in our training set to allow our model to learn how to differentiate between leaflet and chordae, and label additional structures of interest within the image. Additionally, sub-optimal image quality can cause the segmentation to perform poorly. This is a fundamental limitation when working with cardiac ultrasound, as it is possible for acquisitions to be very noisy, or lack detail of the mitral leaflets due to signal dropout. Expanding our data-set to include wider variations in image quality has again improved results in DeepMitral v2. Further investigation is still required to establish a threshold in image quality for which automated segmentation is feasible.

The results demonstrated with DeepMitral show promise for further devel-

opment in automated segmentation of 3D TEE volumes. We demonstrate good performance only on a single, diastolic frame, however the patient cases all include 3D plus time volume sequences. DeepMitral could be trained on a dataset with the complete cardiac cycle segmented to enable accurate segmentation at any time point. Incorporating the cyclical nature of cardiac motion into the network architecture could potentially further improve the accuracy of the segmentations. Since different structures are better imaged at different phases of the cardiac cycle, this technique has the potential to further improve our results and overcome limitations due to image quality. Our methods could also be extended to other areas of interest for cardiac ultrasound through transfer learning. This could be applied to adult tricuspid valves, enabling improved results as data availability for the tricuspid valve is more limited and image quality is generally poor. Additional areas of interest could include transfer learning for the left atrial appendage segmentation, as well as the left-ventricular-outflow-tract, which are of clinical interest for virtual modelling of device positioning.

4.5 Conclusions

In this chapter, we describe a deep learning architecture trained on a dataset created using the semi-automatic method to produce the labelled volumes. The results demonstrate state-of-the-art performance in segmentation accuracy, taking roughly five seconds to complete a single segmentation. This provides a platform for producing very fast and accurate segmentations that can be integrated into workflows for patient-specific valve modelling and valve quantification. The results from DeepMitral successfully replicate the gold standard segmentations with improved performance over existing state-of-the-art methods. Sub-millimetre average surface error in the segmentation stage is sufficient for use in patient specific

valve modelling without manual intervention. DeepMitral improves the workflow of the mitral valve modelling process by reducing the time required for completing an accurate mitral valve segmentation and providing more consistent results.

To our knowledge, we are the first to demonstrate the effectiveness of CNN based segmentation approaches for the mitral valve leaflets from 3D TEE volumes. We also report the first publicly available dataset of annotated TEE volumes with labelled leaflets. This will enable the broader research community to build upon this work to further improve the robustness and accuracy of automated mitral valve segmentation. Overall this work represents progress towards robust, fully automatic mitral valve segmentation which enables improvements in mitral valve modelling and valve quantification workflows.

Chapter 5

Real-time mitral annulus detection

The mitral annulus is an important structure for valve quantification, and is a useful visualization target for image guidance systems. In this chapter we present a fully automatic mitral annulus segmentation framework with real-time performance.

This chapter is adapted from the following manuscript:

[4] P. K. Carnahan, A. Bharucha, M. Eskandari, D. Bainbridge, E. C. S. Chen, and T. M. Peters, "Real-time mitral annulus segmentation from 4D transesophageal echocardiography using deep learning regression," in *Medical Imaging 2023: Image Processing* (I. Išgum and O. Colliot, eds.), SPIE, Apr. 2023

5.1 Introduction

Echocardiography is used extensively in diagnostic and intra-operative imaging for MV procedures. Transesophageal echocardiography uses a 3D ultrasound probe which is passed through the esophagus, allowing for clear images of the mitral valve from the mid-esophageal position, an example of which we see in Figure 5.1. Identification of the mitral annulus shape is essential during diagnosis for a number of applications including identifying pathologies, surgical planning and implant design[88, 89, 90]. The mitral annulus is currently typically identi-

fied using manual or semi-automated methods, such as the Phlips' QLAB Mitral Valve Navigator tool with anatomic intelligence (Philips Healthcare, Andover, MA, USA), which introduces additional workload for clinicians. Additionally, for trans-catheter mitral valve procedures, real-time annulus tracking significantly improves the procedure accuracy as part of an IGS system by providing a clear, simple target to navigate towards [91].

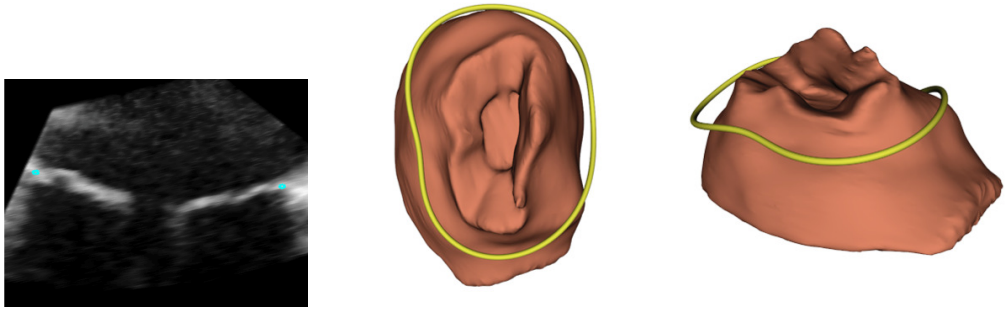

(a) (b) (c)

Figure 5.1: AP slice from TEE volume of mitral valve with annulus intersection shown in blue (a). Mitral leaflet segmentation with corresponding annulus contour (b and c).

Prior methods have been developed that initially identify the mitral annulus using a manual approach, then apply image registration between subsequent ultrasound frames to warp the existing annulus, and in this way track and update the annulus shape and position in real-time [92]. While these methods are effective for real-time tracking of the annulus, they have the potential to accumulate error, as each position is updated based on the relative change compared to the previous frame. Several methods which directly segment the annulus from ultrasound volumes have also been proposed. Early work based on optical flow can accurately identify the annulus, however it could only be applied to systolic images, and took 30-60 seconds to compute [81]. As a result, it is not possible to apply this technique for IGS applications which require real-time tracking of the annulus throughout the entire cardiac cycle.

More recently, deep learning based approaches have been proposed, primarily by taking 2D cross-sectional images through the 3D volume, which are rotated around the mitral valve [93, 86]. These methods achieve good performance, and achieve an accuracy of approximately 3.5 mm measured by the symmetric curve-to-curve error, which is computed by averaging the distances between each point on both curves to the nearest point on the other. The drawbacks of these methods are however, tied to the use of 2D images, where the mitral annulus is approximated by a spline fit through limited set of control points that ignores much of the available information that could be useful for automated analysis. Recently, Andreassen *et al.* [116] proposed a method utilizing fully 3D CNNs to predict a heatmap, which is then converted into coordinates using the geometric median, with reported accuracy of 1.9 mm curve-to-curve distance error. Although they are using 3D CNNs, they utilize a modified volume composed of a series of rotational planes stacked together into a new volume, which may introduce issues related to the distance between points on adjacent rotational planes, which increases further away from the centre of rotation. Additionally, only systolic frames were used from the examinations in their experiments.

Currently, for real-time applications, semi-automatic annulus tracking methods are the only approaches with sufficiently fast runtime to be suitable. Existing fully automatic approaches achieve very good accuracy, with the tradeoff of runtime performance. The best deep-learning based approach by Andreassen *et al.*[116] takes 1.8 seconds in full-resolution mode and 0.13 seconds in the reduced resolution fast mode. Ideally, for real-time ultrasound applications, runtime should be below 0.06 seconds, or 15 frames-per-second.

We propose a novel deep learning based mitral annulus detection algorithm, that performs directly in 3D, and is structured as a regression problem predicting a set of Fourier coefficients that define the mitral annulus coordinates. In the

SlicerHeart[117] extension for 3D Slicer, low-pass smoothing of the mitral annulus is performed in the spatial-frequency domain, where a 1D fast Fourier transform (FFT) of the coordinates in each of the three axes is completed, and then low-pass filtering is applied, and the smoothed annulus coordinates are recovered using the inverse FFT. In our work, we directly predict the corresponding Fourier coefficients of the annulus, and then through the inverse Fourier transform we generate the resulting set of 3D coordinates describing the mitral annulus, bypassing the need for an intermediate heatmap. This architecture was chosen in order to enable highly optimized inference, with fewer post-processing steps enabling its use in real-time surgical guidance applications.

5.2 Methods

From the 4D TEE datasets described in Chapters 3 and 4, we selected 90 cases to perform annulus segmentation for this work. These 90 cases contain a total of 2190 volumes. We split our dataset by case into training, validation and test sets with 78, 6, and 6 cases, respectively, corresponding to 1862, 186, and 142 volumes, respectively. We obtained ground-truth annulus labels through manual delineation of a single frame by an expert clinical user. We then track the annulus through the remainder of the cardiac cycle using an image registration approach, and manually verify and adjust the resulting annulus for each frame.

We apply a pre-processing pipeline to the volumes and annulus predictions including re-sampling, data re-formatting, cropping, and train-time data augmentation. We re-sample the ultrasound volumes to 0.5 mm isotropic spacing, and reorient them to the right-anterior-superior coordinate system for consistency between cases. Next, we centre crop the images to a constant size of 152 x 152 x 128 voxels. The annulus curves are initially defined as varying length lists of 3D coor-

dinates relative to the left, posterior, inferior corner of the volume. We re-sample the curves to a length of 200 points, and redefine the coordinates to be relative to the image centre. This enables consistent prediction from centre cropped volumes, as the locations in space of the corners may change, but the centre does not. Data augmentation was employed during training consisting of random rotations, flips, and translations applied to 25% of samples in each batch. Rotations of up to 20° are applied randomly on each axis, translations of up to 6.0 mm are used on all axes, and flips are applied only on the right-left axis. These augmentations are used to improve the generalizability of the prediction model, as the position of the valve and annulus within ultrasound volumes can vary significantly between cases.

Our network architecture uses a regressor approach based on an encoder backbone using EfficientNetB0 [118], followed by five fully connected layers of size 64, 32, 16 and 33 nodes, as shown in Figure 5.2 . The final layer outputs 33 values which then pass through a *tanh* activation function, scaling the output to between -1 and +1. Of these 33 values, 3 represent the origin, or centroid of the annulus. The remaining 30 values correspond to 5 magnitude, and 5 phase values for each of the 3 spatial axes. The annulus centroid coordinates are rescaled to the range of the image size given by ±48.0 mm. The magnitude values are rescaled to the range of 0 to 30, and the phase values to $\pm\pi$. The magnitude and phase values are finally converted into their corresponding real and imaginary components making up 5 smallest complex Fourier coefficients in each axis.

The final output of the model is in the shape (B, 6, 3, 2) where B is the batch size. This corresponds to 5 complex-valued Fourier coefficients for each of the 3 axes of the image plus the annulus centroid encoded as the DC coefficient. Following prediction the full mitral annulus shape can be sampled by zero-padding the coefficients to a size of 200, and taking the inverse FFT to produce set of 200 3D coordinates.

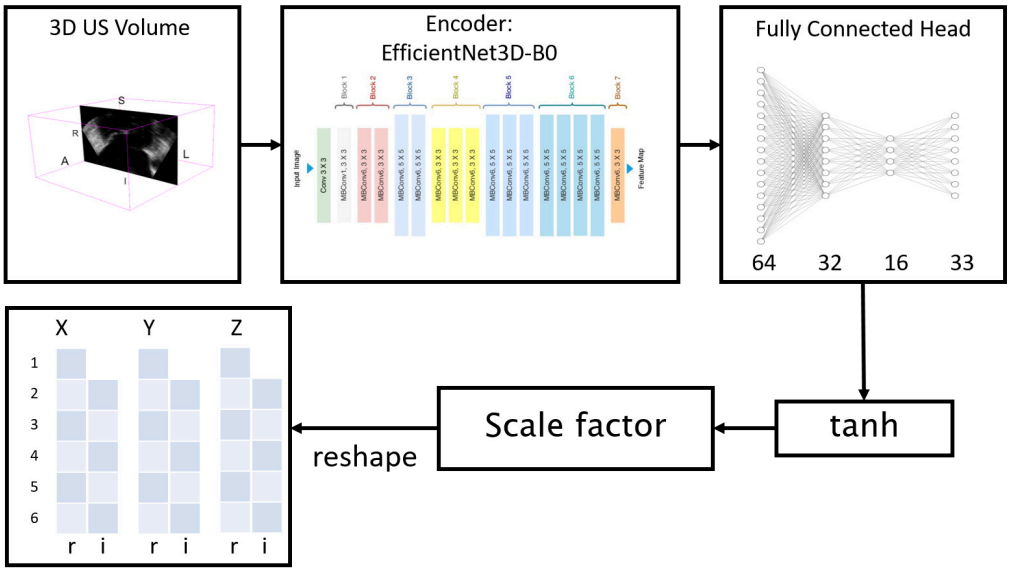

Figure 5.2: Flowchart describing overall network architecture to predict Fourier coefficients representing the mitral annulus.

The coordinate prediction error metrics reported in this work are the mean symmetric curve-to-curve distance as used by Andreassen *et al.* [116], the mean centroid distance, and mean perimeter error. The mean symmetric curve-to-curve distance error is computed by taking the mean of the Euclidean distance to the closest point from each coordinate on the predicted and ground-truth annulus to the other. The centroid error is the Euclidean distance from the centroid of the predicted annulus to the centroid of ground-truth. The perimeter error is the absolute difference between the perimeter of the prediction and the perimeter of the ground-truth.

For network training, we define our loss function as

$$loss = 2m + 0.5c + 0.1p + a \tag{5.1}$$

where m is the mean curve-to-curve distance, c is the mean centroid distance, p is the mean perimeter error and a is given by the angle in radians between 2π

and the total angular rotation of the prediction in the xy plane. This loss function incorporates all three evaluation metrics, with weighting determined through hyper-parameter tuning. The centroid distance is included to ensure the predicted annulus is centered in the correct position. The perimeter error and the final term a serve as regularization parameters to ensure the the predictions consist of one single complete rotation in the xy plane.

5.3 Results

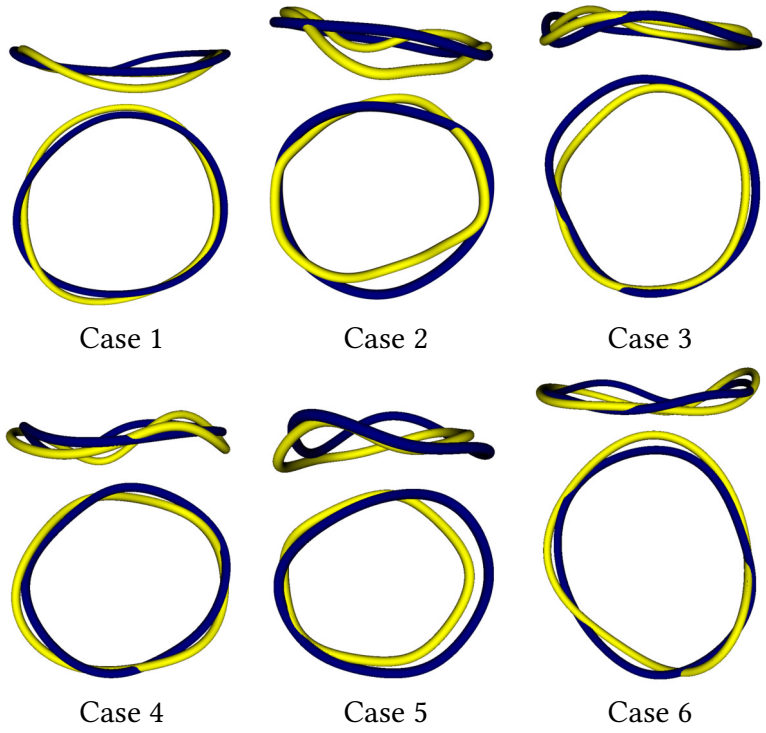

Figure 5.3: Predicted (blue) and ground-truth (yellow) annuli for six test set cases. For each case included is the side-view (top) and top-down view (bottom).

On our test set of 6 cases and 146 volumes, our method achieves a curve-to-curve error of 2.7 ± 0.4 mm, a centroid error of 2.3 ± 1.3 mm, and a perimeter error of 8.7 ± 4.3 mm. In our test data, average annulus diameter was 47.0 ± 7.7 mm, and average perimeter was 144.4 ± 21.6 mm. As indicated in Figure 5.3, from the top-

down view all six cases show good agreement between the predicted and ground-truth annuli. In cases two, three and five, there is a larger error over just a small portion of the annulus curve. From the side-on view, we see more inconsistencies between the prediction and ground-truth. Notably visible in cases two and five, the predicted annulus curve shows larger deviations, corresponding to a mis-prediction of the height of the annulus along the MV leaflets. The training error of our model reaches 0.46 ± 0.21 mm curve-to-curve distance, indicating our model is at present over-fitting the training data. The large discrepancy between the accuracy achieved on the training set compared to the test set indicates that the model is to an extent memorizing the training data, but does not generalize as well to unseen test data.

As shown in Figure 5.4, the accuracy of the model has large variability between cases, indicating that a larger dataset may be required to improve the consistency of the model. Looking across the six test cases, we see that the curve-to-curve and centroid errors are relatively similar between cases, with good accuracy in the curve-to-curve error corresponding with good accuracy in the centroid error. However, we see that in some cases where performance was poor in the curve-to-curve and centroid metric, the perimeter error is not correspondingly poor. This can indicate that the predicted annulus may be the correct size or shape, but positioned in the wrong location. We can isolate the curve-to-curve error by translating the predicted annuli to the ground-truth so the the centroids match, after which curve-to-curve error is reduced to 2.2 ± 0.3 mm. This demonstrates the coupling between curve-to-curve error and centroid error, as the model needs to accurately predict both the annulus shape and position relative to the image centre to achieve a low curve-to-curve error.

Our model achieves a total runtime of 26ms when using GPU acceleration, and 181ms when using only the CPU, when tested on a workstation with an Intel

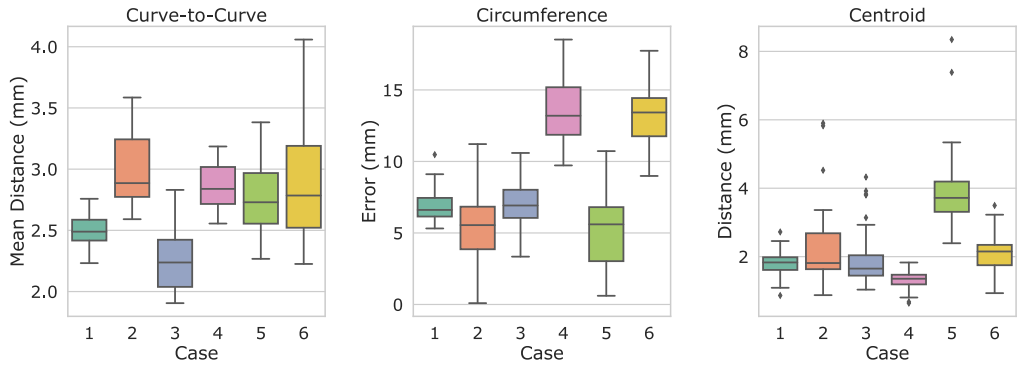

Figure 5.4: Results for all volumes separated by case including curve-to-curve distance, circumference error and centroid error.

i7 6700k processor, 32gb of memory, and an Nvidia GTX 1080 GPU with 8gb of memory. This runtime includes all stepss to go from the original US volume to predicted annulus coordinates. Image re-sampling takes approximately 16ms, our optimized model with GPU acceleration takes approximately 8ms, and the inverse FFT using the GPU takes 2ms.

5.4 Discussion

Our results demonstrate similar performance to prior work utilizing 2D based approaches with spline fitting to post process the predictions into a 3D annulus shape. We currently see higher prediction error than Andreassen *et al.* [116], who reported accuracy of 1.96 ± 1.62 mm using the curve-to-curve distance metric. However, we are not limited to using only systolic frames, which may have introduced additional variability in the manual segmentations, as they were using a semi-automated approach which can only be used at systole. Our method achieves real-time performance, taking only 26ms per frame to produce an annulus prediction, (approximately 40 frames-per-second). This approach would therefore be suitable for use in real-time applications such as image-guided procedures,

compared to prior methods[116] which take 1.7s at full resolution, or 0.17s at a reduced resolution with a reduction in accuracy to results similar to those shown here. By including the full cardiac cycle, our model will be able to track the mitral annulus at all points, enabling applications in image guidance where mitral annulus tracking can be beneficial [92].

To our knowledge, this is the first work to apply a regression model directly predicting Fourier coefficients to mitral annulus segmentation. This approach contributes to a well-defined, continuous and smooth annulus profile, which can be re-sampled to any number of points without compromising the annular shape. Since we only predict five coefficients, there is an inherent low-pass filter applied to the final annulus shape. This is not the case in heatmap based methods, where a single miss-prediction can create an incontinuity in the annulus, which is not desirable when performing quantification. As such, we see greater potential in the Fourier coefficient based approach for generalizing to new cases.

Currently, our reported error is slightly higher than existing state-of-the-art methods, although with greater potential inference speed. This work provides a foundation for further development, as we have demonstrated the feasibility of direct regression of the mitral annulus from 3D volumes. The use of the Fourier coefficient predictions enables very fast inference speeds and point sampling using the inverse FFT. Currently, our training set only includes 75 cases, which is sufficient for mitral valve leaflet segmentation [3], however may be insufficient for the less bounded annulus identification problem. Although we have a total of 1862 volumes for training, since they come from only 75 cases, there are limits in terms of range of valve pathology and image quality, as these will be relatively consistent within a single case. Heatmap based approaches may generalize better with a small number of images as they solve a segmentation problem, which is then sampled to identify the annulus as a set of coordinates. By directly predicting

the annulus shape, our model may have a greater ability to fit the data, however this also leads to a greater data requirement during training.

We see that our model is currently still over-fitting the training data, as there is a very small training error corresponding to relatively high validation and test error. Through hyper-parameter tuning we found that common techniques, such as employing dropout and data augmentation, produced only small improvements in validation error with our given architecture. To address this in future work we will aim to further increase the size of the dataset to provide a wider range of training examples. Additionally, further exploration of alternative encoding architectures may yield models with greater ability to generalize to the test data. Vision transformer networks have shown promise in medical imaging applications such as image registration due to their ability to encode non-local spatial relationships, which conventional CNN based approaches cannot[119]. Alternatively, there is a wide range of architectures that can be used for CNN based encoders that offer various trade offs between complexity and performance, with differing data requirements for training. Since our network architecture is separated into two components, with a CNN based encoder followed by flattening and a prediction head using fully-connected layers, we can further experiment with drop-in replacements to the EfficientNet based encoder used here.

5.5 Conclusions

Delineation of the mitral annulus is an important step for valve quantification, patient-specific modelling, and real-time guidance applications. In this chapter, we present a 3D CNN based model for segmenting the mitral annulus. Our method uses a novel approach in which a regression model predicts the five smallest Fourier coefficients of the mitral annulus in each of the three axes, which can then

be converted to coordinates with any desired sample density through the inverse Fourier transform. This representation allows us to achieve real-time inference speed, enabling the use of this work in surgical guidance applications. Overall, the results of this work demonstrate state-of-the-art runtime speed, with good overall accuracy. The algorithm described can be integrated into a patient-specific modelling workflow to further reduce manual overhead, and can also enable more robust annulus tracking in surgical guidance applications.

Chapter 6

Conclusions

Mitral valve disease is a common pathologic problem occurring increasingly in an aging population. Many patients suffering from mitral valve disease require surgical intervention to restore normal valve function. Diagnostic imaging available for the mitral valve includes ultrasound, cardiac CT, and CMR, with ultrasound in the form of 3D TEE being the primary method used. Mitral valve interventions are difficult procedures, and planning a surgical or transcatheter approach from diagnostic imaging alone remains one of the most significant clinical challenges. While TEE is used as the primary imaging modality, it can be limited in image quality, signal dropout and field-of-view, contributing to the difficulty in planning an interventional approach. The development of simulation approaches utilizing patient-specific mitral valve models has shown promise for both training and procedure planning. However, a major barrier to producing accurate models of a patient's valve is the necessity of deriving the leaflet geometry through segmentation of diagnostic TEE imaging. The goal of this thesis is to address the challenge of producing patient-specific mitral valve models through the development of volume compounding and automated image analysis to more accurately and quickly capture the relevant valve geometry.

6.1 Thesis Contributions

In this thesis I present a collection of methods aimed towards addressing the challenges in using cardiac ultrasound imaging for mitral valve quantification and modelling. Chapter 2 describes the methods used to register and blend multiple views acquired with a standard TEE probe without external tracking hardware. Standard TEE volumes can visualize the mitral valve, however, structures beyond the valve are difficult to see. Alternative imaging approaches such as cardiac CT are often needed to accurately image the sub-valvular structures, however, not all patients are eligible for CT imaging. The work explores the acquisition protocol used to acquire the separate views, as well as the registration algorithm used to align the volumes, and the blending strategy used to create the final image. The results indicate that I successfully demonstrated the creation of extended field-of-view volumes of the mitral valve and LV, which can clearly visualize otherwise difficult-to-see structures such as the chordae tendineae and papillary muscles using standard ultrasound hardware. I have described a workflow for capturing a series of volumes using a TEE probe during standard diagnostic imaging that can then be registered and compounded together. I demonstrate improvements to the compounding process in terms of registration robustness and final image quality. These compounded volumes capture the sub-valvular structures of interest for cardiac procedure planning such as the LVOT, chordae tendineae and papillary muscles. This method is able to provide clinicians with a single volume that captures the mitral valve and the sub-valvular structures using existing standard-of-care ultrasound imaging. For patients who are not eligible for cardiac CT imaging, this provides an alternative approach that captures the same anatomical detail which may not otherwise be visible. Furthermore, we can incorporate the additional detail available in compounded volumes to create more accurate patient-specific models, particularly in regard to the papillary muscles and chor-

dae tendineae. Overall, this represents potential improvements in both diagnostics and procedure planning from 3D TEE imaging.

Identifying, or segmenting, the mitral leaflets from TEE volumes is an important step in diagnosis for quantification of the valve, as well as patient-specific valve modelling. In Chapters 3 and 4 I present methods developed for automating the segmentation process, as well as the curation and release of a public dataset through a conference challenge. In Chapter 3 I describe a semi-automatic workflow that keeps the user in the loop through an iterative active contour algorithm. The results indicate that this workflow enables accurate segmentation with a reduction in the time required when compared to manual annotation. I also describe the 3D Slicer module that serves as the user interface for this method, as well as the automated further mesh modelling steps required to generate a 3D printable mold. Overall, the software presented in this chapter enables a user to quickly go from a patient TEE volume to a 3D printable mesh in a series of four steps. This serves to simplify patient-specific valve modelling workflow and was actively used as part of a study evaluating physical valve replication and simulation through the use of a pulse duplicator device. There is a strong need for purpose built software for valve modelling applications to enable clinical translation, as relying on complicated computer-aided-design software and manual segmentations maintains a burden of expertise and time that may not be feasible for clinical or commercial adoption.

In Chapter 4 I present a follow up method to that discussed in Chapter 3 expanding on my work on mitral valve segmentation. While the semi-automatic approach achieved sufficient accuracy for the application of patient-spefic modelling, there was room to improve upon both the speed and accuracy of the approach. The goal of this chapter was to develop a fully automatic mitral valve segmentation pipeline based on deep learning using CNNs. The first challenge I

addressed towards using deep learning was the requirement of a sufficiently large dataset to train and evaluate a machine learning method. Through the use of my semi-automatic segmentation software in the valve modelling validation study, I was able to curate a dataset sufficient for demonstrating the applicability of CNNs for mitral valve leaflet segmentation with DeepMitral v1. Moving from active contours to deep learning enabled the reduction in runtime from ten minutes down to only a few seconds, while simultaneously improving the accuracy of the segmentation to sub-millimetre average surface distance. This represents a substantial step towards fully automating leaflet segmentation, both for valve modelling and additional clinical quantification work. DeepMitral v1 was then integrated into the 3D Slicer module described in Chapter 3, and I continued to work on curating a larger dataset of expert annotations suitable for public release. The culmination of this work was a public dataset of 150 cases with 3D TEE and labelled mitral valve leaflets, initially released through a MICCAI 2023 challenge. This will serve as a valuable resource to the wider research community working on the mitral valve, and may open opportunities of research not otherwise possible due to limited access to data.

While the previous two chapters focused on automated segmentation of the mitral valve leaflets, there are many other structures of interest related to the mitral valve. Chapter 5 moves beyond the valve leaflets to dicuss the automatic detection and tracking of the mitral valve annulus. Leaflet segmentation is the most important step for mitral valve modelling to accurately capture the valve geometry, however, to accurately replicate the valve dynamics it is necessary to identify the annulus to determine the hinge point of the leaflet. In addition to its importance for replicating valve dynamics, the annulus is used as a key structure for valve quantification and classification of pathology, and has also been used as a visualization target in surgical navigation systems for trans-catheter mitral

valve procedures. This chapter demonstrates how a deep learning method using a CNN backbone can directly predict the mitral annulus shape and position through the use of the Fourier representation of the annulus curve's 3D coordinates. This method works directly with 3D volumes, and can be deployed in real-time using GPU acceleration. This annulus detection algorithm contributes to the research community by demonstrating the feasibility of a novel approach to annulus tracking in real-time, and could be integrated into future projects incorporating the annulus as a structure of interest in surgical navigation systems.

It is my hope that by developing the techniques described in this thesis mitral valve modelling and procedure planning using TEE imaging can be improved. This thesis demonstrates how volume compounding can expand the field-of-view and range of structures visible with a standard TEE probe, expanding the potential clinical utility of the existing standard-of-care imaging modality. Furthermore, it demonstrated how automated processing 3D TEE volumes of the mitral valve can automatically extract key geometric information critical for valve modelling and valve quantification. This geometric information was used to automate several steps in a mitral valve modelling workflow helping to improve the accessibility and consistency of the valve replicas. These advances have the potential to enable clinicians to better plan their mitral valve repair strategy through the combination of improved imaging, automated ultrasound image analysis, and more accessible patient-specific valve modelling.

Bibliography

[1] P. Carnahan, J. Moore, D. Bainbridge, E. C. S. Chen, and T. M. Peters, "Multi-view 3D transesophageal echocardiography registration and volume compounding for mitral valve procedure planning," *Applied Sciences*, vol. 12, p. 4562, Apr. 2022.

[2] P. Carnahan, O. Ginty, J. Moore, A. Lasso, M. A. Jolley, C. Herz, M. Eskandari, D. Bainbridge, and T. M. Peters, "Interactive-Automatic Segmentation and Modelling of the Mitral Valve," in *Functional Imaging and Modeling of the Heart*, pp. 397–404, Springer International Publishing, June 2019.

[3] P. Carnahan, J. Moore, D. Bainbridge, M. Eskandari, E. C. S. Chen, and T. M. Peters, "DeepMitral: Fully automatic 3D echocardiography segmentation for patient specific mitral valve modelling," in *Medical Image Computing and Computer Assisted Intervention – MICCAI 2021*, pp. 459–468, Springer International Publishing, 2021.

[4] P. K. Carnahan, A. Bharucha, M. Eskandari, D. Bainbridge, E. C. S. Chen, and T. M. Peters, "Real-time mitral annulus segmentation from 4D transesophageal echocardiography using deep learning regression," in *Medical Imaging 2023: Image Processing* (I. Išgum and O. Colliot, eds.), SPIE, Apr. 2023.

[5] K. P. McCarthy, L. Ring, and B. S. Rana, "Anatomy of the mitral valve: understanding the mitral valve complex in mitral regurgitation," *European Journal of Echocardiography*, vol. 11, pp. i3–i9, Nov. 2010.

[6] J. L. Quill, A. J. Hill, T. G. Laske, O. Alfieri, and P. A. Iaizzo, "Mitral leaflet anatomy revisited," *The Journal of Thoracic and Cardiovascular Surgery*, vol. 137, pp. 1077–1081, May 2009.

[7] G. Gogoladze, S. L. Dellis, R. Donnino, G. Ribakove, D. G. Greenhouse, A. Galloway, and E. Grossi, "Analysis of the mitral coaptation zone in normal and functional regurgitant valves," *The Annals of Thoracic Surgery*, vol. 89, pp. 1158–1161, Apr. 2010.

[8] R. Yamada, N. Watanabe, T. Kume, M. Tsukiji, T. Kawamoto, Y. Neishi, A. Hayashida, E. Toyota, H. Okura, and K. Yoshida, "Quantitative measurement of mitral valve coaptation in functional mitral regurgitation: In vivo experimental study by real-time three-dimensional echocardiography," *Journal of Cardiology*, vol. 53, pp. 94–101, Feb. 2009.

[9] J. A. Ormiston, P. M. Shah, C. Tei, and M. Wong, "Size and motion of the mitral valve annulus in man. i. a two-dimensional echocardiographic method and findings in normal subjects.," *Circulation*, vol. 64, pp. 113–120, July 1981.

[10] J. H. C. Lam, N. Ranganathan, E. D. Wigle, and M. D. Silver, "Morphology of the human mitral valve: I. chordae tendineae: A new classification," *Circulation*, vol. 41, no. 3, pp. 449–458, 1970.

[11] I. E. Rusted, C. H. Scheifley, and J. E. Edwards, "Studies of the mitral valve. i. anatomic features of the normal mitral valve and associated structures," *Circulation*, vol. 6, no. 6, pp. 825–831, 1952.

[12] G. A. Fishbein and M. C. Fishbein, "Mitral valve pathology," *Current Cardiology Reports*, vol. 21, May 2019.

[13] A. Sagie, N. Freitas, L. R. Padial, M. Leavitt, E. Morris, A. E. Weyman, and R. A. Levine, "Doppler echocardiographic assessment of long-term progression of mitral stenosis in 103 patients: Valve area and right heart disease," *Journal of the American College of Cardiology*, vol. 28, pp. 472–479, Aug. 1996.

[14] S. Ray, "Changing epidemiology and natural history of valvular heart disease," *Clinical Medicine*, vol. 10, no. 2, pp. 168–171, 2010.

[15] G. Ailawadi, B. R. Swenson, M. E. Girotti, L. M. Gazoni, B. B. Peeler, J. A. Kern, L. M. Fedoruk, and I. L. Kron, "Is Mitral Valve Repair Superior to Replacement in Elderly Patients?," *The Annals of Thoracic Surgery*, vol. 86, pp. 77–86, July 2008.

[16] C. A. McNeely and C. M. Vassileva, "Long-term outcomes of mitral valve repair versus replacement for degenerative disease: a systematic review.," *Current Cardiology Reviews*, vol. 11, no. 2, pp. 157–62, 2015.

[17] M. H. Eng and D. D. Wang, "Transcatheter mitral valve therapy: Defining the patient who will benefit," *Current Cardiology Reports*, vol. 20, Sept. 2018.

[18] E. A. Grossi, A. C. Galloway, G. H. Ribakove, P. K. Zakow, C. C. Derivaux, F. G. Baumann, D. Schwesinger, and S. B. Colvin, "Impact of minimally invasive valvular heart surgery: a case-control study," *The Annals of Thoracic Surgery*, vol. 71, pp. 807–810, Mar. 2001.

[19] D. M. Holzhey, J. Seeburger, M. Misfeld, M. A. Borger, and F. W. Mohr, "Learning Minimally Invasive Mitral Valve Surgery," *Circulation*, vol. 128, pp. 483–491, July 2013.

[20] L. Gheorghe, J. Brouwer, D. D. Wang, N. Wunderlich, B. Rana, B. Rensing, F. Eefting, L. Timmers, and M. Swaans, "Current devices in mitral valve replacement and their potential complications," *Frontiers in Cardiovascular Medicine*, vol. 7, Nov. 2020.

[21] A. W. Asgar, E. Horlick, K. McKenzie, N. Brass, W. J. Cantor, A. Chan, A. Della Siega, J. F. Gobeil, S. Kassam, M. P. Love, *et al.*, "Structural heart disease intervention: the Canadian landscape," *Canadian Journal of Cardiology*, vol. 33, pp. 1197–1200, Sept. 2017.

[22] A. M. Gillinov, K. Tantiwongkosri, E. H. Blackstone, P. L. Houghtaling, E. R. Nowicki, J. F. Sabik, D. R. Johnston, L. G. Svensson, and T. Mihaljevic, "Is prosthetic anuloplasty necessary for durable mitral valve repair?," *The Annals of Thoracic Surgery*, vol. 88, pp. 76–82, July 2009.

[23] M. Marin Cuartas, H. Javadikasgari, B. Pfannmueller, J. Seeburger, A. M. Gillinov, R. M. Suri, and M. A. Borger, "Mitral valve repair: Robotic and other minimally invasive approaches.," *Progress in cardiovascular diseases*, vol. 60, pp. 394–404, 2017.

[24] P. C. Saunders, E. A. Grossi, C. F. Schwartz, J. B. Grau, G. H. Ribakove, A. T. Culliford, R. M. Applebaum, A. C. Galloway, and S. B. Colvin, "Anterior leaflet resection of the mitral valve," *Seminars in Thoracic and Cardiovascular Surgery*, vol. 16, pp. 188–193, June 2004.

[25] O. Alfieri, F. Maisano, M. De Bonis, P. L. Stefano, L. Torracca, M. Oppizzi, and G. La Canna, "The double-orifice technique in mitral valve repair: a simple solution for complex problems.," *The Journal of thoracic and cardiovascular surgery*, vol. 122, pp. 674–681, Oct. 2001.

[26] S. K. Bhudia, P. M. McCarthy, N. G. Smedira, B.-K. Lam, J. Rajeswaran, and E. H. Blackstone, "Edge-to-edge (Alfieri) mitral repair: results in diverse clinical settings.," *The Annals of thoracic surgery*, vol. 77, pp. 1598–1606, May 2004.

[27] M. Gavazzoni, M. Taramasso, M. Zuber, G. Russo, A. Pozzoli, M. Miura, and F. Maisano, "Conceiving MitraClip as a tool: percutaneous edge-to-edge repair in complex mitral valve anatomies.," *European heart journal. Cardiovascular Imaging*, vol. 21, pp. 1059–1067, Oct. 2020.

[28] T. E. David, "Artificial chordae," *Seminars in Thoracic and Cardiovascular Surgery*, vol. 16, pp. 161–168, jun 2004.

[29] A. Colli, E. Manzan, F. Z. Fabio, C. Sarais, D. Pittarello, G. Speziali, and G. Gerosa, "TEE-guided transapical beating-heart neochord implantation in mitral regurgitation.," *JACC. Cardiovascular imaging*, vol. 7, pp. 322–323, Mar. 2014.

[30] D. Burckhardt, A. Hoffmann, and W. Kiowski, "Treatment of mitral stenosis.," *European heart journal*, vol. 12 Suppl B, pp. 95–98, July 1991.

[31] Y. Chandrashekhar, S. Westaby, and J. Narula, "Mitral stenosis.," *Lancet (London, England)*, vol. 374, pp. 1271–1283, Oct. 2009.

[32] M. Taramasso, A. Candreva, A. Pozzoli, A. Guidotti, O. Gaemperli, F. Nietlispach, J. Barthelmes, M. Y. Emmert, A. Weber, S. Benussi, *et al.*, "Current challenges in interventional mitral valve treatment," *Journal of thoracic disease*, vol. 7, no. 9, p. 1536, 2015.

[33] A. Sengupta, S. L. Alexis, S. Zaid, G. H. L. Tang, S. Lerakis, and R. P. Martin, "Imaging the mitral valve: a primer for the interventional surgeon," *Annals of Cardiothoracic Surgery*, vol. 10, pp. 28–42, jan 2021.

[34] F. Mahmood and R. Matyal, "A Quantitative Approach to the Intraoperative Echocardiographic Assessment of the Mitral Valve for Repair," *Anesthesia & Analgesia*, vol. 121, pp. 34–58, July 2015.

[35] R. T. Hahn, T. Abraham, M. S. Adams, C. J. Bruce, K. E. Glas, R. M. Lang, S. T. Reeves, J. S. Shanewise, S. C. Siu, W. Stewart, and M. H. Picard, "Guidelines for performing a comprehensive transesophageal echocardiographic examination: recommendations from the American Society of Echocardiography and the Society of Cardiovascular Anesthesiologists.," *Journal of the American Society of Echocardiography : official publication of the American Society of Echocardiography*, vol. 26, pp. 921–964, Sept. 2013.

[36] J. J. Bax, P. Debonnaire, P. Lancellotti, N. A. Marsan, L. F. Tops, J. K. Min, N. Piazza, J. Leipsic, R. T. Hahn, and V. Delgado, "Transcatheter interventions for mitral regurgitation," *JACC: Cardiovascular Imaging*, vol. 12, pp. 2029–2048, Oct. 2019.

[37] S. Uretsky, E. Argulian, J. Narula, and S. D. Wolff, "Use of cardiac magnetic resonance imaging in assessing mitral regurgitation," *Journal of the American College of Cardiology*, vol. 71, pp. 547–563, Feb. 2018.

[38] W. A. Zoghbi, D. Adams, R. O. Bonow, M. Enriquez-Sarano, E. Foster, P. A. Grayburn, R. T. Hahn, Y. Han, J. Hung, R. M. Lang, S. H. Little, D. J. Shah, S. Shernan, P. Thavendiranathan, J. D. Thomas, and N. J. Weissman, "Recommendations for noninvasive evaluation of native valvular regurgitation," *Journal of the American Society of Echocardiography*, vol. 30, pp. 303–371, Apr. 2017.

[39] J. Leipsic, S. Abbara, S. Achenbach, R. Cury, J. P. Earls, G. B. J. Mancini, K. Nieman, G. Pontone, and G. L. Raff, "SCCT guidelines for the interpreta-

tion and reporting of coronary CT angiography: A report of the Society of Cardiovascular Computed Tomography Guidelines Committee," *Journal of Cardiovascular Computed Tomography*, vol. 8, pp. 342–358, Sept. 2014.

[40] G. Feuchtner, "Imaging of cardiac valves by computed tomography," *Scientifica*, vol. 2013, pp. 1–13, Dec. 2013.

[41] K. S. Kunzelman, R. P. Cochran, E. D. Verrier, and R. C. Eberhart, "Anatomic basis for mitral valve modelling.," *The Journal of heart valve disease*, vol. 3, pp. 491–496, Sept. 1994.

[42] M. G. Bateman and P. A. Iaizzo, "Imaging in the context of replacement heart valve development: use of the Visible Heart(®) methodologies.," *Cardiovascular diagnosis and therapy*, vol. 2, pp. 220–230, Sept. 2012.

[43] D. Oliveira, J. Srinivasan, D. Espino, K. Buchan, D. Dawson, and D. Shepherd, "Geometric description for the anatomy of the mitral valve: A review," *Journal of Anatomy*, vol. 237, pp. 209–224, Apr. 2020.

[44] F. Mahmood, K. Owais, M. Montealegre-Gallegos, R. Matyal, P. Panzica, A. Maslow, and K. R. Khabbaz, "Echocardiography derived three-dimensional printing of normal and abnormal mitral annuli.," *Annals of cardiac anaesthesia*, vol. 17, pp. 279–283, Dec. 2014.

[45] O. Ginty, J. Moore, T. Peters, and D. Bainbridge, "Modeling patient-specific deformable mitral valves," *Journal of Cardiothoracic and Vascular Anesthesia*, vol. 32, pp. 1368–1373, June 2018.

[46] A. E. Morgan, J. L. Pantoja, J. Weinsaft, E. Grossi, J. M. Guccione, L. Ge, and M. Ratcliffe, "Finite element modeling of mitral valve repair," *Journal of Biomechanical Engineering*, vol. 138, Jan. 2016.

[47] J. Park, A. Geirsson, and P. N. Bonde, "Mathematical blueprint of a mitral valve," *Seminars in Thoracic and Cardiovascular Surgery*, vol. 31, no. 3, pp. 399–411, 2019.

[48] S. Schievano, K. Kunzelman, M. A. Nicosia, R. P. Cochran, D. R. Einstein, S. Khambadkone, and P. Bonhoeffer, "Percutaneous mitral valve dilatation: single balloon versus double balloon. a finite element study.," *The Journal of heart valve disease*, vol. 18, pp. 28–34, Jan. 2009.

[49] K. S. Kunzelman, R. P. Cochran, C. Chuong, W. S. Ring, E. D. Verrier, and R. D. Eberhart, "Finite element analysis of the mitral valve.," *The Journal of heart valve disease*, vol. 2, pp. 326–340, May 1993.

[50] K. May-Newman and F. C. Yin, "A constitutive law for mitral valve tissue.," *Journal of biomechanical engineering*, vol. 120, pp. 38–47, Feb. 1998.

[51] V. Prot, B. Skallerud, G. Sommer, and G. A. Holzapfel, "On modelling and analysis of healthy and pathological human mitral valves: two case studies.," *Journal of the mechanical behavior of biomedical materials*, vol. 3, pp. 167–177, Feb. 2010.

[52] M. Stevanella, E. Votta, and A. Redaelli, "Mitral valve finite element modeling: implications of tissues' nonlinear response and annular motion.," *Journal of biomechanical engineering*, vol. 131, p. 121010, Dec. 2009.

[53] E. Votta, F. Maisano, S. F. Bolling, O. Alfieri, F. M. Montevecchi, and A. Redaelli, "The Geoform disease-specific annuloplasty system: a finite element study.," *The Annals of thoracic surgery*, vol. 84, pp. 92–101, July 2007.

[54] M. Stevanella, F. Maffessanti, C. A. Conti, E. Votta, A. Arnoldi, M. Lombardi, O. Parodi, E. G. Caiani, and A. Redaelli, "Mitral valve patient-specific finite

element modeling from cardiac MRI: Application to an annuloplasty procedure," *Cardiovascular Engineering and Technology*, vol. 2, pp. 66–76, jan 2011.

[55] A. Avanzini, "A computational procedure for prediction of structural effects of edge-to-edge repair on mitral valve.," *Journal of biomechanical engineering*, vol. 130, p. 031015, June 2008.

[56] K. D. Lau, V. Díaz-Zuccarini, P. Scambler, and G. Burriesci, "Fluid-structure interaction study of the edge-to-edge repair technique on the mitral valve.," *Journal of biomechanics*, vol. 44, pp. 2409–2417, Sept. 2011.

[57] A. Avanzini, G. Donzella, and L. Libretti, "Functional and structural effects of percutaneous edge-to-edge double-orifice repair under cardiac cycle in comparison with suture repair.," *Proceedings of the Institution of Mechanical Engineers. Part H, Journal of engineering in medicine*, vol. 225, pp. 959–971, Oct. 2011.

[58] K. Rangarajan, H. Davis, and P. H. Pucher, "Systematic review of virtual haptics in surgical simulation: A valid educational tool?," *Journal of Surgical Education*, vol. 77, pp. 337–347, mar 2020.

[59] T. Shirakawa, M. Yoshitatsu, Y. Koyama, A. Kurata, T. Miyoshi, H. Mizoguchi, T. Masai, K. Toda, and Y. Sawa, "To what extent can 3D model replicate dimensions of individual mitral valve prolapse?," *Journal of artificial organs : the official journal of the Japanese Society for Artificial Organs*, vol. 21, pp. 348–355, Sept. 2018.

[60] P. Sardari Nia, S. Heuts, J. Daemen, P. Luyten, J. Vainer, J. Hoorntje, E. Cheriex, and J. Maessen, "Preoperative planning with three-dimensional reconstruction of patient's anatomy, rapid prototyping and simulation

for endoscopic mitral valve repair.," *Interactive cardiovascular and thoracic surgery*, vol. 24, pp. 163–168, Feb. 2017.

[61] Y. Yang, H. Wang, H. Song, Y. Hu, Q. Gong, Y. Xiong, J. Liu, W. Ren, and Q. Zhou, "Morphological evaluation of mitral valve based on three-dimensional printing models: Potential implication for mitral valve repair," *BIO Integration*, vol. 2, pp. 143–151, dec 2021.

[62] J. Chikwe, N. Toyoda, A. C. Anyanwu, S. Itagaki, N. N. Egorova, P. Boateng, A. El-Eshmawi, and D. H. Adams, "Relation of mitral valve surgery volume to repair rate, durability, and survival," *Journal of the American College of Cardiology*, vol. 69, no. 19, pp. 2397–2406, 2017.

[63] D. J. LaPar, G. Ailawadi, J. M. Isbell, I. K. Crosby, J. A. Kern, J. B. Rich, A. M. Speir, I. L. Kron, I. for the Virginia Cardiac Surgery Quality Initiative, *et al.*, "Mitral valve repair rates correlate with surgeon and institutional experience," *The Journal of thoracic and cardiovascular surgery*, vol. 148, no. 3, pp. 995–1004, 2014.

[64] J. Vozenilek, "See one, do one, teach one: Advanced technology in medical education," *Academic Emergency Medicine*, vol. 11, pp. 1149–1154, nov 2004.

[65] R. Rocha e Silva, A. L. Jr., M. Goncharov, and F. B. Jatene, "Low cost simulator for heart surgery training," *Brazilian Journal of Cardiovascular Surgery*, vol. 31, pp. 449–453, 2016.

[66] P. Kozlowski, R. S. Bandaru, J. D'hooge, and E. Samset, "Real-time catheter localization and visualization using three-dimensional echocardiography," in *Medical Imaging 2017: Image-Guided Procedures, Robotic Interventions, and Modeling* (R. J. Webster and B. Fei, eds.), SPIE, Mar. 2017.

[67] A. Mashari, Z. Knio, J. Jeganathan, M. Montealegre-Gallegos, L. Yeh, Y. Amador, R. Matyal, R. Saraf, K. Khabbaz, and F. Mahmood, "Hemodynamic Testing of Patient-Specific Mitral Valves Using a Pulse Duplicator: A Clinical Application of Three-Dimensional Printing," *Journal of Cardiothoracic and Vascular Anesthesia*, vol. 30, pp. 1278–1285, Oct. 2016.

[68] O. K. Ginty, J. T. Moore, M. Eskandari, P. Carnahan, A. Lasso, M. A. Jolley, M. Monaghan, and T. M. Peters, "Dynamic, patient-specific mitral valve modelling for planning transcatheter repairs," *International Journal of Computer Assisted Radiology and Surgery*, vol. 14, pp. 1227–1235, May 2019.

[69] A. Perperidis, "Postprocessing Approaches for the Improvement of Cardiac Ultrasound B-Mode Images: A Review," *IEEE Transactions on Ultrasonics, Ferroelectrics, and Frequency Control*, vol. 63, pp. 470–485, Mar. 2016.

[70] P. Soler, G. Delso, N. Villain, E. Angelini, and I. Bloch, "Superresolution spatial compounding techniques with application to 3D breast ultrasound imaging," in *SPIE Proceedings* (S. Emelianov and W. F. Walker, eds.), SPIE, Mar. 2006.

[71] R. Wright, N. Toussaint, A. Gomez, V. Zimmer, B. Khanal, J. Matthew, E. Skelton, B. Kainz, D. Rueckert, J. V. Hajnal, and J. A. Schnabel, "Complete fetal head compounding from multi-view 3D ultrasound," in *Lecture Notes in Computer Science*, pp. 384–392, Springer International Publishing, 2019.

[72] C. Szmigielski, K. Rajpoot, V. Grau, S. G. Myerson, C. Holloway, J. A. Noble, R. Kerber, and H. Becher, "Real-Time 3D Fusion Echocardiography," *JACC: Cardiovascular Imaging*, vol. 3, pp. 682–690, July 2010.

[73] G. Gao, K. Reddy, Y. Ma, and K. S. Rhode, "Real-time compounding of three-dimensional transesophageal echocardiographic volumes: The phantom study," in *2009 Annual International Conference of the IEEE Engineering in Medicine and Biology Society*, IEEE, Sept. 2009.

[74] P. Biaggi, S. Jedrzkiewicz, C. Gruner, M. Meineri, J. Karski, A. Vegas, F. C. Tanner, H. Rakowski, J. Ivanov, T. E. David, and A. Woo, "Quantification of mitral valve anatomy by three-dimensional transesophageal echocardiography in mitral valve prolapse predicts surgical anatomy and the complexity of mitral valve repair.," *Journal of the American Society of Echocardiography : official publication of the American Society of Echocardiography*, vol. 25, pp. 758–765, July 2012.

[75] K. R. Khabbaz, F. Mahmood, O. Shakil, H. J. Warraich, J. H. Gorman, R. C. Gorman, R. Matyal, P. Panzica, and P. E. Hess, "Dynamic 3-dimensional echocardiographic assessment of mitral annular geometry in patients with functional mitral regurgitation.," *The Annals of thoracic surgery*, vol. 95, pp. 105–110, Jan. 2013.

[76] A. M. Gillinov and M. K. Banbury, "Pre-Measured Artificial Chordae for Mitral Valve Repair," *The Annals of Thoracic Surgery*, vol. 84, pp. 2127–2129, Dec. 2007.

[77] D. Grinberg, M.-Q. Le, Y. J. Kwon, M. A. Fernandez, D. Audigier, F. Ganet, J.-F. Capsal, J. F. Obadia, and P.-J. Cottinet, "Mitral valve repair based on intraoperative objective measurement," *Scientific Reports*, vol. 9, Mar. 2019.

[78] A. S. Jassar, C. J. Brinster, M. Vergnat, J. D. Robb, T. J. Eperjesi, A. M. Pouch, A. T. Cheung, S. J. Weiss, M. A. Acker, J. H. Gorman, R. C. Gorman, and B. M. Jackson, "Quantitative Mitral Valve Modeling Using Real-Time Three-

Dimensional Echocardiography: Technique and Repeatability," *The Annals of Thoracic Surgery*, vol. 91, pp. 165–171, Jan. 2011.

[79] P. Burlina, C. Sprouse, D. DeMenthon, A. Jorstad, R. Juang, F. Contijoch, T. Abraham, D. Yuh, and E. McVeigh, "Patient-Specific Modeling and Analysis of the Mitral Valve Using 3D-TEE," in *Information Processing in Computer-Assisted Interventions*, pp. 135–146, Springer, Jan. 2010.

[80] R. J. Schneider, N. A. Tenenholtz, D. P. Perrin, G. R. Marx, P. J. del Nido, and R. D. Howe, "Patient-Specific Mitral Leaflet Segmentation from 4D Ultrasound," in *Medical Image Computing and Computer-Assisted Intervention – MICCAI 2011* (G. Fichtinger, A. Martel, and T. Peters, eds.), (Berlin, Heidelberg), pp. 520–527, Springer Berlin Heidelberg, 2011.

[81] R. J. Schneider, D. P. Perrin, N. V. Vasilyev, G. R. Marx, P. J. del Nido, and R. D. Howe, "Mitral annulus segmentation from four-dimensional ultrasound using a valve state predictor and constrained optical flow," *Medical Image Analysis*, vol. 16, pp. 497–504, Feb. 2012.

[82] C.-N. Jin, I. S. Salgo, R. J. Schneider, W. Feng, F.-X. Meng, K. K.-H. Kam, W.-K. Chi, C.-Y. So, C. Chan, J.-P. Sun, G. Tsui, K.-Y. K. Wong, C.-M. Yu, S. Wan, R. Wong, M. Underwood, S. Au, S.-K. Ng, and A. P.-W. Lee, "Automated quantification of mitral valve anatomy using anatomical intelligence in three-dimensional echocardiography.," *International journal of cardiology*, vol. 199, pp. 232–238, Nov. 2015.

[83] R. I. Ionasec, I. Voigt, B. Georgescu, Y. Wang, H. Houle, F. Vega-Higuera, N. Navab, and D. Comaniciu, "Patient-Specific Modeling and Quantification of the Aortic and Mitral Valves From 4-D Cardiac CT and TEE," *IEEE Transactions on Medical Imaging*, vol. 29, pp. 1636–1651, Sept. 2010.

[84] I. Voigt, R. I. Ionasec, B. Georgescu, H. Houle, M. Huber, J. Hornegger, and D. Comaniciu, "Model-driven physiological assessment of the mitral valve from 4D TEE," in *SPIE Proceedings* (M. I. Miga and K. H. Wong, eds.), SPIE, feb 2009.

[85] A. M. Pouch, H. Wang, M. Takabe, B. M. Jackson, J. H. Gorman, R. C. Gorman, P. A. Yushkevich, and C. M. Sehgal, "Fully automatic segmentation of the mitral leaflets in 3D transesophageal echocardiographic images using multi-atlas joint label fusion and deformable medial modeling.," *Medical Image Analysis*, vol. 18, pp. 118–129, Jan. 2014.

[86] B. S. Andreassen, F. Veronesi, O. Gerard, A. H. S. Solberg, and E. Samset, "Mitral Annulus Segmentation Using Deep Learning in 3-D Transesophageal Echocardiography," *IEEE Journal of Biomedical and Health Informatics*, vol. 24, pp. 994–1003, Apr. 2020.

[87] E. Costa, N. Martins, M. S. Sultan, D. Veiga, M. Ferreira, S. Mattos, and M. Coimbra, "Mitral Valve Leaflets Segmentation in Echocardiography using Convolutional Neural Networks," in *2019 IEEE 6th Portuguese Meeting on Bioengineering (ENBENG)*, IEEE, Feb. 2019.

[88] H. Alkadhi, L. Desbiolles, P. Stolzmann, S. Leschka, H. Scheffel, A. Plass, T. Schertler, P. T. Trindade, M. Genoni, P. Cattin, B. Marincek, and T. Frauenfelder, "Mitral annular shape, size, and motion in normals and in patients with cardiomyopathy," *Investigative Radiology*, vol. 44, pp. 218–225, Apr. 2009.

[89] A. M. Fabricius, T. Walther, V. Falk, and F. W. Mohr, "Three-dimensional echocardiography for planning of mitral valve surgery: Current applicability?," *The Annals of Thoracic Surgery*, vol. 78, pp. 575–578, Aug. 2004.

[90] P. Ferrazzi, A. Iacovoni, S. Pentiricci, M. Senni, M. Iascone, N. Borenstein, L. Behr, A. Borghi, R. Balossino, and E. Quaini, "Toward the development of a fully elastic mitral ring: Preliminary, acute, in vivo evaluation of physiomechanical behavior," *The Journal of Thoracic and Cardiovascular Surgery*, vol. 137, pp. 174–179, Jan. 2009.

[91] J. T. Moore, M. W. A. Chu, B. Kiaii, D. Bainbridge, G. Guiraudon, C. Wedlake, M. Currie, M. Rajchl, R. V. Patel, and T. M. Peters, "A navigation platform for guidance of beating heart transapical mitral valve repair," *IEEE Transactions on Biomedical Engineering*, vol. 60, pp. 1034–1040, Apr. 2013.

[92] F. P. Li, M. Rajchl, J. Moore, and T. M. Peters, "A mitral annulus tracking approach for navigation of off-pump beating heart mitral valve repair," *Medical Physics*, vol. 42, pp. 456–468, Dec. 2014.

[93] Y. Zhang, A.-a. Amadou, I. Voigt, V. Mihalef, H. Houle, M. John, T. Mansi, and R. Liao, "A bottom-up approach for real-time mitral valve annulus modeling on 3d echo images," in *Medical Image Computing and Computer Assisted Intervention – MICCAI 2020*, pp. 458–467, Springer International Publishing, 2020.

[94] P. M. Shah, "Current concepts in mitral valve prolapse—Diagnosis and management," *Journal of Cardiology*, vol. 56, pp. 125–133, Sept. 2010.

[95] A. Linden, J. Seeburger, T. Noack, V. Falk, and T. Walther, "Imaging in Cardiac Surgery: Visualizing the Heart," *The Thoracic and Cardiovascular Surgeon*, vol. 65, pp. S213–S216, Apr. 2017.

[96] C. Wachinger, W. Wein, and N. Navab, "Registration strategies and similarity measures for three-dimensional ultrasound mosaicing," *Academic Radiology*, vol. 15, pp. 1404–1415, Nov. 2008.

[97] P. Carnahan, J. T. Moore, D. Bainbridge, E. C. S. Chen, and T. M. Peters, "Multi-view 3D echocardiography volume compounding for mitral valve procedure planning," in *Medical Imaging 2020: Image-Guided Procedures, Robotic Interventions, and Modeling* (B. Fei and C. A. Linte, eds.), SPIE, Mar. 2020.

[98] C. Wachinger, W. Wein, and N. Navab, "Three-Dimensional Ultrasound Mosaicing," in *Medical Image Computing and Computer-Assisted Intervention – MICCAI 2007* (N. Ayache, S. Ourselin, and A. Maeder, eds.), (Berlin, Heidelberg), pp. 327–335, Springer Berlin Heidelberg, 2007.

[99] M. Felsberg and G. Sommer, "The monogenic signal," *IEEE Transactions on Signal Processing*, vol. 49, no. 12, pp. 3136–3144, 2001.

[100] E. Bedrosian, "The analytic signal representation of modulated waveforms," *Proceedings of the IRE*, vol. 50, pp. 2071–2076, Oct. 1962.

[101] K. Rajpoot, V. Grau, and J. A. Noble, "Local-phase based 3D boundary detection using monogenic signal and its application to real-time 3-D echocardiography images," in *2009 IEEE International Symposium on Biomedical Imaging: From Nano to Macro*, IEEE, jun 2009.

[102] V. Grau and J. A. Noble, "Adaptive multiscale ultrasound compounding using phase information," in *Lecture Notes in Computer Science*, pp. 589–596, Springer Berlin Heidelberg, 2005.

[103] C. Hohmann, G. Michels, M. Schmidt, R. Pfister, N. Mader, M. Ohler, L. Blanke, N. Jazmati, C. Lehmann, J. Rybniker, S. M. Fünger, G. Fätkenheuer, and N. Jung, "Diagnostic challenges in infective endocarditis: is PET/CT the solution?," *Infection*, vol. 47, no. 4, pp. 579–587, 2019.

[104] W. T. Roberts, J. J. Bax, and L. C. Davies, "Cardiac CT and CT coronary angiography: technology and application," *Heart*, vol. 94, pp. 781–792, June 2008.

[105] E. J. Benjamin, S. S. Virani, C. W. Callaway, A. M. Chamberlain, A. R. Chang, S. Cheng, S. E. Chiuve, M. Cushman, F. N. Delling, R. Deo, *et al.*, "Heart Disease and Stroke Statistics—2018 Update: A Report from the American Heart Association," *Circulation*, vol. 137, pp. E67–E492, Mar. 2018.

[106] M. F. Eleid, G. S. Reeder, J. F. Malouf, R. J. Lennon, S. V. Pislaru, V. T. Nkomo, and C. S. Rihal, "The Learning Curve for Transcatheter Mitral Valve Repair With MitraClip," *Journal of Interventional Cardiology*, vol. 29, pp. 539–545, July 2016.

[107] A. B. Scanlan, A. V. Nguyen, A. Ilina, A. Lasso, L. Cripe, A. Jegatheeswaran, E. Silvestro, F. X. McGowan, C. E. Mascio, S. Fuller, T. L. Spray, M. S. Cohen, G. Fichtinger, and M. A. Jolley, "Comparison of 3D Echocardiogram-Derived 3D Printed Valve Models to Molded Models for Simulated Repair of Pediatric Atrioventricular Valves," *Pediatric Cardiology*, vol. 39, pp. 538–547, Nov. 2017.

[108] A. V. Nguyen, A. Lasso, H. H. Nam, J. Faerber, A. H. Aly, A. M. Pouch, A. B. Scanlan, F. X. McGowan, L. Mercer-Rosa, M. S. Cohen, J. Simpson, G. Fichtinger, and M. A. Jolley, "Dynamic Three-Dimensional Geometry of the Tricuspid Valve Annulus in Hypoplastic Left Heart Syndrome with a Fontan Circulation," *Journal of the American Society of Echocardiography*, Feb. 2019.

[109] E. Kerfoot, J. Clough, I. Oksuz, J. Lee, A. P. King, and J. A. Schnabel, "Left-Ventricle Quantification Using Residual U-Net," in *Statistical Atlases and*

Computational Models of the Heart. Atrial Segmentation and LV Quantification Challenges, pp. 371–380, Springer International Publishing, 2019.

[110] O. Russakovsky, J. Deng, H. Su, J. Krause, S. Satheesh, S. Ma, Z. Huang, A. Karpathy, A. Khosla, M. Bernstein, A. C. Berg, and L. Fei-Fei, "ImageNet Large Scale Visual Recognition Challenge," *International Journal of Computer Vision (IJCV)*, vol. 115, no. 3, pp. 211–252, 2015.

[111] L. M. Prevedello, S. S. Halabi, G. Shih, C. C. Wu, M. D. Kohli, F. H. Chokshi, B. J. Erickson, J. Kalpathy-Cramer, K. P. Andriole, and A. E. Flanders, "Challenges related to artificial intelligence research in medical imaging and the importance of image analysis competitions.," *Radiology. Artificial intelligence*, vol. 1, p. e180031, Jan. 2019.

[112] F. Milletari, N. Navab, and S.-A. Ahmadi, "V-Net: Fully Convolutional Neural Networks for Volumetric Medical Image Segmentation," in *2016 Fourth International Conference on 3D Vision (3DV)*, pp. 565–571, IEEE, Oct. 2016.

[113] S. Liu, D. Xu, S. K. Zhou, O. Pauly, S. Grbic, T. Mertelmeier, J. Wicklein, A. Jerebko, W. Cai, and D. Comaniciu, "3D Anisotropic Hybrid Network: Transferring Convolutional Features from 2D Images to 3D Anisotropic Volumes," in *Medical Image Computing and Computer Assisted Intervention – MICCAI 2018*, pp. 851–858, Springer International Publishing, 2018.

[114] A. Myronenko, "3D MRI Brain Tumor Segmentation Using Autoencoder Regularization," in *Brainlesion: Glioma, Multiple Sclerosis, Stroke and Traumatic Brain Injuries*, pp. 311–320, Springer International Publishing, 2019.

[115] D. P. Kingma and J. L. Ba, "Adam: A Method for Stochastic Optimization," in *CoRR*, vol. 1412.6980, 2014.

[116] B. S. Andreassen, D. Volgyes, E. Samset, and A. H. S. Solberg, "Mitral annulus segmentation and anatomical orientation detection in TEE images using periodic 3d CNN," *IEEE Access*, vol. 10, pp. 51472–51486, 2022.

[117] A. Lasso, C. Herz, H. Nam, A. Cianciulli, S. Pieper, S. Drouin, C. Pinter, S. St-Onge, C. Vigil, S. Ching, K. Sunderland, G. Fichtinger, R. Kikinis, and M. A. Jolley, "SlicerHeart: An open-source computing platform for cardiac image analysis and modeling," *Frontiers in Cardiovascular Medicine*, vol. 9, Sept. 2022.

[118] M. Tan and Q. Le, "EfficientNet: Rethinking model scaling for convolutional neural networks," in *Proceedings of the 36th International Conference on Machine Learning* (K. Chaudhuri and R. Salakhutdinov, eds.), vol. 97 of *Proceedings of Machine Learning Research*, pp. 6105–6114, PMLR, June 2019.

[119] A. Dosovitskiy, L. Beyer, A. Kolesnikov, D. Weissenborn, X. Zhai, T. Unterthiner, M. Dehghani, M. Minderer, G. Heigold, S. Gelly, J. Uszkoreit, and N. Houlsby, "An image is worth 16x16 words: Transformers for image recognition at scale," in *International Conference on Learning Representations*, 2021.

Appendix A

Permissions and Copyrights

For the chapters that were adapted from previously published articles, permission to reprint was obtained. As authors of the publications, we are entitled to reuse the articles in this thesis as per the publishers' guidelines.

ELSEVIER LICENSE TERMS AND CONDITIONS

Sep 13, 2023

This Agreement between Western University -- Patrick Carnahan ("You") and Elsevier ("Elsevier") consists of your license details and the terms and conditions provided by Elsevier and Copyright Clearance Center.

License Number	5627120298051
License date	Sep 13, 2023
Licensed Content Publisher	Elsevier
Licensed Content Publication	Journal of the American Society of Echocardiography
Licensed Content Title	Guidelines for Performing a Comprehensive Transesophageal Echocardiographic Examination: Recommendations from the American Society of Echocardiography and the Society of Cardiovascular Anesthesiologists
Licensed Content Author	Rebecca T. Hahn,Theodore Abraham,Mark S. Adams,Charles J. Bruce,Kathryn E. Glas,Roberto M. Lang,Scott T. Reeves,Jack S. Shanewise,Samuel C. Siu,William Stewart,Michael H. Picard
Licensed Content Date	Sep 1, 2013
Licensed Content Volume	26
Licensed Content Issue	9
Licensed Content Pages	44
Start Page	921
End Page	964
Type of Use	reuse in a thesis/dissertation
Portion	figures/tables/illustrations
Number of figures/tables /illustrations	1
Format	electronic
Are you the author of this Elsevier article?	No
Will you be translating?	No
Title	Echocardiography image processing for mitral valve interventions
Institution name	Western university
Expected presentation date	Jan 2024
Order reference number	1
Portions	Figure 1
Requestor Location	Western University 1151 Richmond St London, ON N6A 3K7 Canada Attn: Patrick Carnahan
Publisher Tax ID	GB 494 6272 12
Total	**0.00 CAD**
Terms and Conditions	

INTRODUCTION

1. The publisher for this copyrighted material is Elsevier. By clicking "accept" in connection with completing this licensing transaction, you agree that the following terms and conditions apply to this transaction (along with the Billing and Payment terms and conditions established by Copyright Clearance Center, Inc. ("CCC"), at the time that you opened your RightsLink account and that are available at any time at https://myaccount.copyright.com).

GENERAL TERMS

2. Elsevier hereby grants you permission to reproduce the aforementioned material subject to the terms and conditions indicated.
3. Acknowledgement: If any part of the material to be used (for example, figures) has appeared in our publication with credit or acknowledgement to another source, permission must also be sought from that source. If such permission is not obtained then that material may not be included in your publication/copies. Suitable acknowledgement to the source must be made, either as a footnote or in a reference list at the end of your publication, as follows:
"Reprinted from Publication title, Vol /edition number, Author(s), Title of article / title of chapter, Pages No., Copyright (Year), with permission from Elsevier [OR APPLICABLE SOCIETY COPYRIGHT OWNER]." Also Lancet special credit - "Reprinted from The Lancet, Vol. number, Author(s), Title of article, Pages No., Copyright (Year), with permission from Elsevier."
4. Reproduction of this material is confined to the purpose and/or media for which permission is hereby given. The material may not be reproduced or used in any other way, including use in combination with an artificial intelligence tool (including to train an algorithm, test, process, analyse, generate output and/or develop any form of artificial intelligence tool), or to create any derivative work and/or service (including resulting from the use of artificial intelligence tools).
5. Altering/Modifying Material: Not Permitted. However figures and illustrations may be altered/adapted minimally to serve your work. Any other abbreviations, additions, deletions and/or any other alterations shall be made only with prior written authorization of Elsevier Ltd. (Please contact Elsevier's permissions helpdesk here). No modifications can be made to any Lancet figures/tables and they must be reproduced in full.
6. If the permission fee for the requested use of our material is waived in this instance, please be advised that your future requests for Elsevier materials may attract a fee.
7. Reservation of Rights: Publisher reserves all rights not specifically granted in the combination of (i) the license details provided by you and accepted in the course of this licensing transaction, (ii) these terms and conditions and (iii) CCC's Billing and Payment terms and conditions.
8. License Contingent Upon Payment: While you may exercise the rights licensed immediately upon issuance of the license at the end of the licensing process for the transaction, provided that you have disclosed complete and accurate details of your proposed use, no license is finally effective unless and until full payment is received from you (either by publisher or by CCC) as provided in CCC's Billing and Payment terms and conditions. If full payment is not received on a timely basis, then any license preliminarily granted shall be deemed automatically revoked and shall be void as if never granted. Further, in the event that you breach any of these terms and conditions or any of CCC's Billing and Payment terms and conditions, the license is automatically revoked and shall be void as if never granted. Use of materials as described in a revoked license, as well as any use of the materials beyond the scope of an unrevoked license, may constitute copyright infringement and publisher reserves the right to take any and all action to protect its copyright in the materials.
9. Warranties: Publisher makes no representations or warranties with respect to the licensed material.
10. Indemnity: You hereby indemnify and agree to hold harmless publisher and CCC, and their respective officers, directors, employees and agents, from and against any and all claims arising out of your use of the licensed material other than as specifically authorized pursuant to this license.
11. No Transfer of License: This license is personal to you and may not be sublicensed, assigned, or transferred by you to any other person without publisher's written permission.
12. No Amendment Except in Writing: This license may not be amended except in a writing signed by both parties (or, in the case of publisher, by CCC on publisher's behalf).
13. Objection to Contrary Terms: Publisher hereby objects to any terms contained in any purchase order, acknowledgment, check endorsement or other writing prepared by you, which terms are inconsistent with these terms and conditions or CCC's Billing and Payment terms and conditions. These terms and conditions, together with CCC's Billing and Payment terms and conditions (which are incorporated herein), comprise the entire agreement between you and publisher (and CCC) concerning this licensing transaction. In the event of any conflict between your obligations established by these terms and conditions and those established by CCC's Billing and Payment terms and conditions, these terms and conditions shall control.
14. Revocation: Elsevier or Copyright Clearance Center may deny the permissions described in this License at their sole discretion, for any reason or no reason, with a full refund payable to you. Notice of such denial will be made using the contact information provided by you. Failure to receive such notice will not alter or invalidate the denial. In no event will Elsevier or Copyright Clearance Center be responsible or liable for any costs, expenses or damage incurred by you as a result of a denial of your permission request, other than a refund of the amount(s) paid by you to Elsevier and/or Copyright Clearance Center for denied permissions.

LIMITED LICENSE

The following terms and conditions apply only to specific license types:
15. **Translation**: This permission is granted for non-exclusive world **English** rights only unless your license was granted for

translation rights. If you licensed translation rights you may only translate this content into the languages you requested. A professional translator must perform all translations and reproduce the content word for word preserving the integrity of the article.

16. **Posting licensed content on any Website**: The following terms and conditions apply as follows: Licensing material from an Elsevier journal: All content posted to the web site must maintain the copyright information line on the bottom of each image; A hyper-text must be included to the Homepage of the journal from which you are licensing at http://www.sciencedirect.com/science/journal/xxxxx or the Elsevier homepage for books at http://www.elsevier.com; Central Storage: This license does not include permission for a scanned version of the material to be stored in a central repository such as that provided by Heron/XanEdu. Licensing material from an Elsevier book: A hyper-text link must be included to the Elsevier homepage at http://www.elsevier.com . All content posted to the web site must maintain the copyright information line on the bottom of each image.

Posting licensed content on Electronic reserve: In addition to the above the following clauses are applicable: The web site must be password-protected and made available only to bona fide students registered on a relevant course. This permission is granted for 1 year only. You may obtain a new license for future website posting.

17. **For journal authors:** the following clauses are applicable in addition to the above:

Preprints:

A preprint is an author's own write-up of research results and analysis, it has not been peer-reviewed, nor has it had any other value added to it by a publisher (such as formatting, copyright, technical enhancement etc.).

Authors can share their preprints anywhere at any time. Preprints should not be added to or enhanced in any way in order to appear more like, or to substitute for, the final versions of articles however authors can update their preprints on arXiv or RePEc with their Accepted Author Manuscript (see below).

If accepted for publication, we encourage authors to link from the preprint to their formal publication via its DOI. Millions of researchers have access to the formal publications on ScienceDirect, and so links will help users to find, access, cite and use the best available version. Please note that Cell Press, The Lancet and some society-owned have different preprint policies. Information on these policies is available on the journal homepage.

Accepted Author Manuscripts: An accepted author manuscript is the manuscript of an article that has been accepted for publication and which typically includes author-incorporated changes suggested during submission, peer review and editor-author communications.

Authors can share their accepted author manuscript:

- immediately
  - via their non-commercial person homepage or blog
  - by updating a preprint in arXiv or RePEc with the accepted manuscript
  - via their research institute or institutional repository for internal institutional uses or as part of an invitation-only research collaboration work-group
  - directly by providing copies to their students or to research collaborators for their personal use
  - for private scholarly sharing as part of an invitation-only work group on commercial sites with which Elsevier has an agreement
- After the embargo period
  - via non-commercial hosting platforms such as their institutional repository
  - via commercial sites with which Elsevier has an agreement

In all cases accepted manuscripts should:

- link to the formal publication via its DOI
- bear a CC-BY-NC-ND license - this is easy to do
- if aggregated with other manuscripts, for example in a repository or other site, be shared in alignment with our hosting policy not be added to or enhanced in any way to appear more like, or to substitute for, the published journal article.

Published journal article (JPA): A published journal article (PJA) is the definitive final record of published research that appears or will appear in the journal and embodies all value-adding publishing activities including peer review co-ordination, copy-editing, formatting, (if relevant) pagination and online enrichment.

Policies for sharing publishing journal articles differ for subscription and gold open access articles:

Subscription Articles: If you are an author, please share a link to your article rather than the full-text. Millions of researchers have access to the formal publications on ScienceDirect, and so links will help your users to find, access, cite, and use the best available version.

Theses and dissertations which contain embedded PJAs as part of the formal submission can be posted publicly by the awarding institution with DOI links back to the formal publications on ScienceDirect.

If you are affiliated with a library that subscribes to ScienceDirect you have additional private sharing rights for others' research accessed under that agreement. This includes use for classroom teaching and internal training at the institution (including use in

course packs and courseware programs), and inclusion of the article for grant funding purposes.
Gold Open Access Articles: May be shared according to the author-selected end-user license and should contain a CrossMark logo, the end user license, and a DOI link to the formal publication on ScienceDirect.
Please refer to Elsevier's posting policy for further information.
18. **For book authors** the following clauses are applicable in addition to the above: Authors are permitted to place a brief summary of their work online only. You are not allowed to download and post the published electronic version of your chapter, nor may you scan the printed edition to create an electronic version. **Posting to a repository:** Authors are permitted to post a summary of their chapter only in their institution's repository.
19. **Thesis/Dissertation**: If your license is for use in a thesis/dissertation your thesis may be submitted to your institution in either print or electronic form. Should your thesis be published commercially, please reapply for permission. These requirements include permission for the Library and Archives of Canada to supply single copies, on demand, of the complete thesis and include permission for Proquest/UMI to supply single copies, on demand, of the complete thesis. Should your thesis be published commercially, please reapply for permission. Theses and dissertations which contain embedded PJAs as part of the formal submission can be posted publicly by the awarding institution with DOI links back to the formal publications on ScienceDirect.

Elsevier Open Access Terms and Conditions
You can publish open access with Elsevier in hundreds of open access journals or in nearly 2000 established subscription journals that support open access publishing. Permitted third party re-use of these open access articles is defined by the author's choice of Creative Commons user license. See our open access license policy for more information.
Terms & Conditions applicable to all Open Access articles published with Elsevier:
Any reuse of the article must not represent the author as endorsing the adaptation of the article nor should the article be modified in such a way as to damage the author's honour or reputation. If any changes have been made, such changes must be clearly indicated.
The author(s) must be appropriately credited and we ask that you include the end user license and a DOI link to the formal publication on ScienceDirect.
If any part of the material to be used (for example, figures) has appeared in our publication with credit or acknowledgement to another source it is the responsibility of the user to ensure their reuse complies with the terms and conditions determined by the rights holder.
Additional Terms & Conditions applicable to each Creative Commons user license:
CC BY: The CC-BY license allows users to copy, to create extracts, abstracts and new works from the Article, to alter and revise the Article and to make commercial use of the Article (including reuse and/or resale of the Article by commercial entities), provided the user gives appropriate credit (with a link to the formal publication through the relevant DOI), provides a link to the license, indicates if changes were made and the licensor is not represented as endorsing the use made of the work. The full details of the license are available at http://creativecommons.org/licenses/by/4.0.
CC BY NC SA: The CC BY-NC-SA license allows users to copy, to create extracts, abstracts and new works from the Article, to alter and revise the Article, provided this is not done for commercial purposes, and that the user gives appropriate credit (with a link to the formal publication through the relevant DOI), provides a link to the license, indicates if changes were made and the licensor is not represented as endorsing the use made of the work. Further, any new works must be made available on the same conditions. The full details of the license are available at http://creativecommons.org/licenses/by-nc-sa/4.0.
CC BY NC ND: The CC BY-NC-ND license allows users to copy and distribute the Article, provided this is not done for commercial purposes and further does not permit distribution of the Article if it is changed or edited in any way, and provided the user gives appropriate credit (with a link to the formal publication through the relevant DOI), provides a link to the license, and that the licensor is not represented as endorsing the use made of the work. The full details of the license are available at http://creativecommons.org/licenses/by-nc-nd/4.0. Any commercial reuse of Open Access articles published with a CC BY NC SA or CC BY NC ND license requires permission from Elsevier and will be subject to a fee.
Commercial reuse includes:

- Associating advertising with the full text of the Article
- Charging fees for document delivery or access
- Article aggregation
- Systematic distribution via e-mail lists or share buttons

Posting or linking by commercial companies for use by customers of those companies.

20. **Other Conditions**:

v1.10

Questions? E-mail us at customercare@copyright.com.

SPRINGER NATURE LICENSE
TERMS AND CONDITIONS

Sep 20, 2023

This Agreement between Western University -- Patrick Carnahan ("You") and Springer Nature ("Springer Nature") consists of your license details and the terms and conditions provided by Springer Nature and Copyright Clearance Center.

License Number	5633190559839
License date	Sep 20, 2023
Licensed Content Publisher	Springer Nature
Licensed Content Publication	International Journal of Computer Assisted Radiology and Surgery
Licensed Content Title	Dynamic, patient-specific mitral valve modelling for planning transcatheter repairs
Licensed Content Author	Olivia K. Ginty et al
Licensed Content Date	May 21, 2019
Type of Use	Thesis/Dissertation
Requestor type	academic/university or research institute
Format	electronic
Portion	figures/tables/illustrations
Number of figures/tables/illustrations	1

Will you be translating?	no
Circulation/distribution	1 - 29
Author of this Springer Nature content	yes
Title	Echocardiography image processing for mitral valve interventions
Institution name	Western university
Expected presentation date	Jan 2024
Portions	Figure 4
Requestor Location	Western University 1151 Richmond St London, ON N6A 3K7 Canada Attn: Western University
Total	0.00 CAD

Terms and Conditions

Springer Nature Customer Service Centre GmbH Terms and Conditions

The following terms and conditions ("Terms and Conditions") together with the terms specified in your [RightsLink] constitute the License ("License") between you as Licensee and Springer Nature Customer Service Centre GmbH as Licensor. By clicking 'accept' and completing the transaction for your use of the material ("Licensed Material"), you confirm your acceptance of and obligation to be bound by these Terms and Conditions.

1. Grant and Scope of License

1. 1. The Licensor grants you a personal, non-exclusive, non-transferable, non-sublicensable, revocable, world-wide License to reproduce, distribute, communicate to

the public, make available, broadcast, electronically transmit or create derivative works using the Licensed Material for the purpose(s) specified in your RightsLink Licence Details only. Licenses are granted for the specific use requested in the order and for no other use, subject to these Terms and Conditions. You acknowledge and agree that the rights granted to you under this License do not include the right to modify, edit, translate, include in collective works, or create derivative works of the Licensed Material in whole or in part unless expressly stated in your RightsLink Licence Details. You may use the Licensed Material only as permitted under this Agreement and will not reproduce, distribute, display, perform, or otherwise use or exploit any Licensed Material in any way, in whole or in part, except as expressly permitted by this License.

1. 2. You may only use the Licensed Content in the manner and to the extent permitted by these Terms and Conditions, by your RightsLink Licence Details and by any applicable laws.

1. 3. A separate license may be required for any additional use of the Licensed Material, e.g. where a license has been purchased for print use only, separate permission must be obtained for electronic re-use. Similarly, a License is only valid in the language selected and does not apply for editions in other languages unless additional translation rights have been granted separately in the License.

1. 4. Any content within the Licensed Material that is owned by third parties is expressly excluded from the License.

1. 5. Rights for additional reuses such as custom editions, computer/mobile applications, film or TV reuses and/or any other derivative rights requests require additional permission and may be subject to an additional fee. Please apply to journalpermissions@springernature.com or bookpermissions@springernature.com for these rights.

2. Reservation of Rights

Licensor reserves all rights not expressly granted to you under this License. You acknowledge and agree that nothing in this License limits or restricts Licensor's rights in or use of the Licensed Material in any way. Neither this License, nor any act, omission, or statement by Licensor or you, conveys any ownership right to you in any Licensed Material, or to any element or portion thereof. As between Licensor and you, Licensor owns and retains all right, title, and interest in and to the Licensed Material subject to the license granted in Section 1.1. Your permission to use the Licensed Material is expressly conditioned on you not impairing Licensor's or the applicable copyright owner's rights in the Licensed Material in any way.

3. Restrictions on use

3. 1. Minor editing privileges are allowed for adaptations for stylistic purposes or formatting purposes provided such alterations do not alter the original meaning or intention of the Licensed Material and the new figure(s) are still accurate and representative of the Licensed Material. Any other changes including but not limited to, cropping, adapting, and/or omitting material that affect the meaning, intention or moral rights of the author(s) are strictly prohibited.

3. 2. You must not use any Licensed Material as part of any design or trademark.

3. 3. Licensed Material may be used in Open Access Publications (OAP), but any such reuse must include a clear acknowledgment of this permission visible at the same time as the figures/tables/illustration or abstract and which must indicate that the Licensed Material is not part of the governing OA license but has been reproduced with permission. This may be indicated according to any standard referencing system but must include at a minimum 'Book/Journal title, Author, Journal Name (if applicable), Volume (if applicable), Publisher, Year, reproduced with permission from SNCSC'.

4. STM Permission Guidelines

4. 1. An alternative scope of license may apply to signatories of the STM Permissions Guidelines ("STM PG") as amended from time to time and made available at https://www.stm-assoc.org/intellectual-property/permissions/permissions-guidelines/.

4. 2. For content reuse requests that qualify for permission under the STM PG, and which may be updated from time to time, the STM PG supersede the terms and conditions contained in this License.

4. 3. If a License has been granted under the STM PG, but the STM PG no longer apply at the time of publication, further permission must be sought from the Rightsholder. Contact journalpermissions@springernature.com or bookpermissions@springernature.com for these rights.

5. Duration of License

5. 1. Unless otherwise indicated on your License, a License is valid from the date of purchase ("License Date") until the end of the relevant period in the below table:

Reuse in a medical communications project	Reuse up to distribution or time period indicated in License
Reuse in a dissertation/thesis	Lifetime of thesis
Reuse in a journal/magazine	Lifetime of journal/magazine
Reuse in a book/textbook	Lifetime of edition
Reuse on a website	1 year unless otherwise specified in the License
Reuse in a presentation/slide kit/poster	Lifetime of presentation/slide kit/poster. Note: publication whether electronic or in print of presentation/slide kit/poster may require further permission.
Reuse in conference proceedings	Lifetime of conference proceedings
Reuse in an annual report	Lifetime of annual report
Reuse in training/CME materials	Reuse up to distribution or time period indicated in License
Reuse in newsmedia	Lifetime of newsmedia

Reuse in coursepack/classroom materials	Reuse up to distribution and/or time period indicated in license

6. Acknowledgement

6. 1. The Licensor's permission must be acknowledged next to the Licensed Material in print. In electronic form, this acknowledgement must be visible at the same time as the figures/tables/illustrations or abstract and must be hyperlinked to the journal/book's homepage.

6. 2. Acknowledgement may be provided according to any standard referencing system and at a minimum should include "Author, Article/Book Title, Journal name/Book imprint, volume, page number, year, Springer Nature".

7. Reuse in a dissertation or thesis

7. 1. Where 'reuse in a dissertation/thesis' has been selected, the following terms apply: Print rights of the Version of Record are provided for; electronic rights for use only on institutional repository as defined by the Sherpa guideline (www.sherpa.ac.uk/romeo/) and only up to what is required by the awarding institution.

7. 2. For theses published under an ISBN or ISSN, separate permission is required. Please contact journalpermissions@springernature.com or bookpermissions@springernature.com for these rights.

7. 3. Authors must properly cite the published manuscript in their thesis according to current citation standards and include the following acknowledgement: '*Reproduced with permission from Springer Nature*'.

8. License Fee

You must pay the fee set forth in the License Agreement (the "License Fees"). All amounts payable by you under this License are exclusive of any sales, use, withholding, value added or similar taxes, government fees or levies or other assessments. Collection and/or remittance of such taxes to the relevant tax authority shall be the responsibility of the party who has the legal obligation to do so.

9. Warranty

9. 1. The Licensor warrants that it has, to the best of its knowledge, the rights to license reuse of the Licensed Material. **You are solely responsible for ensuring that the material you wish to license is original to the Licensor and does not carry the copyright of another entity or third party (as credited in the published version).** If the credit line on any part of the Licensed Material indicates that it was reprinted or adapted with permission from another source, then you should seek additional permission from that source to reuse the material.

9. 2. EXCEPT FOR THE EXPRESS WARRANTY STATED HEREIN AND TO THE EXTENT PERMITTED BY APPLICABLE LAW, LICENSOR PROVIDES THE

LICENSED MATERIAL "AS IS" AND MAKES NO OTHER REPRESENTATION OR WARRANTY. LICENSOR EXPRESSLY DISCLAIMS ANY LIABILITY FOR ANY CLAIM ARISING FROM OR OUT OF THE CONTENT, INCLUDING BUT NOT LIMITED TO ANY ERRORS, INACCURACIES, OMISSIONS, OR DEFECTS CONTAINED THEREIN, AND ANY IMPLIED OR EXPRESS WARRANTY AS TO MERCHANTABILITY OR FITNESS FOR A PARTICULAR PURPOSE. IN NO EVENT SHALL LICENSOR BE LIABLE TO YOU OR ANY OTHER PARTY OR ANY OTHER PERSON OR FOR ANY SPECIAL, CONSEQUENTIAL, INCIDENTAL, INDIRECT, PUNITIVE, OR EXEMPLARY DAMAGES, HOWEVER CAUSED, ARISING OUT OF OR IN CONNECTION WITH THE DOWNLOADING, VIEWING OR USE OF THE LICENSED MATERIAL REGARDLESS OF THE FORM OF ACTION, WHETHER FOR BREACH OF CONTRACT, BREACH OF WARRANTY, TORT, NEGLIGENCE, INFRINGEMENT OR OTHERWISE (INCLUDING, WITHOUT LIMITATION, DAMAGES BASED ON LOSS OF PROFITS, DATA, FILES, USE, BUSINESS OPPORTUNITY OR CLAIMS OF THIRD PARTIES), AND WHETHER OR NOT THE PARTY HAS BEEN ADVISED OF THE POSSIBILITY OF SUCH DAMAGES. THIS LIMITATION APPLIES NOTWITHSTANDING ANY FAILURE OF ESSENTIAL PURPOSE OF ANY LIMITED REMEDY PROVIDED HEREIN.

10. Termination and Cancellation

10. 1. The License and all rights granted hereunder will continue until the end of the applicable period shown in Clause 5.1 above. Thereafter, this license will be terminated and all rights granted hereunder will cease.

10. 2. Licensor reserves the right to terminate the License in the event that payment is not received in full or if you breach the terms of this License.

11. General

11. 1. The License and the rights and obligations of the parties hereto shall be construed, interpreted and determined in accordance with the laws of the Federal Republic of Germany without reference to the stipulations of the CISG (United Nations Convention on Contracts for the International Sale of Goods) or to Germany´s choice-of-law principle.

11. 2. The parties acknowledge and agree that any controversies and disputes arising out of this License shall be decided exclusively by the courts of or having jurisdiction for Heidelberg, Germany, as far as legally permissible.

11. 3. This License is solely for Licensor's and Licensee's benefit. It is not for the benefit of any other person or entity.

Questions? For questions on Copyright Clearance Center accounts or website issues please contact springernaturesupport@copyright.com or +1-855-239-3415 (toll free in the US) or +1-978-646-2777. For questions on Springer Nature licensing please visit https://www.springernature.com/gp/partners/rights-permissions-third-party-distribution

Other Conditions:

Version 1.4 - Dec 2022

Questions? customercare@copyright.com.

PATRICK CARNAHAN

EDUCATION

PhD **University of Western Ontario**, Biomedical Engineering 2023

BSc **University of Western Ontario**, Computer Science 2018
Honors Specialization
Graduated with Distinction
Minor in Theoretical Computer Science

HONORS AND AWARDS

NSERC – PGSD 2021
$63,000, three-year, merit-based scholarship awarded to PhD candidates in engineering

Ontario Graduate Scholarship - Queen Elizabeth II 2020
$15,000, merit-based scholarship available to students in science and technology disciplines

NSERC – CGSM (Accepted) 2019
$17,500, merit-based scholarship awarded to graduate students in engineering

Ontario Graduate Scholarship (Awarded) 2019
$15,000, merit-based scholarship available to students in all disciplines of graduate study

Western Gold Medal – Honors Specialization in Computer Science 2018
Awarded to the student graduating with the highest standing in computer science.

Edna Jeffery Scholarship 2016
$600, awarded to the student with the highest standing in computer science after second year.

Western University - Four Year Continuing Admission Scholarship 2014
$10,000 over 4 years, awarded to students with admission average of 95% or higher

PUBLICATIONS

A.H. Bharucha, J. Moore, **P. Carnahan**, P. MacCarthy, M.J. Monaghan, M. Baghai, R. Deshpande, J. Byrne, R. Dwarakowski, M. Eskandari, “Three-dimensional printing in modelling mitral valve interventions,” in *Echo Research & Practice*, vol. 10, 2023.

P. Carnahan, A. Bharucha, M. Eskandari, D. Bainbridge, E. C. S. Chen and T. M. Peters, " Real-time mitral annulus segmentation from 4D transesophageal echocardiography using deep learning regression," in *Proceedings of SPIE Medical Imaging*, vol. 12464, pp. 437-443, 2023.

H. Nissar, **P. Carnahan,** D. Bainbridge, E.C.S. Chen, T.M. Peters, “An open-source 3D Slicer module for fluoro-free transcatheter vessel navigation,” in *Proceedings of SPIE Medical Imaging*, vol. 12034, pp. 467-476, 2023.

P. Carnahan, J. Moore, D. Bainbridge, E.C.S. Chen, T.M. Peters, “Multi-View 3D Transesophageal Echocardiography Registration and Volume Compounding for Mitral Valve Procedure Planning,” in *Applied Sciences*, vol. 12 (9), 4562, 2022.

H. Nisar, **P. Carnahan**, D. Fakim, H. Akhuanzada, D. Hocking, T.M. Peters, E.C.S. Chen, “Towards ultrasound-based navigation: deep learning based IVC lumen segmentation from intracardiac echocardiography,” in *Proceedings of SPIE Medical Imaging*, vol. 12034, pp. 467-476, 2022.

P. Carnahan, J. Moore, D. Bainbridge, M. Eskandari, E.C.S. Chen, T.M. Peters, “DeepMitral: Fully automatic 3D echocardiography segmentation for patient specific mitral valve modelling,” in *Medical Image Computing and Computer Assisted Intervention – MICCAI 21*, Lecture Notes in Computer Science, vol. 12905, pp. 459-468, 2021.

P. Carnahan, J. Moore, D. Bainbridge, E. C. S. Chen and T. M. Peters, "Multi-view 3D echocardiography volume compounding for mitral valve procedure planning," in *Proceedings of SPIE Medical Imaging*, vol 11315, pp. 255-262, 2020.

P. Carnahan, J. Moore, D. Bainbridge, G. Wheeler, S. Deng, K. Pushparajah, E. C. S. Chen, J. M. Simpson and T. M. Peters, "Applications of VR medical image visualization to chordal length measurements for cardiac procedures," in *Proceedings of SPIE Medical Imaging*, vol 11315, pp. 578-584, 2020.

N. Boone, H. H. Nam, J. Moore, **P. Carnahan**, O. Ginty, M. A. Jolley and T. M. Peters, "Patient-specific, dynamic models of the tricuspid valve for simulation and planning," in *Proceedings of SPIE Medical Imaging*, vol 11315, pp. 613-621, 2020.

P. Carnahan, O. Ginty, J. Moore, A. Lasso, M. A. Jolley, C. Herz, M. Eskandari, D. Bainbridge and T. M. Peters, "Interactive-Automatic Segmentation and Modelling of the Mitral Valve," in *Functional Imaging and Modeling of the Heart*, Springer International Publishing, 2019, pp. 397-404.

L. A. Groves, **P. Carnahan**, D. R. Allen, R. Adam, T. M. Peters and E. C. S. Chen, "Accuracy assessment for the co-registration between optical and VIVE head-mounted display tracking," *International Journal of Computer Assisted Radiology and Surgery,* vol. 14, pp. 1207-1215, 5 2019.

O. K. Ginty, J. T. Moore, M. Eskandari, **P. Carnahan**, A. Lasso, M. A. Jolley, M. Monaghan and T. M. Peters, "Dynamic, patient-specific mitral valve modelling for planning transcatheter repairs," *International Journal of Computer Assisted Radiology and Surgery,* vol. 14, pp. 1227-1235, 5 2019.

CONFERENCE AWARDS

Oral Presentation Award, Oral Session 8, Cardiac and Lung Imaging. March 2023.
Imaging Network Ontario, London, Canada

Oral Presentation Honorable Mention, June 2019.
London Imaging Discovery Day, London, Canada

INTERNATIONAL CONFERENCE PRESENTATIONS

Workshop Organizer, Oct 2023: "Segmentation of the Mitral Valve from 3D TEE"
MICCAI, Vancouver, Canada

Platform, June 2023: "From 4D Transesophageal Echocardiography to Patient Specific Mitral Valve Models"
Hamlyn Symposium on Medical Robotics, London, UK

Poster, Feb 2023: "Real-time mitral annulus segmentation from 4D transesophageal echocardiography using deep learning regression"
SPIE Medical Imaging, San Diego, USA

Virtual Platform, Sept 2021: "DeepMitral: Fully automatic 3D echocardiography segmentation for patient specific mitral valve modelling"
MICCAI, Virtual Event

Platform, Feb 2020: "Multi-view 3D echocardiography volume compounding for mitral valve procedure planning"
SPIE Medical Imaging, Houston, USA

Poster, Feb 2020: "Applications of VR medical image visualization to chordal length measurements for cardiac procedures"
SPIE Medical Imaging, Houston, USA

Video Platform, Sept 2019: "EMERGING TECHNOLOGIES : ECHO AND VR IN CARDIAC INTERVENTIONS". T.M Peters and P. Carnahan
Echo Supervisor Summit, Australia

Poster, June 2019: "Interactive-Automatic Segmentation and Modelling of the Mitral Valve"
Functional Imaging and Modelling of the Heart, Bordeaux, France

LOCAL CONFERENCE PRESENTATIONS

Platform, June 2023: "Real time mitral annulus segmentation from 4D transesophageal echocardiography using deep learning regression"
London Imaging Discovery Day, London, Canada

Platform, March 2023: "Real time mitral annulus segmentation from 4D transesophageal echocardiography using deep learning regression"
Imaging Network Ontario, London, Canada

Platform, June 2022: "Multi-view 3D echocardiography volume compounding for mitral valve procedure planning"
Robarts Research Retreat, London, Canada

Platform, June 2022: "Multi-view 3D echocardiography volume compounding for mitral valve procedure planning"
London Imaging Discovery Day, London, Canada

Poster, March 2022: "Multi-view 3D echocardiography volume compounding for mitral valve procedure planning"
Imaging Network Ontario, London, Canada

Platform, June 2021: "DeepMV: Fully Automatic Ultrasound Segmentation for Patient Specific Mitral Valve Modelling"
Robarts Research Retreat, London, Canada

Virtual Poster, May 2021: "DeepMV: Fully Automatic Ultrasound Segmentation for Patient Specific Mitral Valve Modelling"
London Health Research Day, London, Canada

Platform, March 2021: "DeepMV: Fully Automatic Ultrasound Segmentation for Patient Specific Mitral Valve Modelling"
Imaging Network Ontario, London, Canada

Platform, March 2020: "Multi-view 3D echocardiography volume compounding for mitral valve procedure planning"
Imaging Network Ontario, London, Canada

Platform, June 2019: "Interactive-Automatic Segmentation and Modelling of the Mitral Valve"
London Imaging Discovery Day, London, Canada

Poster, April 2019: "Interactive-Automatic Ultrasound Segmentation for Mitral Valve Modelling"
London Health Research Day, London, Canada

Poster, March 2019: "Interactive-Automatic Ultrasound Segmentation for Mitral Valve Modelling" Imaging Network Ontario, London, Canada

TEACHING EXPERIENCE

University of Western Ontario Sept 2022-Dec 2022
Teaching Assistant, Software Engineering
- Algorithms and Data Structures (SE2205) - Dr. Quazi Rahman

University of Western Ontario Jan 2022-Apr 2022
Teaching Assistant, Software Engineering
- Software Engineering Design I (SE3350) – Dr. Shaimaa Ali

University of Western Ontario Sept 2021-Dec 2021
Teaching Assistant, Software Engineering
- Software Requirements and Analysis (SE3352) – Dr. Shaimaa Ali

University of Western Ontario Sept 2020-Dec 2020
Teaching Assistant, Software Engineering
- Software Requirements and Analysis (SE3352) - Dr. Luiz Capretz

University of Western Ontario Jan 2020-Apr 2020
Teaching Assistant, Engineering Sciences
- Programming Fundamentals for Engineers (ES1036) - Dr. Quazi Rahman

University of Western Ontario Sept 2019-Dec 2019
Teaching Assistant, Software Engineering
- Algorithms and Data Structures (SE2205) - Dr. Mehdi Delrobaei

University of Western Ontario Jan 2019-Apr 2019
Teaching Assistant, Engineering Sciences
- Programming Fundamentals for Engineers (ES1036) - Dr. Quazi Rahman

SERVICE AND INVOLVEMENT

Organizer: Segmentation of the Mitral Valve from 3D TEE (MICCAI 2023 Challenge and Workshop)

Reviewer: IEEE Trans. Med. Imaging, Computer Methods in Biomechanics and Biomedical Engineering: Imaging & Visualization, AE-CAI

Student Member: SPIE, MICCAI

ACADEMIC OUTREACH / VOLUNTEER EXPERIENCE

Canadian Medical Hall of Fame, London — Sept 2018 - Present
Volunteer, Image Guided Interventions Workshops

Western Engineering Summer Academy, London — August 2019
Volunteer, Biomedical Engineering Imaging Workshop

Western Engineering Summer Academy, London — August 2018
Volunteer, Biomedical Engineering Imaging Workshop

Western Scholars Honors Society, London — 2014-2018
Undergraduate member